Thesis for the degree
Doctor of Philosophy

עבודת גמר (תזה) לתואר
דוקטור לפילוסופיה

Submitted to the Scientific Council of the
Weizmann Institute of Science
Rehovot, Israel

מוגשת למועצה המדעית של
מכון ויצמן למדע
רחובות, ישראל

By
Tegest Aychek

מאת
טאגסט אייצק

תפקיד התאים החד-גרעיניים של ה-lamina propria בבקרה על הומאוסטזיס ובהתפתחות מחלות מעיים דלקתיות

The role of lamina propria mononuclear phagocytes in gut homeostasis and the development of inflammatory bowel disorders

Advisor:
Prof. Steffen Jung

מנחה:
פרופ'.סטפן יונג

Month and Year
February 2013

חודש ושנה עבריים
שבט תשע"ג

Abstract

The monolayer of intestinal epithelial cells that separates the gut lumen from host tissue is constantly exposed to dietary antigens and a complex community of commensal bacteria. It is in this vulnerable setting that inflammatory bowel disorders (IBD), such as Crohn's disease (CD) and ulcerative colitis (UC), occur in genetically predisposed individuals. Strategically positioned intestinal *lamina propria* mononuclear phagocytes are considered crucial for maintaining gut homeostasis and immune defense. This includes: monocyte-derived CX_3CR1^+ cells, displaying macrophage (MΦ) features and migratory $CD103^+$ $CD11c^+$ cells that are derived from dedicated dendritic cell (DC) precursors and display DC hallmarks. Understanding the differential contributions of these two cell types and their intercellular communication is likely to provide critical insights into the mechanisms that maintain the gut homeostasis or lead to IBD.

Here we focused on the two cytokines IL-12 and IL-23 that are considered to play key roles in the development of Th1 and Th17 cell responses. To define the importance of cytokine production by the specific mononuclear phagocyte populations, we used a cell ablation strategy combined with a challenge by the murine Attaching & Effacing (A&E) pathogen *Citrobacter rodentium*. Chimeras generated with CD11c-DTR and IL-23 $(p19)^{-/-}$ BM allowed us to show that DC/MΦ-derived IL-23 is required for the induction of IL-22 and anti-microbial peptides (AMPs). Moreover, also when the IL23 deficiency was restricted to CX_3CR1^+ cells using newly established CX_3CR1^{Cre}:iDTR mice AMP and IL22 production were impaired. Surprisingly though, *C. rodentium*-challenged mice carrying IL-23 deficiencies died from the challenge. Our results suggest that in an IL-23 deficient environment, IL-12 secreted by $CD103^+$ DCs drives uncontrolled IFN-γ production by T cells causing severe immunopathology. In support of this notion, the immunopathology was prevented by neutralization of IFN-γ that rescued the mice.

Acknowledgements

I would like to thank my supervisor, Professor Steffen Jung, who guided me during this research with both his words and deeds. I am extremely grateful and indebted to him for his professional support, guidance and dedication.

I wish to express my sincere thanks to Professor Michal Neeman for her guidance and support in the MRI project.

I also would like to thank:
Dr. Katrien Vandoorne, for her dynamic collaboration and scientific help.
Dr. Alexander Mildner for creating a fertile working environment, scientific help and collegiality.

List of abbreviation

APCs: antigen-presenting cells
BM: Bone Marrow
DC: Dendritic Cell
DN: Double Negative
DTx: Diphtheria Toxin
DSS: Dextran Sulfate Sodium
ECM: Extra Cellular Matrix
ELISA: Enzyme-Linked ImmunoSorbent Assay
EBI3: Epstein–Barr virus-induced gene 3
GFP: Green Fluorescent Protein
IBD: Inflammatory Bowel Disease
IFNγ: Interferon γ
ILFs: isolated lymphoid follicles
IL-27: Interleukin 27
IL-23: Interleukin 23
IL-12: Interleukin 12
IL-10: Interleukin 10
IL-6: Interleukin 6
IL-17: Interleukin 17
LpDC: lamina propria Dendritic Cell
MΦ: Macrophages
MLNs: Mesenteric lymph nodes
MDPs: Macrophage/ DC precursors
MHC: Major Histocompatibility Complex
NK cell: Natural Killer cell
PCR: Polymerase Chain Reaction
PDCs: Plasmacytoid Dendritic Cells
PP: Peyer's Patches
PAMPs: pathogen-associated molecular patterns
PRRs: pattern-recognition receptors
RT-PCR: Reverse Transcriptase PCR

TBP: TATA box binding protein

TNF-α: Tumor Necrosis Factor-alpha

TGF-β: Tumor Growth Factor-beta

TCR: T Cell Receptor

TLR: Toll-like receptors

TNF: Tumor Necrosis Factor

TRIF: TIR-domain-containing adapter-inducing interferon-β

T_{reg}: Regulatory T cells

Th-17: T helper 17 cells

1. Introduction

1.1 Mononuclear phagocytes in the intestinal mucosa.

The intestinal immune system maintains tolerance to harmless food antigens and commensals, yet robustly responds to harmful pathogens. Dysregulation of this delicate balance results in uncontrolled inflammatory disorders, such as Inflammatory Bowel Disease (IBD) in humans [1]. Homeostasis maintenance is believed to be decisively influenced by mononuclear phagocytes, including macrophages and dendritic cells (DCs) [2]. Mononuclear phagocytes are highly abundant in mucosal tissue and can be found both in organized lymphoid organs, such as the Peyer's Patches (PPs), as well as in isolated lymphoid follicles (ILFs). Moreover, mononuclear phagocytes are also very frequent in the loose connective tissue underlying the epithelium, the *lamina propria* [3]. *Lamina propria* mononuclear phagocytes first aroused attention when they were shown to penetrate epithelial tight junctions to reach the gut lumen [4]. More recent reports have highlighted the phenotypic and functional heterogeneity of *lamina propria* mononuclear phagocytes and the existence of discrete subpopulations, which express the α integrin chain CD103 (αE) and the chemokine receptor CX3CR1, respectively [5].

1.1.2 Classification of mononuclear phagocytes according to functions and their *in vivo* origin.

Functional assays for *lamina propria* DCs (lpDCs) and MΦ have largely been restricted to *ex vivo* isolates and it hence remains unclear, whether reported activities exist in the tissue and microbiota context. Moreover, while lpDCs could act upon migration to the local draining mesenteric lymph nodes (MLNs) [6], macrophages might display their activities within the *lamina propria* itself [7]. Specific mononuclear phagocyte differentiation begins with clonotypic MΦ/ DC precursors (MDPs) that lost the potential to give rise to granulocytes [8]. In the past, it was established that classical splenic DCs (cDCs) do not arise from non-monocytic precursors [9]. Monocytes, on the other hand, could give efficient rise to mononuclear phagocytes in the gut. Using a combination of conditional cell ablation and precursor cell-mediated *in vivo* reconstitution Varol and

colleagues demonstrated that intestinal CX3CR1+ mononuclear phagocytes derive from Ly6C^{hi}, but not Ly6C^{lo} monocytes. CD103+ lpDCs on the other hand are replenished via dedicated circulating DC precursors, the so-called pre-cDCs [10] (Fig. 1). Interestingly, results from our laboratory indicated that the balance of CD103+ and CX3CR1+ cells might be critical for the maintenance of robust intestinal homeostasis. Thus, a *lamina propria* that was exclusively populated by CX3CR1+ mononuclear phagocytes was found prone to develop severe colitis in a dextran sodium sulfate (DSS) challenge modelwith [11]. The proinflammatory activity of the CX3CR1+ cells in these experiments strictly depended on their ability to produce TNFα [11]. These results support the notion that CD103+ and CX3CR1+ mononuclear phagocytes exert distinct functions.

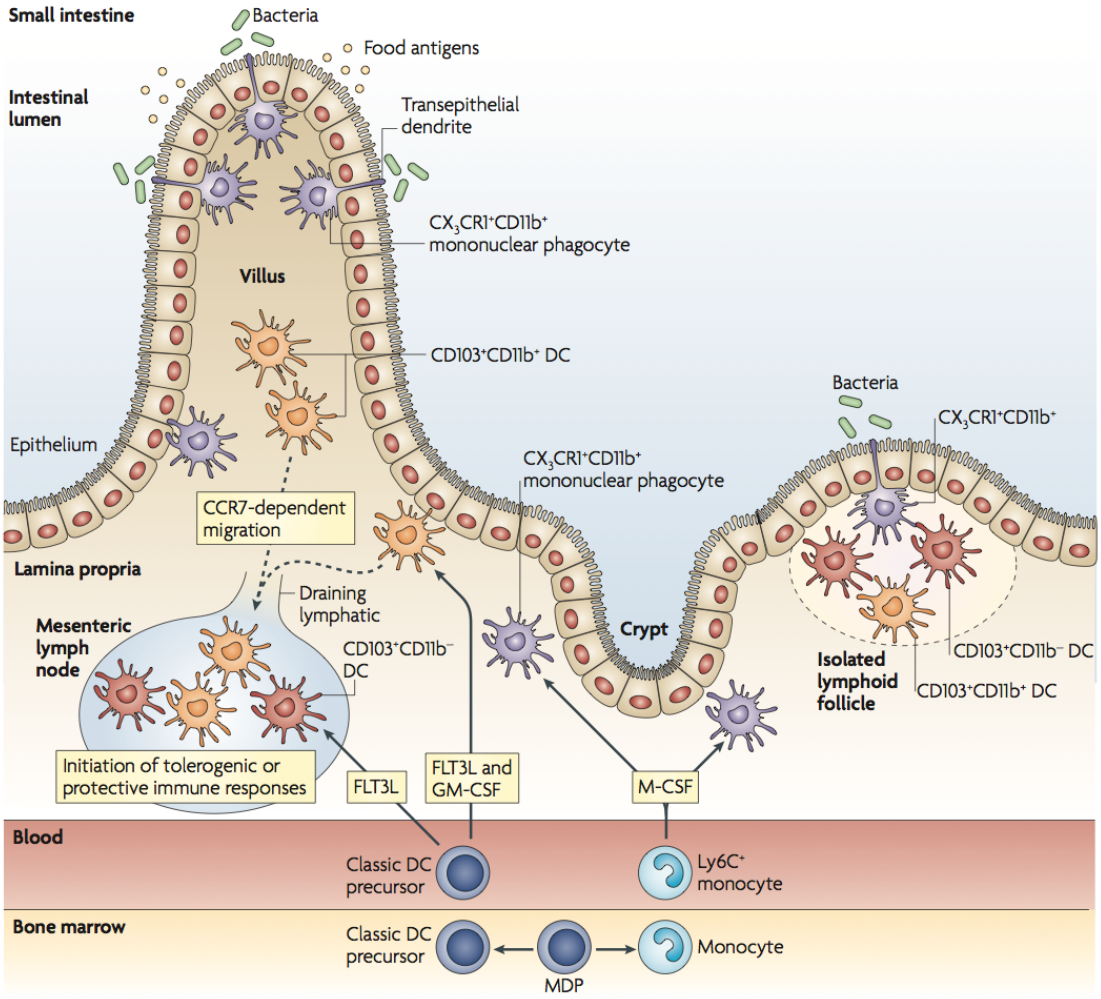

Fig. 1. The intestinal mononuclear phagocyte compartment. adopted from reference # 2

1.1.3 Mononuclear phagocytes in IBD.

Commensal microflora plays a critical role in the maintenance of intestinal epithelial homeostasis through the triggering of pattern recognition receptors, such as Toll-like receptors (TLRs) [12]. In vitro studies suggest that the epithelium secretes factors such as the cytokine thymic stromal lymphopoietin (TSLP) that conditions DCs in the underlying lamina propria to acquire the Th2-promoting phenotype [13]. Collectively in their native environment mononuclear phagocytes are exposed to complex signals derived from the microflora, the epithelium and probably other cellular components. Arguably, investigations of the contributions of mononuclear phagocyte to the development or resolution of chronic intestinal inflammation should hence preferably to be performed in their physiological context.

Monocyte-derived CX3CR1+ mononuclear phagocytes display a number of unique characteristics [11]. Expression of the CX3CR1 chemokine receptor allows these cells to interact with CX3CL1-expressing columnar epithelial cells and form characteristic transepithelial dendrites (TEDs) that penetrate the epithelial barrier [14,15]. By means of their TEDs, CX3CR1+ cells could capture luminal antigens or even bacteria[16] and contribute to tolerance establishment or immune defense. However surprisingly, recent studies have revealed that CX3CR1+ mononuclear phagocytes do not directly relate antigens or information to deeper lymphoid organs. Thus, only CD103+ lpDCs, but not CX3CR1+ cells migrate to mesenteric LNs (MsnLN) [17]. In fact the absence of this DC hallmark, combined with the notion that CX3CR1+ cells are poor stimulators of naïve T cells [17] led to the notion that these cells might be a special subset of macrophages [2]. Taken together, CX3CR1+ cells seem to exert unique yet-to-be defined local functions within the *lamina propria*. Strategically positioned in immediate proximity to the epithelium, CX3CR1+ cells could contribute to phagocytosis and killing of invading bacteria. Moreover, CX3CR1+ cells have even been shown to migrate into the intestinal lumen in a MyD88-dependent manner [18], although the physiological relevance of this route remains elusive. Interestingly, isolated CX3CR1+ *lamina propria* cells were shown

to be activated by microflora-derived ATP to produce IL-6 and IL-23, as well as to activate TGFβ [19]. This cytokine spectrum might allow these cells to promote the generation or maintenance of Th17 cells in the *lamina propria*. In support of this notion CD47 knockout mice that display a reduced percentage of SIRPα+ CD103neg DCs, i.e. CX3CR1+ cells, have impaired Th17 responses and are relatively protected from TNBS-induced colitis. Other studies have implied CX3CR1+ cells in the generation of Foxp3+ T regulatory cells based on their production of the regulatory cytokines IL-10 and TGFβ. Moreover, recently CD11c+ CD11b+ F4/80+ myeloid cells, likely to represent the CX3CR1+ population, were shown to release IL- 10 that acts in a paracrine manner on Treg cells to maintain Foxp3 expression and prevent colitis [20]. Upon antigen encounter in lymphoid organs pluripotent naive CD4+ T cells integrate signals from antigen-presenting DCs and the surrounding cytokine milieu, rapidly divide and acquire the capacity to secrete effector cytokines. After emigration to the tissues the resulting CD4+ helper T (TH) cells then orchestrate host immunity by secreting cytokines that act on immune and non-immune cells. Canonical TH subsets comprise IFNγ-secreting TH1 and IL4-secreting TH2 subsets. More recently, the T effector cell family has expanded to include IL-17-producing TH17 cells and peripherally-induced FoxP3+ regulatory T cells (Treg) [21]. Development of TH17 cells depends on the presence of a normal gut microflora [22]. Moreover, variations of the TH17 prevalence in C57BL/6 mice could be linked to the composition of the gut microflora of the animals [22]. Recently, it was shown that colonization of the small intestine with a single commensal microbe, the *segmented filamentous bacterium* (SFB), has a major impact on the intestinal T cell compartment [23]. Whereas it is now evident that the prevalence of T helper subsets and regulatory T cells has a decisive impact on the robustness of homeostasis and host response to pathogen challenge, it remains unclear whether the compartment is shaped in the draining lymph nodes or the tissue, i.e. *lamina propria*. For instance, different IL-10 requirements of Treg cells have been reported dependent on the site of their action. Suppression of naive T cell transfer colitis, which probably occurs primarily in the spleen or lymph nodes, is an IL10-independent mechanism [24]. In contrast IL10 is required to control *Helicobacter*-triggered local inflammation, as well as to cure colitis, where effector cells have probably already accumulated in the *lamina propria* [24]. While we have a considerable understanding of the

reactions in the lymph node, immune reactions in the tissue proper remain poorly understood. Emerging evidence suggests that T cell fates in the MLNs and the *lamina propria* are controlled by CD103+ DCs and CX3CR1+ macrophages, respectively [25]. Beyond the clinical relevance of IBD-related studies, the intestine provides hence also a unique opportunity to investigate this issue of general importance for our understanding of the functional organization of the immune system.

1. 2 Cytokine involvement in immunity and inflammation

Cytokines coordinate virtually every aspect of immunity and inflammation. They play a critical role in the decision whether a response occurs after an immune insult. Moreover, the production of particular cytokines subsequently orchestrates the nature of the response (cytotoxic, humoral, cell mediated, or allergic) or non-responsiveness and active immune suppression. Understanding the function of individual cytokines is a major challenge because their functional role may vary depending on the cellular source, target, and phase of the immune response. Moreover, numerous cytokines have both pro- and anti-inflammatory potential, with the contrasting outcome determined by the immune cells present and their state of responsiveness to the cytokine[26].

1.2.1 The IL-12 cytokine family (IL-12, IL-23, IL-27, IL-35)

Members of the IL-12 cytokine family are heterodimeric complexes of helical subunits. They all bind to a β-chain -ike receptor (Scheme 3). The IL-12 cytokine family contains four members:

IL-12p70 comprises two disulphide-linked proteins: the **p35** chain and the **p40** chain [27]. IL-12 promotes the polarization of naïve T cells to TH1 cells and induces the secretion of interferon-γ (IFNγ) from CD4+ and CD8+ T cells and by natural-killer (NK) cells.

IL-23 comprises **p40** and **p19**, which was discovered based on its homology with IL-6 and the p35 chain. IL-23 enhances TH17-cell activities by acting on differentiated TH17 cells, which express the IL-23 receptor (IL-23R). IL-23 is dispensable for TH17 formation. IL-23 has also been reported to mediate intercellular communication between myeloid cells [28].

IL-27 comprises the **p28** and **EBI3** (Epstein–Barr virus-induced gene 3) chains and

promotes TH1-cell differentiation, an effect that is most prominent in the absence of IL-12. However, IL-27 also has a major regulatory role by directly antagonizing the development of TH17-cell responses and to limit IL-17-cell-driven inflammation in the central nervous system.

IL-35 comprises the **p35** and **EBI3** chains. Ebi3–/– and Il12a–/– Treg cells have significantly reduced regulatory activity *in vitro* and fail to control homeostatic proliferation and to cure inflammatory bowel disease *in vivo* [29]. This suggests that IL-35 is an inhibitory cytokine that may be specifically produced by Treg cells and is required for maximal suppressive activity. IL-35 and IL-10 induce the generation of T cells with IL-35 induced regulatory population (iTr35). These cells mediated repression by means of IL-35 but not by the use of the inhibitory cytokines IL-10 TGF-b under inflammatory conditions in intestines infected with *Trichuris muris* [30].

DCs can produce IL-12p70, IL-23 and IL-27 following exposure to pathogen-associated molecular patterns (PAMPs) that act through TLRs. Because TLRs use distinct adaptor molecules that lead to different gene-induction programs [31], the synthesis of IL-12 family members can be differentially regulated downstream of TLRs. There are important differences in the transcriptional control of genes that encode the different polypeptide chains of the IL-12 family members. For example systemic injection of flagellin leads to IL-23 secretion by CD103+CD11b+ lpDCs in the small intestine within one hour of exposure. This fast production of IL-23 was mediated by TLR5 and followed by induces expression of RegIIIγ via the epithelial [32]. However the source of IL-23 in the colon *in vivo* remains undefined. In addition p40 can be regulated by microRNAs. It is a target of microRNA10a (miR-10a) that is expressed in the colon and negatively regulated by intestinal microbiota in a MyD88 dependent pathway [33]. Accordingly, a miR-10a inhibitor promoted the expression of p40 in DCs which contribute to the maintenance of the intestinal homeostasis [33].

IL-12p70 is a key factor driving TH1-cell differentiation, whereas IL-10 inhibits TH1-cell responses. The balance between IL-12 and IL-10 was considered to be the crucial parameter that controls the development of T cell-mediated inflammation. The discovery of IL-23 and IL-27 has led to a re-evaluation of this view. Now several

experimental studies and clinical investigations suggest that IL6 and IL-23-driven TH17 cells, rather than the TH1-cell subset, mediate the inflammatory responses of autoimmune or infectious origin[34].

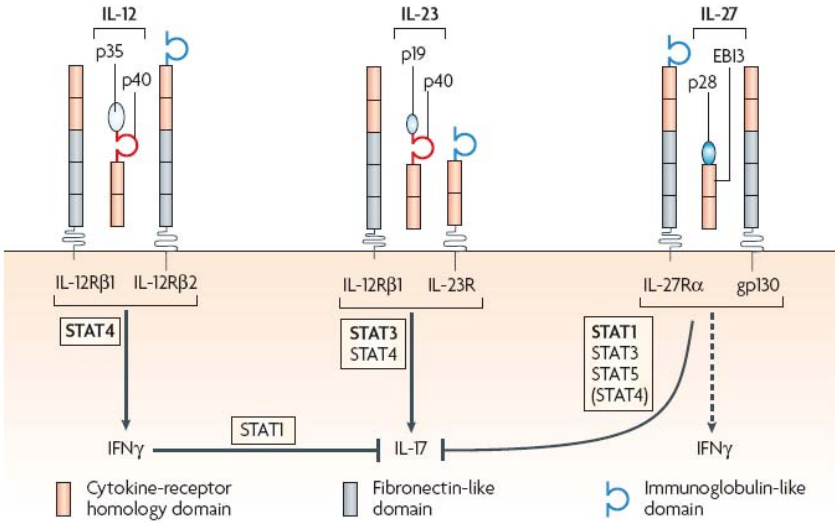

Scheme 3. Key features of IL-12 family members (adopted from reference #35). The IL-12 family of cytokines comprises a helical subunit (blue ovals) and a receptor-like β-chain an immunoglobulin-like domain; fibronectin-like domains. IL-12p70 and IL-23 share a common chain (p40) and their receptors share the IL-12 receptor β1 (IL-12Rβ1) chain. IL-12 induces the expression of IFNγ. IFNγ suppresses the development of IL-17-secreting T cells and thereby limits IL-17-mediated inflammatory events. IL-23 (comprising p40 and p19) promotes IL-17 production by several T cell types including the T helper 17 (TH17)-cell subset. IL-17 is a potent pro-inflammatory cytokine that induces tissue damage. IL-27 shares homology with IL-12p70 and IL-23 and signals through a receptor that shares the gp130 chain with the IL-6 receptor. IL-27 also has a major regulatory role by limiting TH17-cell differentiation. Signalling pathways that induce IL-12 family members include the JAK-STAT (signal transducer and activator of transcription) pathway.

Interestingly, transgenic mice expressing firefly luciferase under the control of the

IL-12 p40 promoter display high constitutive transgene expression in the small intestine [36], whereas the reporter gene activity was low in other tissues. Within the small bowel, constitutive IL-12 p40 promoter activity was restricted to the terminal ileum and associated with high expression of p40 mRNA as well as p40 and IL-23 p19/p40 proteins. Furthermore, little or no p40 protein expression in lpDCs was found in the terminal ileum of germfree mice, indicating a key role of the intestinal flora in driving constitutive p40 expression. In addition, analysis of transgenic mice with a mutated NF-κB target site in the p40 promoter showed a critical role of NF-κB in driving constitutive transgene expression.[36].

1.2.3 The IL-10-related family of cytokines (IL-10, IL-22)

IL-10 and its related cytokines share 20-30% amino acid identity and also have homologous secondary structures [37]. IL-10 signals through homodimeric IL-10R, while IL-22 signals through a heterodimeric receptor that consists of IL-22R and IL-10R [37]. Because IL-10R is ubiquitously expressed, signaling specificity is conferred by IL-10R and IL-22R expression; IL-10R expression is limited to cells of the immune system, whereas IL-22R expression is limited to tissue cells, such as epithelial cells [38]. In addition IL-22 has a soluble receptor known as IL-22-binding protein or IL-22RA2; however the function and the pathways that control its expression are still under investigation [37]. Just as IL-10 is believed to protect the immune system from overwhelming itself, IL-22 was proposed to protect the tissues during inflammation via a Stat3-mediated mechanism.

IL-22 has recently been shown to be protective during acute inflammation in a model of hepatitis [39,40]. In contrast, in the skin IL-22 has been shown to mediate inflammation [41,42]. The dual nature of this cytokine, acting in both anti- and pro- inflammatory fashion, depends thus on the context. This includes, but is not limited to, the duration and amount of IL-22 present, the overall cytokine milieu and the involved tissues. In vitro, IL-22 production can be induced directly in CD4+ T cells by IL-23 or IL-6 [42]. Mice deficient in IL-23 lose their ability to control infections by Attaching and Effacing enterobacteria (*C. rodentium*) suggesting that IL-22 may exert an important function in the anti-microbial host defense[45]. Indeed IL-22 seems to directly target colonic epithelial cells to induce the expression of the RegIII family of lectins, which can directly bind and kill Gram-positive

bacteria. IL-22 is involved in induction of genes encoding for host defense proteins including S100A7, S100A8, S100A10, β-defensin-2 and β-defensin-3 [38,43,44]. IL-22 also triggers expression of the chemokines CXCL1, CXCL5 and CXCL9 and the cytokines IL-6 and G-CSF [45,46]. IL-22 is adequate to advance protective innate immunity to Citrobacter *rodentium* for several weeks after infection of immuno-deficient mice [47] and delivery of exogenous IL-22 is sufficient to ameliorate the spontaneous intestinal inflammation observed in mice deficient in the TCR α-subunit [48]. This suggests that the IL-22-IL22R pathway enhances mechanisms of innate immunity in the absence of adaptive immune response.

Inhibition of IL-22 in the colon during the recovery phase of DSS induced colitis suppressed the reconstitution of goblet cell, i.e. the epithelial cells that are critical for mucus production [48]. Local delivery of exogenous IL-23 to the skin is sufficient to induce dermal inflammation and epidermal hyperplasia in an IL-22 dependent way [42]. Moreover IL-22 signaling was enough to reconstitute the organization of colonic patches (CLPs) and isolated lymphoid follicles (ILFs) and to re-establish the host defense against infection with *C. rodentium* in mice missing lymphotoxin signals[49]. Taken together these data reveal that dysregulated IL-22 responses can lead to pathological inflammation and can substantially damage barrier surfaces and tissue organization.

IL-22 expression in the innate and adaptive immune system.

IL-22 is known to be produced by Innate TH17 cells (iTH17 cells) 4 days after *C. rodentium* infection. This early induction of IL-22 is crucially controlled by the innate immune receptors Nod1 and Nod2 [50]. In addition to iTH17 cells, a variety of other intestinal cells can secrete both IL-17 and IL-22, including CD8+ T cells, γδ T cells [47,51-54]. Moreover, recent data highlight IL-22 expression in innate lymphoid cells (ILCs), including NK cells and lymphoid tissue inducer cells (LTis), a rising family of innate lymphocytes that do not require the recombination of antigen specific receptors [Spits, H Nat Immunol (2011)]. Furthermore studies revealed IL-22 expression in CD11c+ cells assumed to be DCs in colitis induced by DSS [55].

IL-10 controls T cell tolerance, at the interface between the innate and the adaptive immune systems. Microbial stimulation of antigen-presenting cells (APCs) via the pattern-recognition receptors (PRRs) induces APC maturation, which is associated with

the induction of MHC and costimulatory molecule gene expression. The secretion of innate immune cytokines, such as IL-10, can directly inhibit the APC maturation process. In addition, IL-10 can act on T cells to inhibit effector T cell differentiation stimulated by mature APCs. Upon stimulation by APCs, IL-10 can be produced by multiple T cell types, including Treg, Th17, Th1, Th2, and CTL cells [56]. IL-10 plays an important role in immune regulation in the intestine.

The relationship between IL-10 and IL-23

Colon specimens obtained from IBD patients have considerably lower levels of IgA and IL-10 when compared to normal controls. There is a negative correlation between the levels of IL-10 and IL-23 in the IBD mucosa since the levels of IL-23 were higher in IBD specimens. IL-23 blockage resulted in the enhancement of IL-10 levels by *lamina propria* mononuclear cells in the IBD group. Collectively IL-23 plays a critical role in suppression of the gene transcription of *IL10* in the IBD colon which weakens the defensive barrier by reducing the production of IgA in the gut [57].

Citrobacter rodentium

Citrobacter rodentium is a member of the attaching and effacing (A/E) family of bacterial pathogens, which is characterized by intimate bacterial adherence to host intestinal epithelial cells, effacement of microvilli, and reorganisation of the host actin cytoskeleton to form pedestal-like extensions of epithelial cells beneath the adherent bacteria called A/E lesions [58]. Gastrointestinal colonization and formation of A/E lesions is mediated by a pathogenicity island called the locus of enterocyte effacement (LEE), which is conserved among A/E bacteria [59]. *C. rodentium* is unique amongst *Citrobacter* species in possessing the LEE [60]. As the only known A/E pathogen to naturally infect mice, it is a valuable model organism for the study of pathogenesis of the clinically significant human pathogens, entero-pathogenic *E. coli* (EPEC) and entero-haemorrhagic *E. coli* (EHEC). Infection with C. *rodentium* results in transient reduction of commensals [61]. In the early stages of the infection virulence genes are expressed and necessary for pathogen growth in specific pathogen free mice. These virulence genes are not expressed in germ-free mice although germ-free mice show significantly high levels of C. *rodentium* when

compared to SPF mice[62]. In contrary throughout the late phase of infection the virulence genes expression was down regulated and the pathogen was released to the intestinal lumen where it was out competed by commensals. This points at the capacity of commensals to out-compete C. *rodentium* to some extent by the ability of the pathogen and commensals to grow on structurally similar carbohydrates [62].

Figure 2. Effacement of intestinal microvilli *Citrobacter* on the surface of Caco-2 cells causing a zone of effacement of bush villi around the dividing bacteria. http://www.staff.ncl.ac.uk/p.dean/body_index.html

Immune cell-mediated eradication of *C. rodentium.*

Adoptively transferred Ly6C^{hi} wt monocytes have been shown to traffic to the colon and restore clearance of C. *rodentium* in Ccr2–/– mice; in addition Nod2 controls the colonic recruitment of monocytes through the production of CCL2 in response to pathogen infection [63]. In the unique environment of the gut, IgA+ plasma cells produce the antimicrobial mediators TNF-α and inducible nitric oxide synthase (iNOS) [64]. In response to TLR ligation upon C. *rodentium* infection these plasma cells can acquire monocyte/DC functions and affect the response to microbial attack [64].

2. Objective

The objective of this thesis was to analyze the differential contribution of intestinal dendritic cells and macrophages to the maintenance of gut homeostasis and the immune defense against enterobacteria.

3. Approaches

1. Establishment of *C. rodentium* infection model in WT mice and analysis of kinetics of IL-22-mediated production of antimicrobial peptides in early host defense against the A&E pathogen.
2. Definition of the cellular source of the IL-23 produced in response to the *Citrobacter* infection.
3. Analysis of the involvement the IL-23 produced by DCs or macrophages in the regulation of IL-17A and IFN-γ defense against *C. rodentium* infection.
4. Definition of immunopathology underlying death in *Citrobacter*-infected IL23 mutant mice.
5. Establishment of a novel non-invasive read-out technique for IBD: MRI and fluorescent confocal endomicroscopy for the assessment of colitis based on permeability of the colonic microvasculature.

4. Results

4.1. Establishment of the *C. rodentium* infection model in WT mice.

Citrobacter rodentium is a natural mouse pathogen closely related to the attaching and effacing (A/E) *E. coli* strains EPEC and EHEC and hence provides an *in vivo* model to investigate A/E pathogen-host interactions under physiological conditions, with the ability to manipulate both the pathogen and the host. Visualization of infection using bioluminescence imaging of *C. rodentium* revealed that a few hours after oral challenge with 10^8–10^9 organisms, the site of initial colonization is the cecum, while two to three days later bacteria can be seen in the distal colon [58]. Depending on the mouse strain, bacterial levels in the colon peak between day 5–14 post infection (PI). Clearance of *C. rodentium* parallels the colonization, with clearance of the cecum followed by clearance of the colon by day 21–28 PI. Colonic hyperplasia (measured by increased crypt length and tissue weight) can be detected from day 5–14 PI. The majority of inbred mouse strains tested (C57Bl/6, NIH Swiss and BALB/c) show no mortality, when infected with *C. rodentium* but clear the disease spontaneously.

We decided to use the *C. rodentium* model in order to probe for differential contributions of lamina propria-resident DCs and MΦs in the response to pathogen challenge. Although the experimental procedures are seemingly straightforward, kinetics of *C. rodentium* clearance are known to be influenced by the microflora [67]. Optimization of the model required therefore extensive pilot experiments to establish baseline parameters in our facility. In order to investigate the initial colonization, the peak of the colonization and the clearance kinetics we analyzed colonic tissue of wt C57BL/6 mice during a 12 day time window. Wt mice inoculated with 10^9 *C. rodentium* bacteria showed consistent but minor weight changes **(Fig. 1a)**. Histological analysis revealed segmental colitis at day 8 with increased mucosal hyperplasia and increased crypt length in *C. rodentium* infected animals and widespread colitis on day 12 with thickened colon and extensive mucosal hyperplasia **(Fig. 1b)**.

a

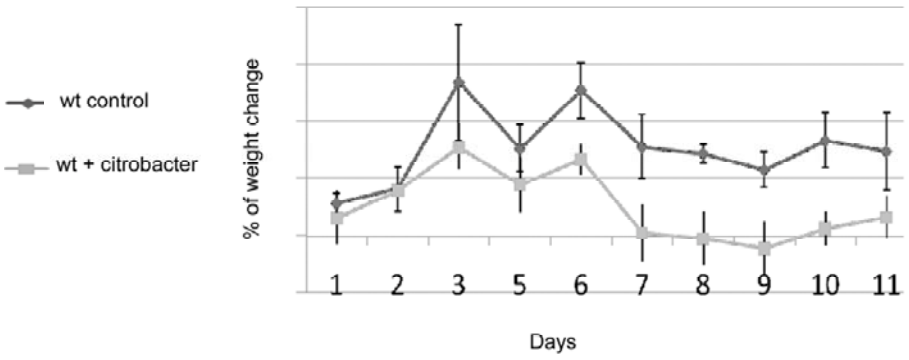
wt control
wt + citrobacter
% of weight change
1
2
3
5
6
7
8
9
10
11
Days

b

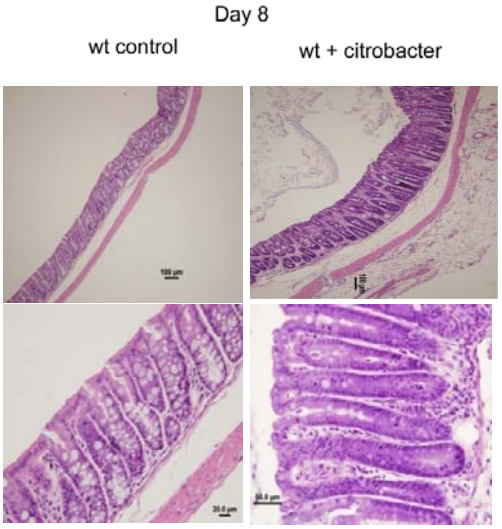
Day 8
wt control
wt + citrobacter

c

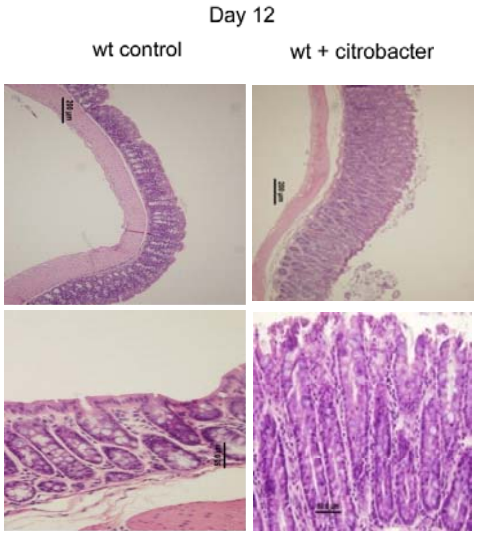
Day 12
wt control
wt + citrobacter

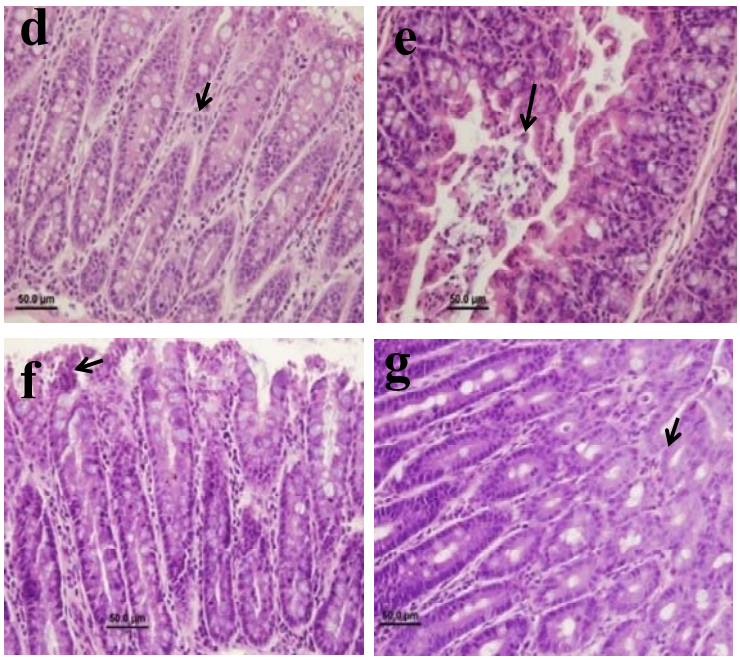

Figure 1: Wt mice display segmental colitis on day 8 and widespread colitis on day 12 after *C. rodentium* challenge. Wt mice (n=6) were orally inoculated with ≈10^8–10^9 CFU of *C. rodentium* by gavage. (a) Average weight changes; day of infection day 0 (b-d) Histological analysis of representative colons from uninfected and infected mice on day 8 and 12 after inoculation. H&E staining illustrates (b) segmental colitis at day 8 with increased mucosal hyperplasia and increased crypt length in infected mice (c) widespread colitis on day 12 with thickened colon and extensive mucosal hyperplasia. (d-g) H&E staining on day 12 illustrates (d) infiltration of immune cells (e) submucosal edema (f) extensive bacterial colonization (g) goblet cell deletion.

4.2. IL-22 induced production of antimicrobial peptides mediates the critical early host defense against *C. rodentium* infection in Wt mice.

Wt mice infected with *C. rodentium* clear the bacteria between day 21–28 post infection. Both intestinal epithelial cells and immune cells are crucial in host defense against the A/E pathogen. Epithelial tight junctions provide the first barrier preventing microbes from leaving the intestinal lumen but epithelial cells also actively secrete antimicrobial peptides to control pathogens in the gastrointestinal tract [68].

In order to establish the kinetics of the early cytokine responses by *C. rodentium* infected Wt mice in our facility, we analyzed colonic tissue of challenged Wt mice at

different time points: day 1-3, day 4, day 8 and day 12 post infection. Real-time PCR analysis of the colon of the infected mice revealed that IL12p19, i.e. IL-23-specific subunit transcripts, were upregulated on day 3 and 12 **(Fig 2a**), IL12p35, the IL-12-specific subunit transcripts, were induced on day 6. IL22 transcripts were upregulated on day 4 and 8 with a lag to IL-23, but downregulated by day 12. Peak expression of the anti-microbial peptide RegIIIβ and the anti microbial proteins S100A9 and A100A8 occurred at day 8, i.e. with a delay to IL22. The same was observed for IL-17A, an indicator of active Th17 cells. Expression of IL12p40, the cytokine subunit shared by IL12 and IL23 was upregulated on day 3 and 12, IL-6 and IL-10 were found expressed only at day 12 **(Fig 2b, Summary Table 1)**. The distinct dynamics of the IL-22 and IL-6, as well as IL-10 are indicative of the existence of a previously reported early and late host defense response.

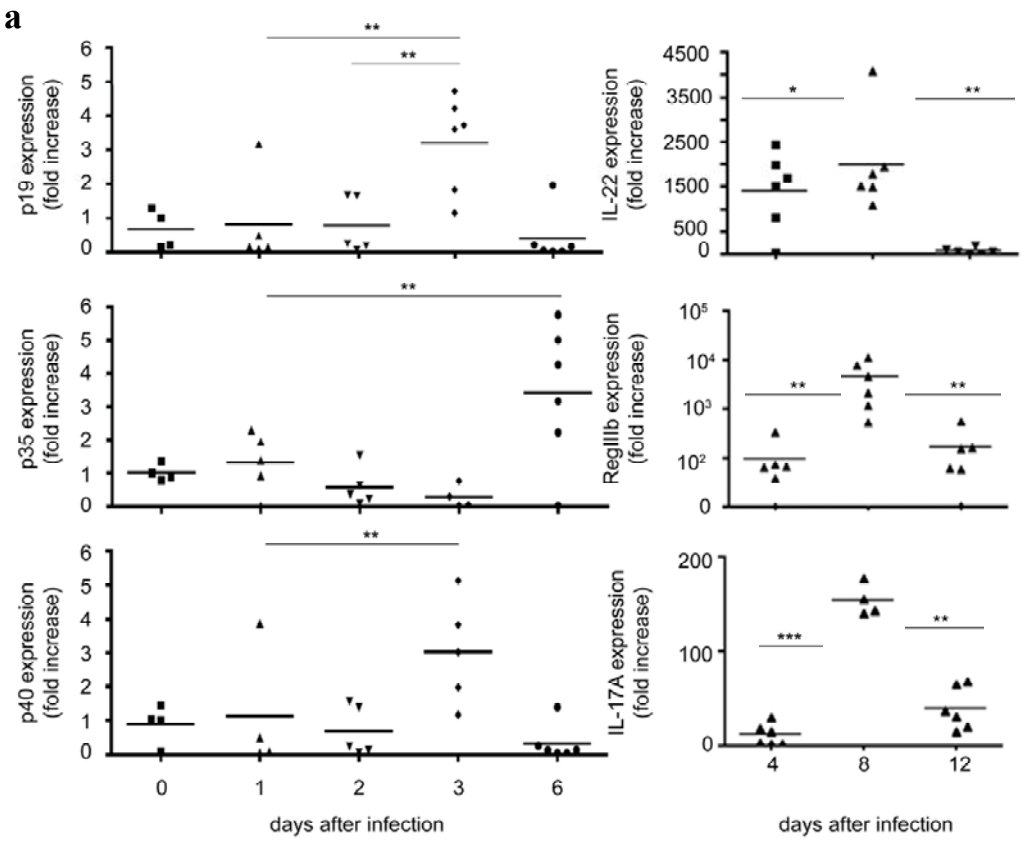

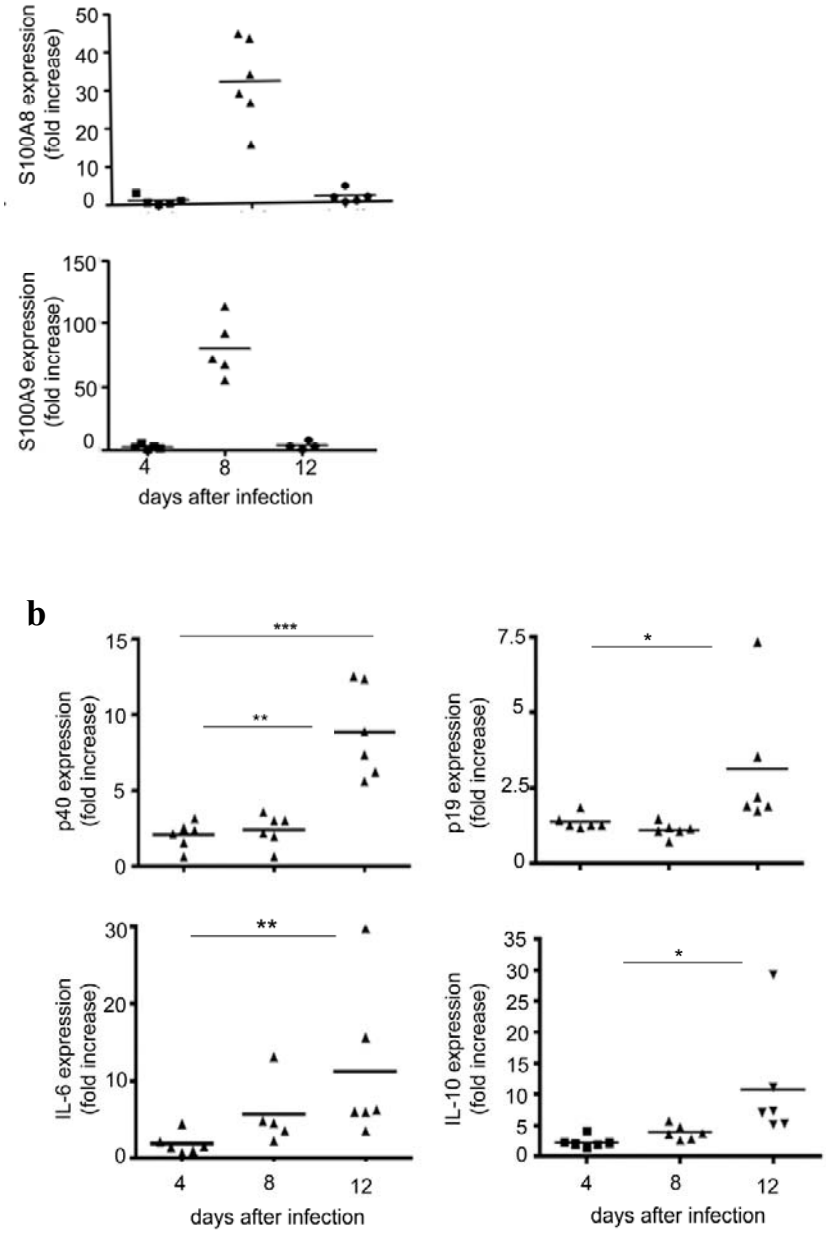

Figure 2: Cytokine dynamics during the early host response to *C. rodentium* infection in Wt mice. Mice were infected with ≈10^8−10^9 CFU of *C. rodentium* by gavage and a time-course RT-PCR analysis of infected colonic tissue (a) was performed. IL23p19 was upregulated on day 3, IL12p35 was upregulated on day 6. IL22 was found upregulated on day 4 and day 8, waning by day 12. IL-17A , RegIIIβ ,S100A9 and

S100A8 were found upregulated on day 8 (n=6). (b) late host defense as represented by IL-23p19, IL-12/23p40, IL-6 and IL-10 up-regulated on day 12 (n=6). Statistics were done by using one way Anova and Tukey as apost hoc. Asterisk P<0.05, two asterisks P<0.01, three asterisks P<0.001.

Table 1: Summary of cytokine production kinetics (m-RNA) in WT mice.

DAY	3	4	6	8	12
IL-23p19	++++	-	-	-	++
IL-12p35	-	-	+++	ND	ND
IL-23/12p40	++++	-	-	-	++
IL-22	ND	++	ND	++++	+
IL-17	ND	+	ND	++++	++
RegIIIβ	ND	++	ND	++++	++
S100A9	ND	+	ND	++++	+
S100A8	ND	+	ND	++++	+
IL-6	ND	+	ND	+	++
IL-10	ND	+	ND	+	++

4.3. IL-23 production by hematopoietic cells is necessary to survive a *C. rodentium* infection.

The key role of IL-23 in the pathogenesis of autoimmune and chronic inflammatory disorders is supported by the identification of IL-23R susceptibility alleles associated with inflammatory bowel disease (IBD), psoriasis and ankylosing spondylitis. IL-23-driven inflammation has been linked to the actions of Th17 cells [65]. To determine the source of IL-23 and specifically ask, whether the IL-23 protecting against the *C. rodentium* challenge is derived from hematopoietic cells, we generated chimeric mice by transplanting bone marrow (BM) of mice deficient for the IL-23 subunit p19 (p19-/-) into lethally irradiated Wt mice. As control we included p40-/- mice that lack the shared subunit of IL-12 and IL-23 and are known to succumb to *C. rodentium* infection.

In support of a critical role of IL-23 in the early response, [p19-/- > wt] BM

chimeras succumbed to the *C. rodentium* challenge, although only by day 12, whereas [wt > wt] BM chimeras mice recovered from the infection.

This establishes that hematopoietic IL-23 is necessary for the animals to survive the *C. rodentium* infection. Interestingly and unlike IL-12/23p40-/- mice [IL-12/23p40-/- > wt] BM chimeras survived the *C. rodentium* infection (**Fig. 3a**) establishing that the additional impairment of IL-12 production by hematopoietic cells can rescue IL23-deficient [IL-23 p19-/- > wt] BM chimeras.

In order to investigate whether the IL-23 is required for the early induction of IL-22 is derived from hematopoietic cells we analyzed [IL-12/23p40-/- > wt] and [IL-23 p19-/- > wt] chimeras for IL-22 production. Both mice displayed significant reductions of IL-22 transcript when compared to infected wt chimeras (**Fig. 3b)**. In addition mice that lacked IL-23 and mice that lacked IL-12/23 exhibited a reduction of the IL-22 induced RegIIIβ (**Fig. 3b)**.

Collectively, these results establish that hematopoietic IL-23 is responsible for IL-22 production, which in turn induces epithelial expression of the anti-microbial protein RegIIIβ.

To determine whether the BM chimeras that have p19 and p40 deficiencies succumb to the infection because of an overwhelming pathogen burden, we assessed *in vivo* bacterial loads using the bioluminescent *C. rodentium* strain. As shown in **Fig. 3c** and **Fig. 3e,** the signal emanating from the infected BM chimeras at day 7 was localized to the distal colon in all the chimeras. A more intense signal was emitted from the BM chimeras that lacked the IL-23 and IL-12/23 production, relative to BM chimeras that had a wt immune system **(Fig. 3c,e).** These findings suggest that IL-23 plays a role in controlling the *C. rodentium* burden. The increased bacterial load is however unlikely the death cause of the [p19-/- > wt] chimeras since it is shared with the [p40-/- > wt] mice surviving the infection. In addition, we observed reduced colon lengths in the chimeras with the IL-12/23 deficiency in comparison to the ones having the IL23 deficiency only, suggesting that the two mice might mount different responses to the pathogen.

Neutralization of IL-22 through treatment with IL-22–binding protein was reported to

suppress goblet cell reconstitution during the recovery phase of a DSS-induced acute colitis [48]. Histological analysis of colon tissue of *Citrobacter* challenged [p19-/- > wt] and [p40-/- > wt] BM chimeras revealed loss of goblet cells in chimeras that have deficiency in IL-23 and IL-23/12 in the hematopoietic compartment, with increased loss of enterocyte architecture in BM chimeras that lack IL-23 **(Fig. 3d, e)**.

Intradermal administration of IL-23 but not IL-12 into mouse skin initiates a TNF dependent, but IL-17A independent cascade of events resulting in psoriasis-like epidermal hyperplasia [69]**.** We observed reduced mucosal hyperplasia in chimeras that lack IL-23/12 and in chimeras that lack IL-23 **(Fig. 3d and e)** suggesting that IL-23 derived from hematopoietic cells leads among other outcomes to mucosal hyperplasia that protects the host from bacteria infiltration.

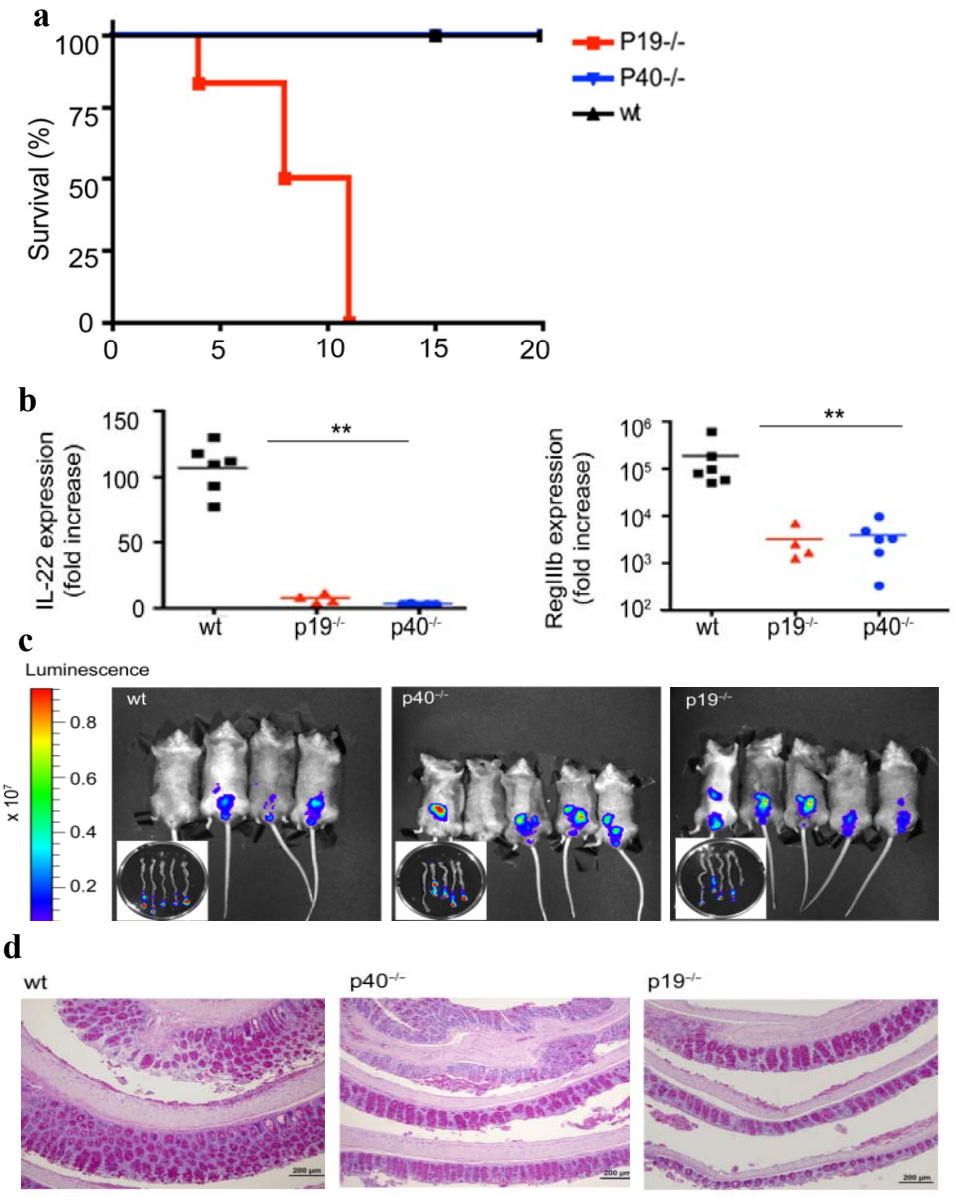
a
Survival (%)
100
75
50
25
0
0
5
10
15
20
P19-/-
P40-/-
wt
b
IL-22 expression (fold increase)
150
100
50
0
**
wt
p19-/-
p40-/-
RegIIIb expression (fold increase)
10^6
10^5
10^4
10^3
10^2
**
wt
p19-/-
p40-/-
c
Luminescence
x 10^7
0.8
0.6
0.4
0.2
wt
p40-/-
p19-/-
d
wt
p40-/-
p19-/-

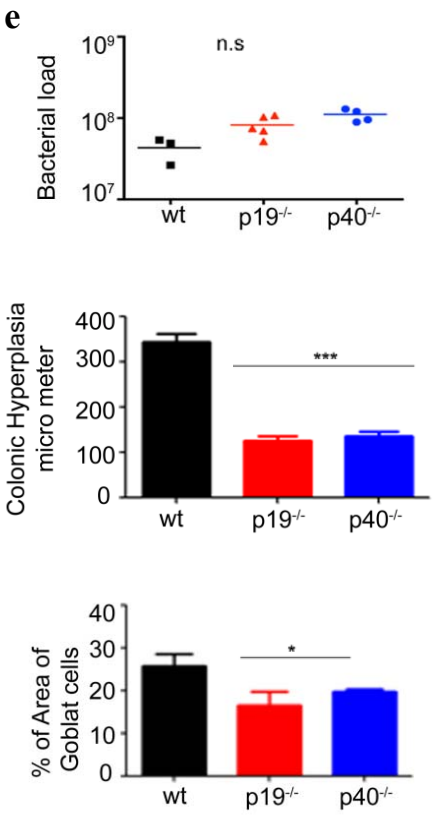

Figure 3: Mice with hematopoietic IL-23 deficiency succumb to *C. rodentium* infection. Mice were infected with ≈10^8–10^9 CFU of *C. rodentium* by gavage. (a) survival curves of $p40^{-/-}$ BM chimeras (n=6), $p19^{-/-}$ BM chimeras (n=6) and wt mice (n=6). Note that 100% of the $p19^{-/-}$ chimeras died by day 12. (b) Real-time PCR analysis IL-22 and RegIIIβ of colonic tissues collected on day 7 PI. $p19^{-/-}$ (n=6), $p40^{-/-}$ (n=6), WT (n=6). (c) bacterial load at day 7. Tissue distribution of the luminescent *C. rodentium* strain. Images were acquired with the IVIS system and are displayed as pseudocolour images of peak bioluminescence, with variations in color representing light intensity at a given location. Note that the group harboring $p19^{-/-}$ and $p40^{-/-}$ immune cells displayed the highest bacterial load. PAS staining illustrates (d-e) goblet cell deletion, loss of enterocyte architecture and decrease in mucosal hyperplasia in $p40^{-/-}$ BM and $p19^{-/-}$ BM chimeras. Statistics were done by using one way Anova and Tukey as apost hoc. Asterisk $P<0.05$, two asterisks $P<0.01$.

4.4 Intestinal CD11c expressing dendritic cells or MΦs are required for IL-23 production during the early phase of *C. rodentium* infection.

IL-22 and RegIIIβ production are known to be preceded by an early peak of IL-23 (p19) expression [42]. In order to investigate whether this IL-23 stems from mononuclear phagocytes, i.e. DCs or MΦs, we took advantage of CD11c-DTR mice that allow for the conditional ablation of these cells [70]. Specifically, we challenged diphtheria-toxin (DTx)-treated and untreated [CD11c-DTR > wt] BM chimeras with *C. rodentium* and analyzed their colonic tissue 8 days post infection. Real-Time PCR results revealed that absence CD11c+ cells resulted in the reduction of IL-22 and RegIIIβ expression (**Fig. 4 a**, **c)**. This supports the notion that DCs or MΦs produce the IL-23 required for the induction of these factors. In contrast expression of S100A9, a antimicrobial protein reported to be differentially expressed in IL-22 knockout mice compared to WT mice [45], was not affected by the loss of CD11c+ cells (**Fig. 4 b)**.

TH17 development and activation are dependent on the inflammatory cytokines IL-6 and IL-23. Furthermore, the homeostatic TH17 response to enteric microbiota [71] and the inflammatory TH17 response to *C. rodentium* [45,72] both require functional IL-6 *in vivo.* Lack of IL-6 production by hematopoietic cells was sufficient to markedly decrease the numbers of TH17 cells at 24 h after Salmonella enterica Serovar Typhimurium (SL1344) infection and 4 days after *C. rodentium* infection [50]. To find out whether MΦs or dendritic cells direct this IL-6 mediated host defense we analyzed colonic tissue of challenged CD11c-DTR chimeras 8 days post infection. Real-time PCR analysis revealed that IL-6 was not affected by the loss of $CD11c^+$ cells (**Fig. 4 d)**. Together, these results establish that $CD11c^+$ cells are critical for IL-23 production and the ensuing induction of IL-22, which in turn results in epithelial expression of the antimicrobial protein RegIIIβ. Furthermore, the antimicrobial S100A9 defense and the IL-6 mediated response of TH17 cells seem not to be orchestrated by MΦs or DCs.

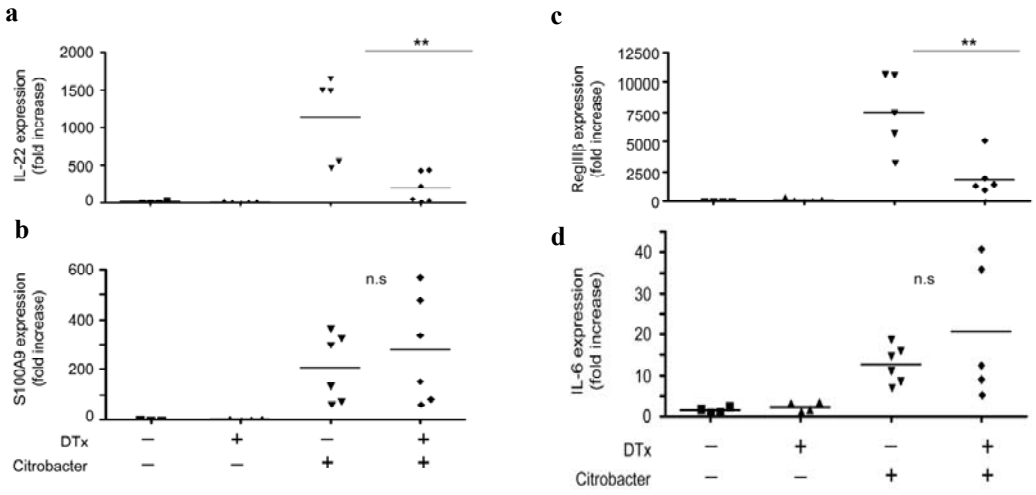

Figure 4: CD11c+ MΦs or DCs are required for IL-23 production and IL-22 and RegIIIβ induction during the early phase *C. rodentium* infection. [CD11c-DTR > WT] BM chimeras were infected with ≈10^8−10^9 CFU of *C. rodentium* by oral gavage. (a-d) Real-time PCR analysis IL-22, RegIIIβ, S100A9 and IL-6 of colonic tissues collected on day 8 PI. IL-22 and RegIIIβ was downregulated in *C. rodentium* infected and DTx treated mice (n=5-6), Statistics were done by using one way Anova and Tukey as apost hoc. Asterisk P<0.05, two asterisks P<0.01.

4.5. IL-23 production by DCs or MΦs is necessary to survive *C. rodentium* infection.

The observed death of the p19-/- BM chimeras (**Fig. 3)** could be due to absence of IL-23 expression by lymphoid or myeloid cells. To distinguish between these options and to further define the critical IL-23 source, we generated three groups of mixed BM chimeras through reconstitution of lethally irradiated Wt recipient mice with an equal mixture of CD11c-DTR (CD45.1) BM with p40-/- and p19-/- (CD45.2). As controls, we included mixed chimeras generated with CD11c-DTR (CD45.1) and Wt (CD45.2) BM.

DTR expression renders CD11c-expressing wt mononuclear phagocytes (CD45.1+) sensitive to DTx-induced cell ablation [70]. Upon DTx treatment, the respective

chimeras are hence left with only mutant mononuclear phagocytes [73]. The lymphocyte compartment of the animals will however still be composed of both wt and mutant cells.

Flow cytometric analysis of spleens and colon tissue of the BM chimeras revealed that mixed chimeras harbored sizable portions of CD11c+ cells derived from the respective mutant BM (CD45.2+). DTx injection specifically depleted DTR transgenic CD45.1+ DCs in the spleen (**Fig. 5a)** and the CD45.1 CD11c+ cells, including CD103+CD11b-/+ DCs and CX3CR1+ CD11b+ MΦs [11] in the colon **(Fig 5b).** As outlined above, in both cases CD11c+ cells left in the tissue are CD45.2+ cells mutant for the different genes. As early events of the *C. rodentium* infection are restricted to the intestinal lamina propria and IL-22R is specifically expressed by non-hematopoetic cells, such as epithelial tissue mediating epithelial innate immunity, our depletion strategy is well suited to study the local crosstalk between intestinal CD11c+ cells and colonic epithelial cells.

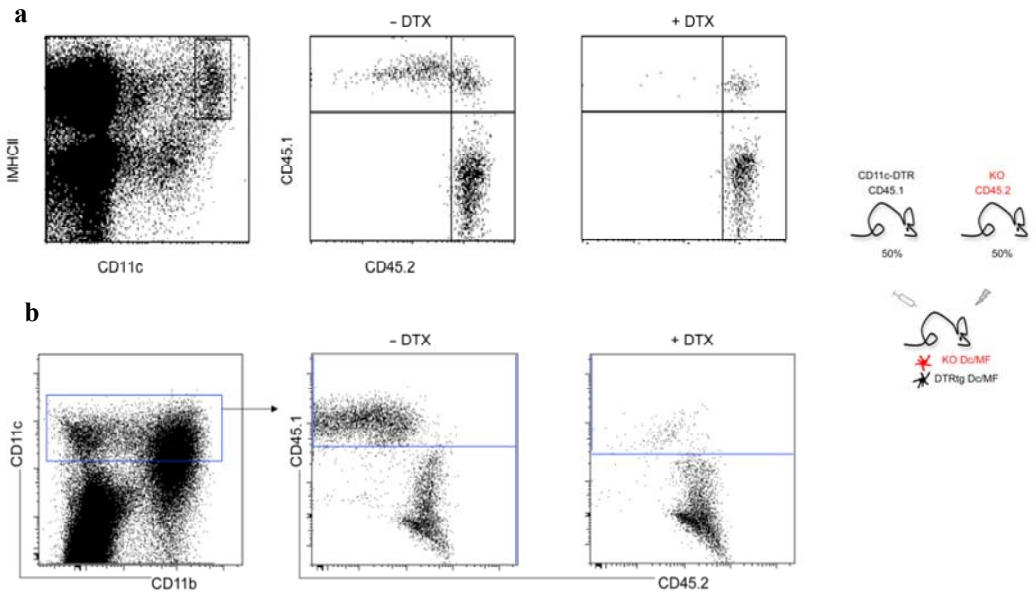

Figure 5: Conditional ablation of CD11c$^+$ cells in mixed BM chimeras. Flow cytometric analysis of cells isolated from mixed BM chimeras (a) spleen analysis of DTx-injected mouse (right) and control (left) showing the depletion on CD45.1$^+$ DTR transgenic DCs (b) Analysis of colon of DTx injected mouse (right) and control (left) showing the depletion of CD11c$^+$ CD45.1$^+$ DTR transgenic cells.

In order to analyze the contribution of DC/macrophage- derived IL-23 to the colonic immune defense, we challenged the various groups of mice (**Table 3**) with *C. rodentium* **(Fig. 6)** Infection of BM chimeras retaining only IL12/23 -deficient $CD11c^+$ cells survived the *C. rodentium* infection. In contrast, BM chimeras retaining IL-23-deficient $CD11c^+$ cells all died by day 8 **(Fig. 6a)**. Collectively these data establish that the critical IL23 source that ensures survival after *C. rodentium* infection are $CD11c^+$ lamina propria DCs or MΦs. Interestingly, and as observed in the complete BM chimeras, combined absence of IL-23 and IL-12 in the [$p40^{-/-}$ / CD11c-DTR > wt] chimeras improved survival.

Mice that lacked IL-23 or IL-12/23 producing $CD11c^+$ cells both displayed a significant reduction of IL-22 transcript when compared to wt chimeras as well as a reduction of the IL-22 induced RegIIIβ (**Fig. 6b)**.

Collectively, these results establish that critical DC or macrophage- derived IL-23 is responsible for the IL-22 production in response to the *Citrobacter* challenge, which in turn seems to directly induce epithelial expression of the antimicrobial protein RegIIIβ.

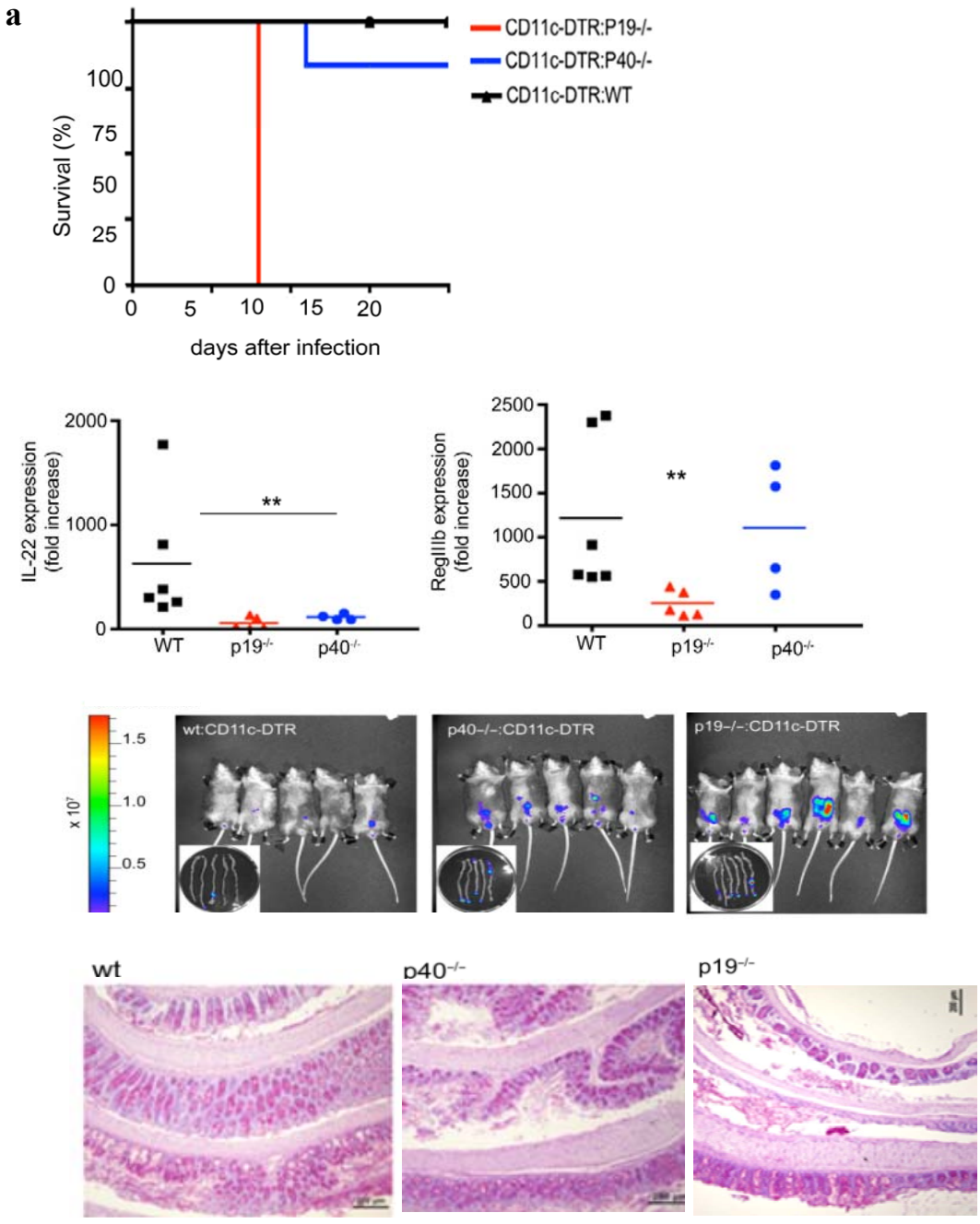
a
CD11c-DTR:P19-/-
CD11c-DTR:P40-/-
CD11c-DTR:WT
Survival (%)
100
75
50
25
0
0
5
10
15
20
days after infection
b
IL-22 expression (fold increase)
2000
1000
0
**
WT
p19-/-
p40-/-
RegIIIb expression (fold increase)
2500
2000
1500
1000
500
0
**
WT
p19-/-
p40-/-
c
x 10^7
1.5
1.0
0.5
wt:CD11c-DTR
p40-/-:CD11c-DTR
p19-/-:CD11c-DTR
d
wt
p40-/-
p19-/-

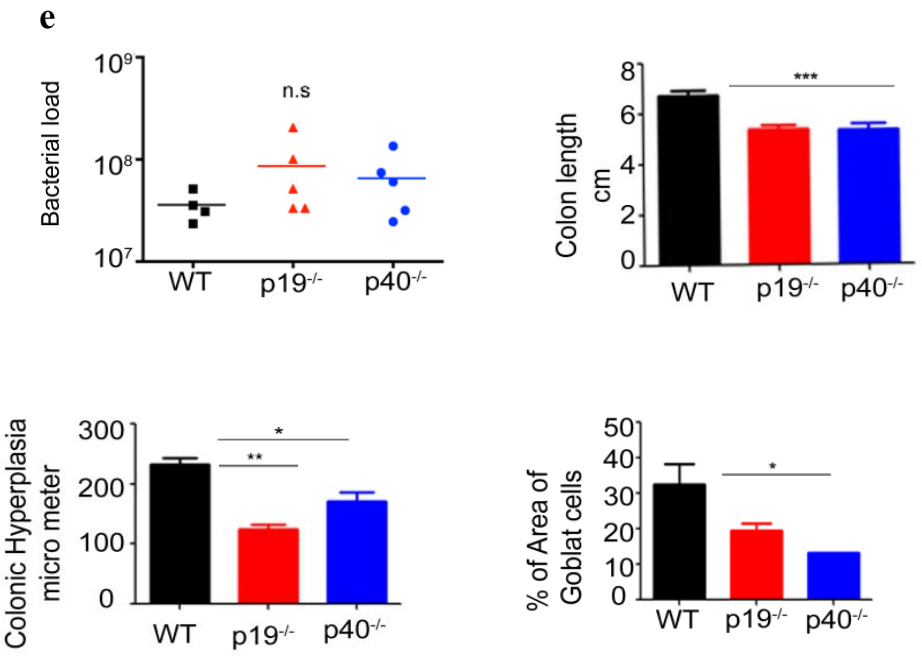

Figure 6: Crucial role of IL-23 produced by CD11c$^+$ lamina propria mononuclear phagocytes in early host defense against *C. rodentium*. Mice harboring a hematopoietic mixture of CD11c:DTR (CD45.1) and p19$^{-/-}$ and p40$^{-/-}$ cells were infected with ≈10^8–10^9 CFU *C. rodentium* by gavage . (a) Note that 100% of the p19$^{-/-}$ chimeras died by day 8. (b) Real-time PCR analysis of IL-22 and RegIIIβ expression in colonic tissues collected on day 7 PI. p19$^{-/-}$ (n=6), p40$^{-/-}$ (n=6), WT (n=6). (c and e) bacterial load at day 7. Tissue distribution of the luminescent *C. rodentium* strain. Images were acquired with the IVIS system. The group harboring mixture of CD11c:DTR (CD45.1) and p19$^{-/-}$and p40$^{-/-}$ cells displayed the highest bacterial load. PAS staining illustrates (d and e) goblet cell deletion loss of Enterocytes architecture and decrease in mucosal hyperplasia in p40$^{-/-}$ BM and p19$^{-/-}$ BM chimeras. Statistics were done by using one way Anova and Tukey as apost hoc. Asterisk P<0.05, two asterisks P<0.01.

We measured bacterial loads *in vivo* using the bioluminescent *C. rodentium* at day 7 to examine the option that the BM chimeras harboring IL-23 deficient DCs and MΦs give in to the infection because of their pathogen load. BM chimeras with IL-23 and IL-12/23 deficient DCs and MΦs had higher bacterial colonization in the distal colon when compared to chimeras with wt DCs or MΦs **(Fig. 6c and e)** suggesting that bacterial burden is indeed controlled by IL-23 produced by DCs or MΦs. Increased bacterial numbers are however unlikely to be the cause of death because they are observed in both chimeras.

Additionally, we observed a reduction in colon length in the chimeras that have IL-12/23 and IL-23 deficient DCs and ΦMΦs in comparison to controls.

Histological analysis revealed loss of goblet cells in chimeras that have deficiency in IL-23 and IL-23/12 in DCs and MΦs, with increased loss enterocytes architecture in BM chimeras harboring the IL-23 deficiency only MΦs**(Fig. 3d, e)**.

Analysis of chimeras that lack IL-23/12 and IL-23 **(Fig. 3d, e)** suggested that this deficiency also leads to mucosal hyperplasia that might protect the host from bacteria infiltration. Together, these results indicate that the critical DC and MΦ derived IL-23 is responsible to the host defense against C. *rodentium* by means of antimicrobial production and maintenance of the epithelial border integrity.

4.6. IL-23 production by MΦs is necessary to survive a *C. rodentium* infection.

The death of the *Citrobacter*-challenged DTx treated [CD11c-DTR / $p19^{-/-}$ > wt] BM chimeras (**Fig. 6)** could be explained by the absence of IL-23 expression from DCs or MΦs. To differentiate between these possibilities, we took advantage of a new mouse strain generated by Simon Yona in our laboratory (Yona et al, *Immunity 2013*). These CX_3CR1^{Cre} mice exploit the prominent activity of the CX_3CR1 promoter in the mononuclear phagocyte system for the genetic manipulation of CX_3CR1^+ monocytes, MΦs and DCs. When crossed to R26-YFP mice or R26-DTR (iDTR) mice, these animals allow the visualization or ablation of CX_3CR1^+ intestinal MΦs, respectively.

4.6.1 Analysis of Mononuclear Phagocytes and Myeloid Precursors in CX_3CR1^{Cre}:R26-YFP and CX_3CR1:iDTR mice

The CX_3CR1 chemokine receptor is expressed in the first dedicated mononuclear phagocyte precursor, the MDP, and expression is maintained in DC-committed precursors (CDPs, preDCs), as well as monocytes. All these cell populations are hence consequently homogeneously marked by reporter gene expression in CX_3CR1^{gfp} mice (Yona et al, *Immunity 2013*). In order to characterize CX_3CR1-Cre expression in the mononuclear compartment for we performed a flow cytometric analysis of spleen and colon tissue of the CX_3CR1^{Cre}:R26-YFP mice. Analysis of classical DCs of CX_3CR1^{Cre}:R26-YFP

animals revealed that about 70% of CD4+ DCs, 60% of DN DCs and 30% of the CD8+ DCs expressed YFP in spleen **(Fig 7 a)**. Examination of the PDCs shows that more than 60% of the PDCs are labeled with YFP. In the intestine the majority of MΦs expressed YFP, as opposed to $CD11b^-$ DCs of which only 20% were YFP^+ in the colon and ileum. 60% of CD11b+ DCs that are mainly abundant in the Peyer's patches of the ileum expressed YFP **(Fig 7 b)**.

Next we analyzed BM chimeras generated with CX_3CR1^{Cre}:iDTR (in short CX_3CR1-DTR) BM before and after DTx treatment. FACS analysis of the myeloid precursors cells revealed that MDPs are ablated upon DTx injection and also 90% of CDPs were affected. However only 30% of the MPs are depleted in these chimeras **(Fig 8a)**. Assessment of the blood and BM myeloid cells revealed that 90% of the $Ly6C^{low}$ monocytes are depleted after DTx treatment. $Ly6C^{high}$ monocytes and Ly6G+ neutrophils in the blood were not affected **(Fig 8b)**. Analysis of the different DC populations of the spleen revealed that 90% of the CD4+ DCs were ablated and DN DCs were absent. On the other hand, only 20% of the CD8+ DCs were affected in the DTx-treated CX_3CR1:iDTR chimeras **(Fig 8c)**. Splenic DCs can be further subdivided according to the expression of the adhesion molecule ESAM (*L.Lewis et al Immunity 2011*). Using this marker we found that ESAM+CD11b+ DCs were 90% depleted, whereas CD11b+ESAM- DCs as well as CD11b-CD8+ESAM+ DCs were hardly affected (10-15%) **(Fig 8c lower panel)**. Analysis of intestinal tissues revealed that more than 90% of the colonic MΦs were ablated upon DTx injection of CX_3CR1:iDTR chimeras. $CD11b^-$ DCs were only partially affected (20%) - consistent with their reporter gene expression. $CD11b^+$ DCs, a cell population hardly discernable in the colon, were found ablated to 80% in these mice **(Fig 8d)**.

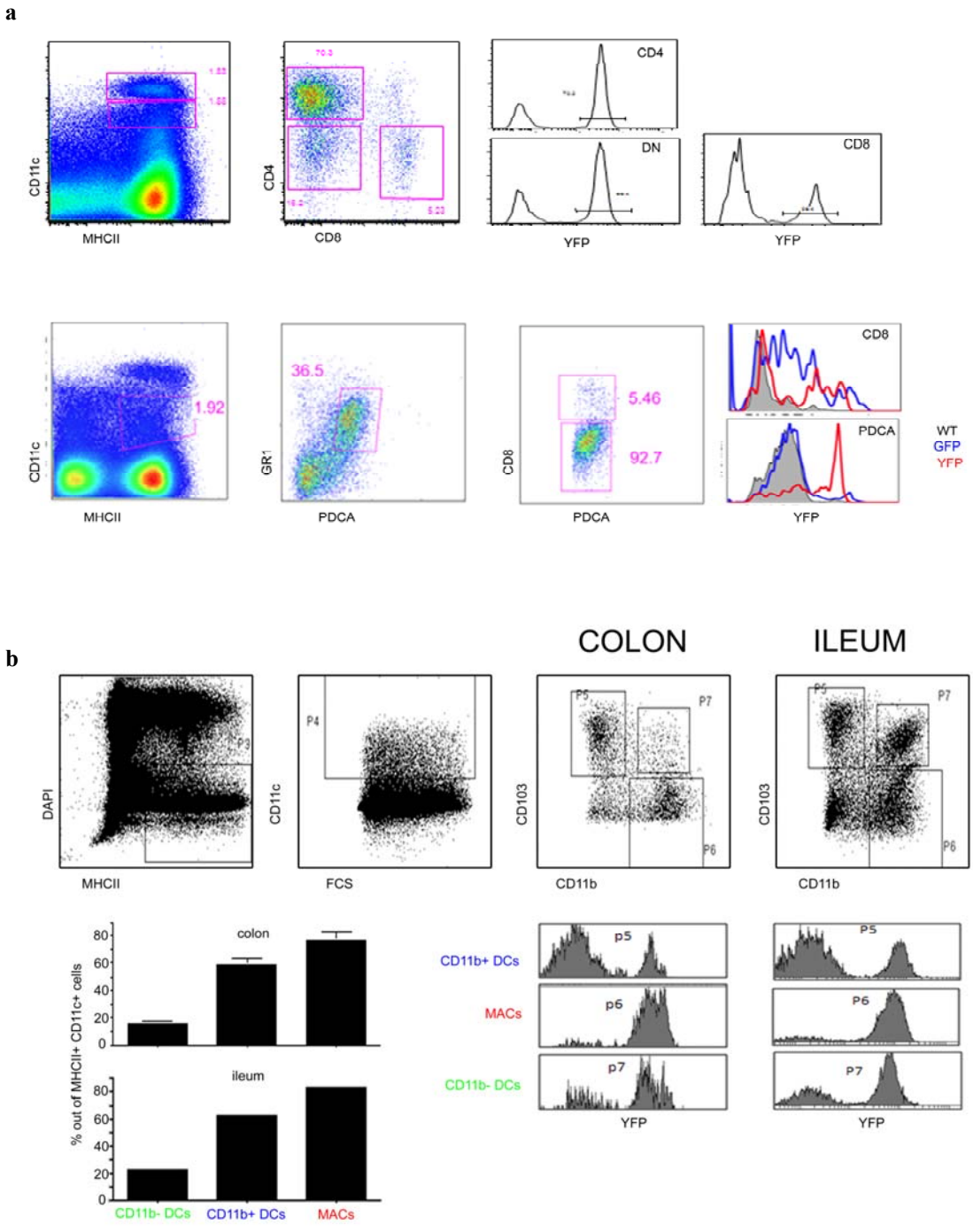

Figure 7: Analysis of Mononuclear Phagocytes and Myeloid precursors in CX_3CR1^{Cre}:R26-YFP BM

chimeras. Flow cytometric analysis of different mononuclear phagocyte population of $CX_3CR1^{Cre/+}$:R26-YFP mice (a-b). (a) Splenic DCs and PDCs (b) colonic and ileal DCs and MΦs.

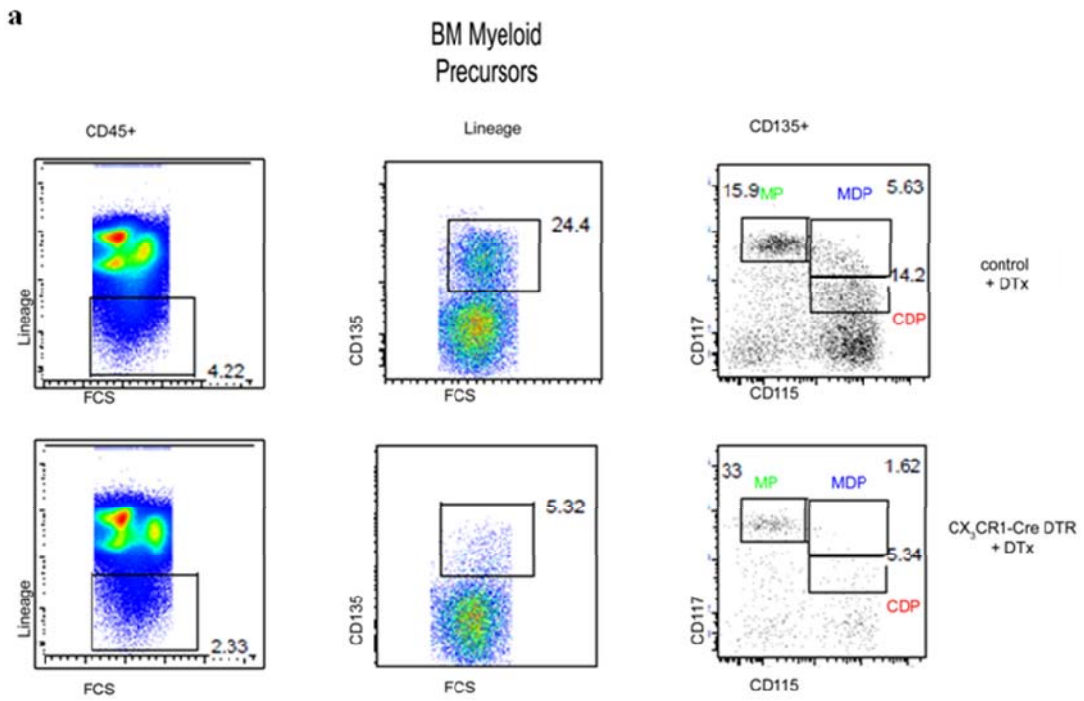

b

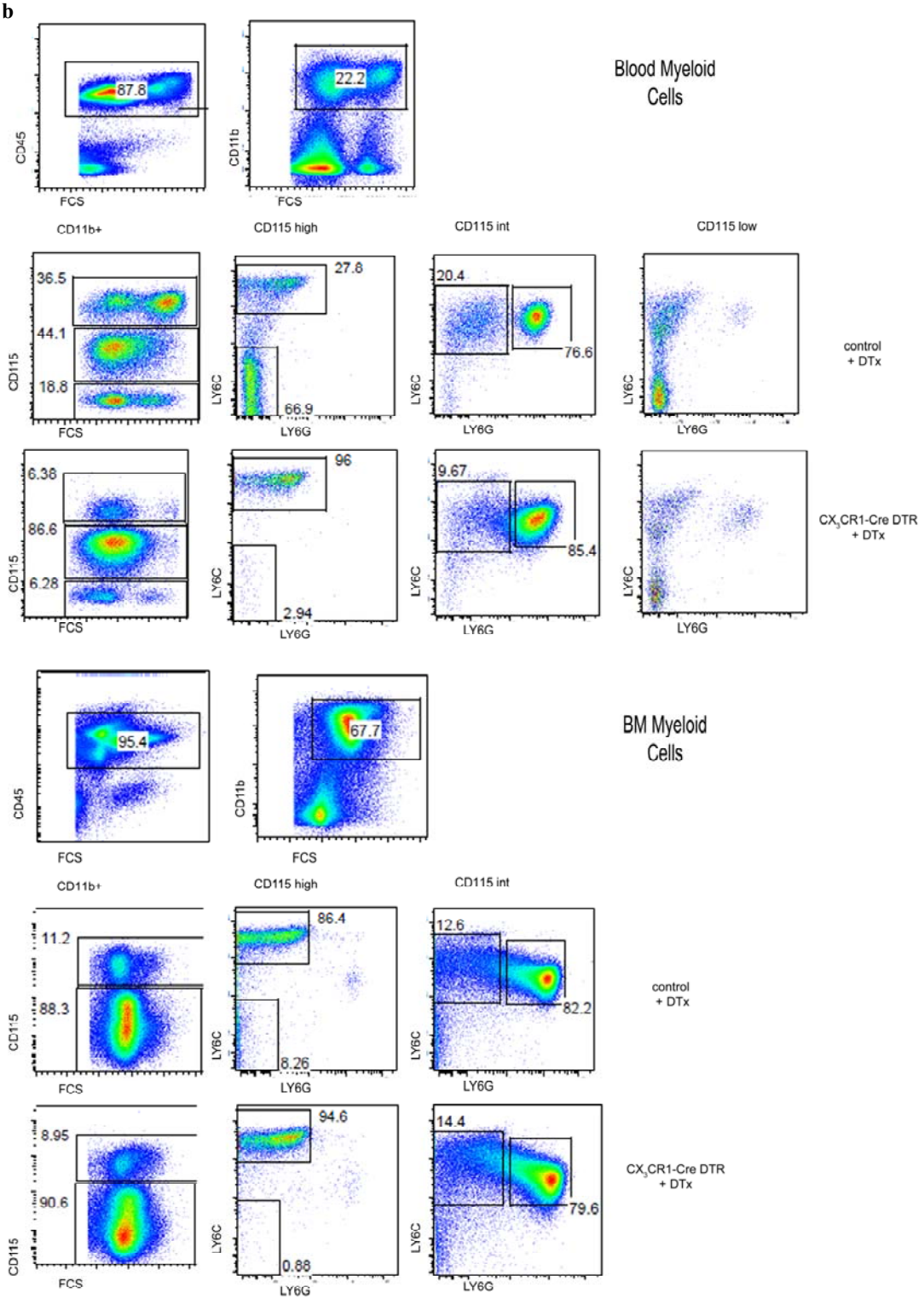
Blood Myeloid Cells
CD45
FCS
87.8
CD11b
22.2
CD11b+
CD115 high
CD115 int
CD115 low
CD115
36.5
44.1
18.8
LY6C
LY6G
27.8
66.9
20.4
76.6
control + DTx
6.38
86.6
6.28
96
2.94
9.67
85.4
CX3CR1-Cre DTR + DTx
BM Myeloid Cells
95.4
67.7
11.2
88.3
86.4
8.26
12.6
82.2
8.95
90.6
94.6
0.88
14.4
79.6

c

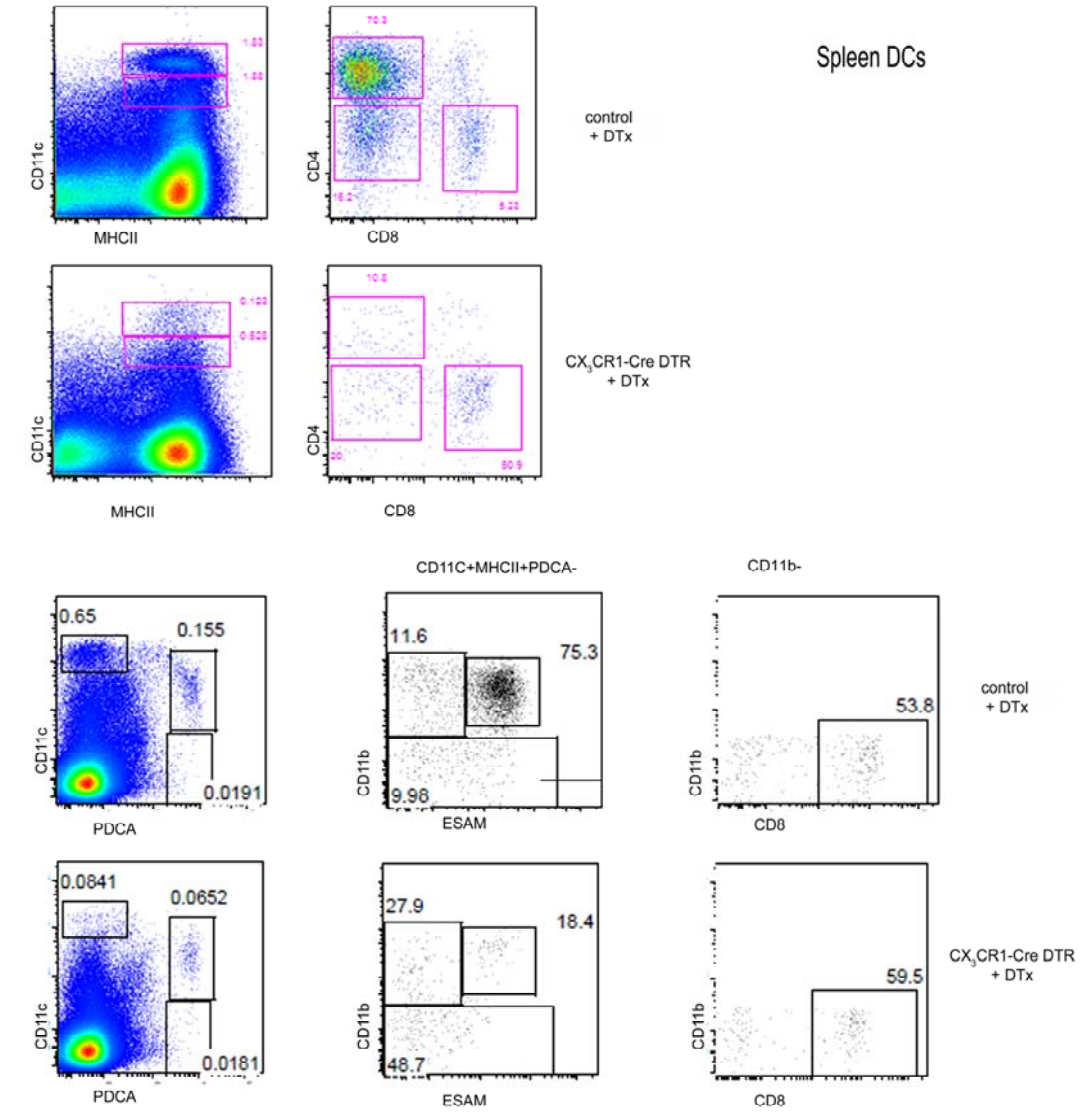
Spleen DCs
control
+ DTx
CX3CR1-Cre DTR
+ DTx
CD11c
MHCII
CD4
CD8
CD11C+MHCII+PDCA-
CD11b-
PDCA
ESAM
0.65
0.155
0.0191
11.6
75.3
9.98
53.8
0.0841
0.0652
0.0181
27.9
18.4
48.7
59.5

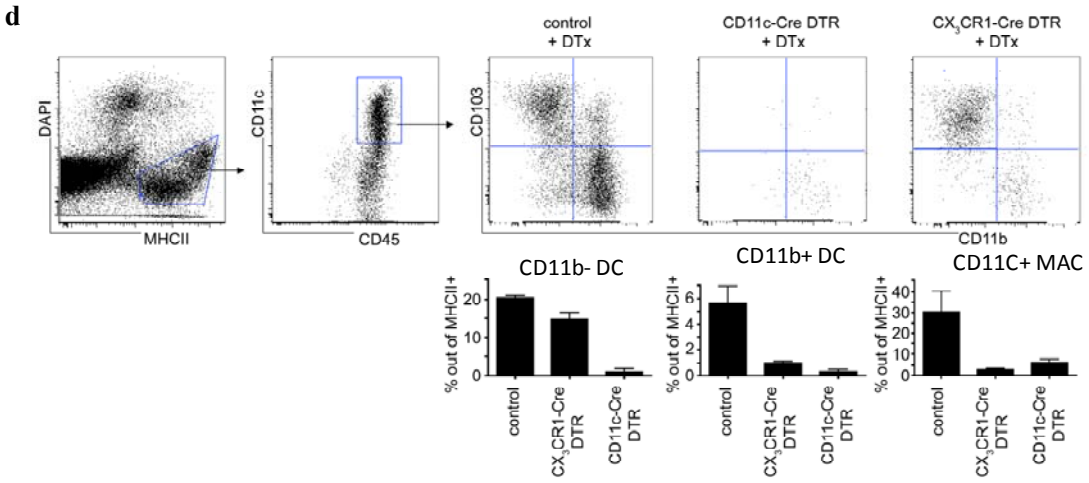

Figure 8: Analysis of Mononuclear Phagocytes and Myeloid precursors in CX_3CR1-DTR BM chimeras. Flow cytometric analysis of different myeloid precursor populations of CX_3CR1-DTR chimeras (a-d). Upper panels show control mice and lower panels show DTx-treated CX_3CR1-DTR chimeras(a). Myeloid precursors, MP, MDP and CDP (b) blood and BM myeloid cells (c)spleen DCs (d) colonic DCs and MΦs in the CX_3CR1-DTR and CD11c-DTR chimeras. Note that in the CD11c-DTR chimeras both DCs and MΦs are depleted as opposed to the macrophage-restricted depletion in CX_3CR1^{iDTR} chimeras (d).

The death of the $p19^{-/-}$ chimeras (**Fig. 6)** could result from the absence of IL-23 expression by DCs or MΦs. To address whether DCs or MΦs are the critical IL-23 source, we generated three groups of mixed BM chimeras through reconstitution of lethally irradiated Wt recipient mice with an equal mixture of CX_3CR1-DTR BM with $p40^{-/-}$ and $p19^{-/-}$ BM. As controls, we included mixed chimeras of CX_3CR1-DTR and Wt BM.

In order to analyze the contribution of MΦ-derived IL-23 to the colonic immune defense, we challenged the groups with *C. rodentium* **(Fig. 9)** Infection of BM chimeras that specifically lacked IL-23 in MΦs died by day 10-12 after *C. rodentium* infection. **(Fig. 9a)**. Interestingly, chimeras that specifically lacked p40 in their MΦs died by day 8-10. These data establish that the critical IL-23 source that ensures survival after *C. rodentium* infection are MΦs.

Mice harboring both IL-23 and IL-12 deficient MΦs displayed a considerable reduction of IL-22 and RegIIIβ transcripts when compared to wt chimeras. However we

observed significantly lower amounts of IL-22 in the chimeras retaining IL-12/23 deficient MΦs (**Fig. 9b)**.

Collectively, these results establish that MΦ derived IL-23 is responsible for IL-22 production, which elicits epithelial expression of the anti-microbial protein RegIIIβ.

To find out whether the BM chimeras that have a MΦ- restricted IL-23 deficiency surrender to the infection because of increased pathogen burdens, we assessed *in vivo* bacterial loads. As shown in **Fig. 9c**, the bioluminescent signal emanating from *C. rodentium* infected BM chimeras at day 8 was strong in BM chimeras that lacked IL-23 or IL-12/23 in MΦ, in comparison to controls. Surprisingly mice harboring IL-12/23 deficient MΦs harbored more bacteria than mice with the IL-23 deficiency. These findings suggest that MΦ- derived IL-23 is critical for the control of the *C. rodentium* burden.

Histological analysis revealed loss of goblet cells in chimeras that have a IL-23/12 deficiency in MΦs exhibited extensive depletion of goblet cells when compared to wt or the IL-23 only deficiency. However increased loss enterocytes architecture was observed only in BM chimeras that harbored IL-23-deficient MΦs.

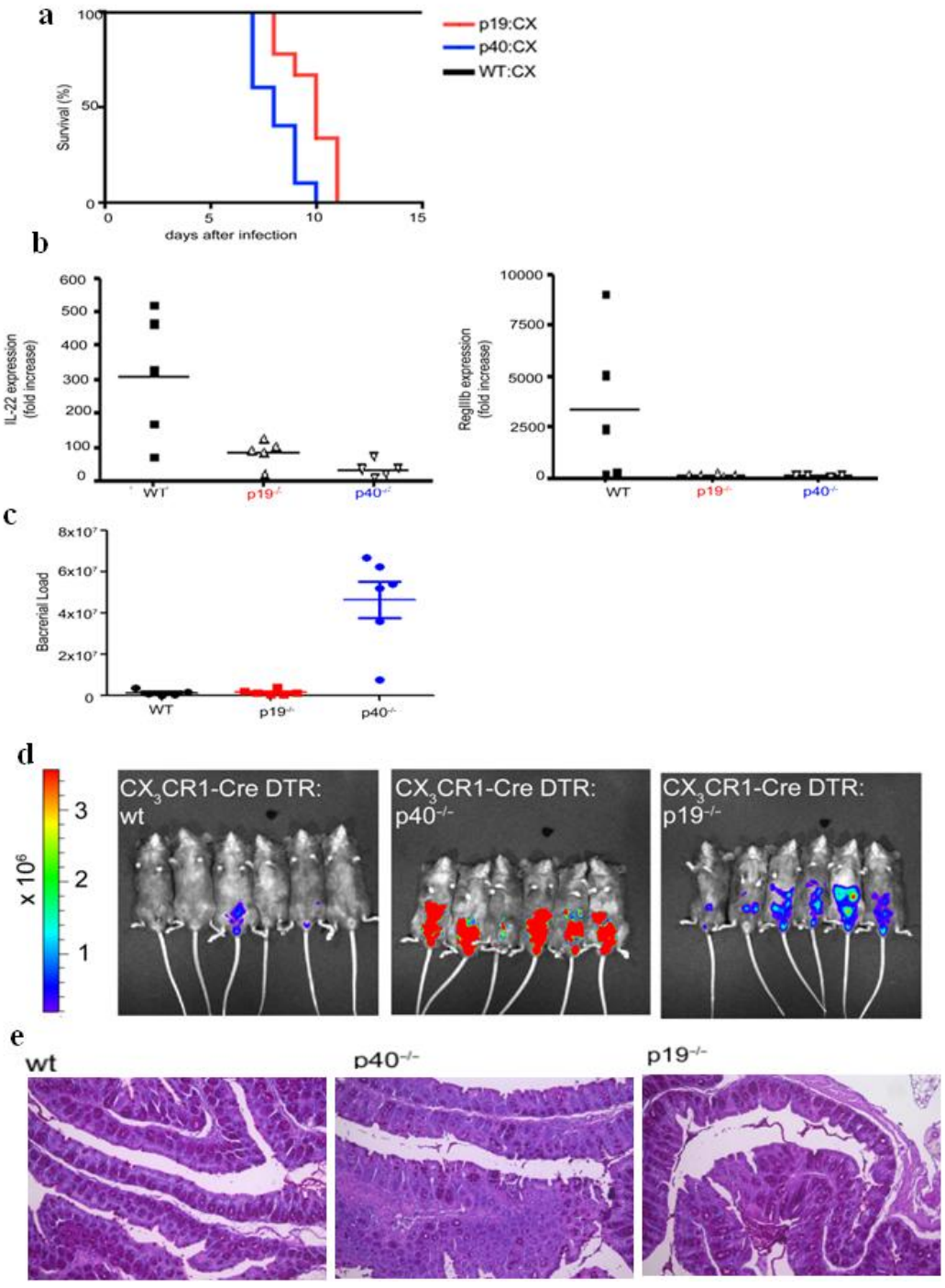
a
Survival (%)
days after infection
p19:CX
p40:CX
WT:CX
b
IL-22 expression (fold increase)
Reglllb expression (fold increase)
WT
p19-/-
p40-/-
c
Bacrerial Load
d
CX3CR1-Cre DTR: wt
CX3CR1-Cre DTR: p40-/-
CX3CR1-Cre DTR: p19-/-
x 10^6
e
wt
p40-/-
p19-/-

Figure 9: Crucial role of macrophage-derived IL-23 in the early host defense against *C. rodentium.* Mice harboring a hematopoietic mixture of CX_3CR1:iDTR and $p19^{-/-}$ or $p40^{-/-}$ cells were infected with $\approx 10^8 - 10^9$ CFU *C. rodentium* by gavage . (a) Note that 100% of the $p19^{-/-}$ and $p40^{-/-}$ chimeras died by day 10-12. (b) Real-time PCR analysis IL-22 and RegIIIβ of colonic tissues collected on day 8 PI. $p19^{-/-}$ (n=6), $p40^{-/-}$ (n=5), WT (n=6). (c) bacterial load at day 8. Tissue distribution of the luminescent *C. rodentium* strain. Images were acquired with the IVIS system. The group harboring mixture of CX_3CR1:iDTR $p19^{-/-}$ and $p40^{-/-}$ cells displayed the highest bacterial load. PAS staining illustrates (e) goblet cell deletion in $p40^{-/-}$ and loss of Enterocytes architecture $p19^{-/-}$ BM chimeras. Statistics were done using one way Anova and Tukey as apost hoc. Asterisk $P<0.05$, two asterisks $P<0.01$.

Collectively, these results indicate that MΦ-derived IL-23 is required for a protective host defense against C. *rodentium* by means of antimicrobial production and maintenance of the epithelial border integrity. Interestingly, mice harboring combined IL-12 and IL-23 deficiency in their MΦs displayed lower levels of IL-22 and had considerably higher bacterial burdens in comparison to mice harboring IL-23 deficient MΦs. This suggests that although both mice succumb to the infection, the cause of the death might differ.

4.6.2 Macrophage derived IL-23 cross-regulates IL-12 production by DCs.

To analyze which cells in the lamina propria express IL-23, IL-12 and IL-23R we performed a gene expression analysis by real-time RT-PCR on FACS sorted, purified cells **(Fig 10 a)**. The results corroborate the notion that $CD11c^+$ MΦs are the main source of IL-23, while the $CD103^+$ $CD11b^-$ DCs are a source of IL-12. Moreover, interestingly, $CD103^+CD11b^-$ DCs upregulated expression of the IL-23 receptor in response to *C. rodentium* infection **(Fig 10 b)**. This led us to examine the direct impact of macrophage-derived IL-23 on IL-12 production by DCs. We sorted $CD103^+$ $CD11b^-$ DCs from mice harboring IL-23 deficient MΦs and compared cells isolated from wt mice. In the absence of IL-23 in MΦs, DCs upregulated the expression of IL-12 and IL-23R. Thus DCs can potentially sense sense macrophage-derived IL-23 and respond by reducing IL-12 expression **(Fig 10 c)**. Such regulatory role of IL23 has previously been proposed (*Becker et al JI 2006*). Under the same condition we performed gene expression analysis of IL-12, IL-23 and IL-23R in FACS purified MΦs that lack IL-23 expression and compared them to wt MΦs. We found that IL-12 expression was high in the wt MΦs, as well as in the IL-23 deficient MΦs. However MΦ- derived IL-23 did not downregulate MΦ- derived IL-

12 in an autocrine lop **(Fig 10 c)**. The high levels of MΦs derived IL-12 in mice that have wt MΦs did not cause the death of the mice, in contrast mice that have elevated levels of DC-derived IL-12 in absence of MΦ-derived IL-23 suffered rapid death **(Fig 9 a)**. In addition,MΦs sorted from mice that are depleted of their wt MΦ exhibit significant reduction of IL-23 in comparison to MΦ that were sorted form mice harboring wt MΦ. Once again we were able to show that our system is highly specific to MΦ depletion and even more than that to IL-23 depletion in the MΦ compartment.

Together these results point out that MΦ-derived IL-23 can cross regulate DC derived IL-12 lading to the protection of the mice from lethality.

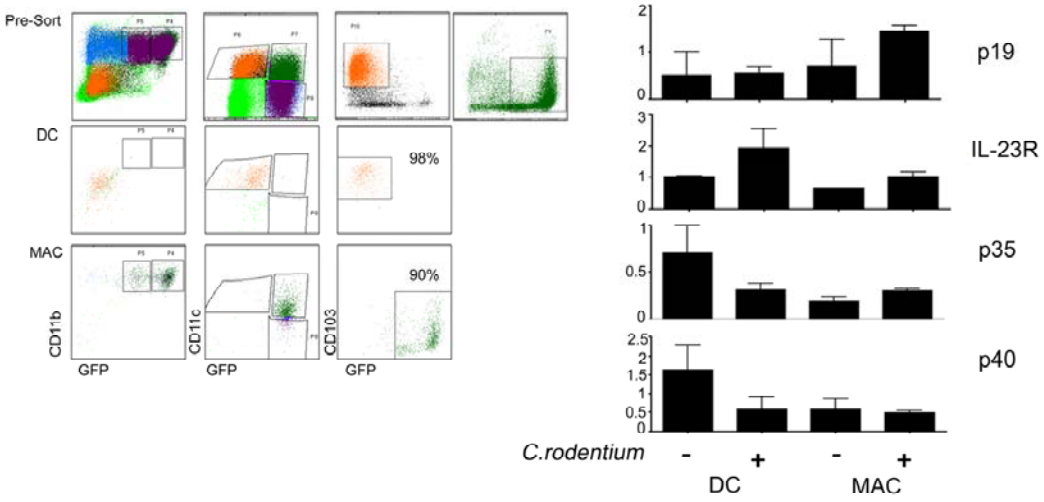
Pre-Sort
DC
MAC
CD11b
CD11c
CD103
GFP
98%
90%
p19
IL-23R
p35
p40
C.rodentium
DC
MAC

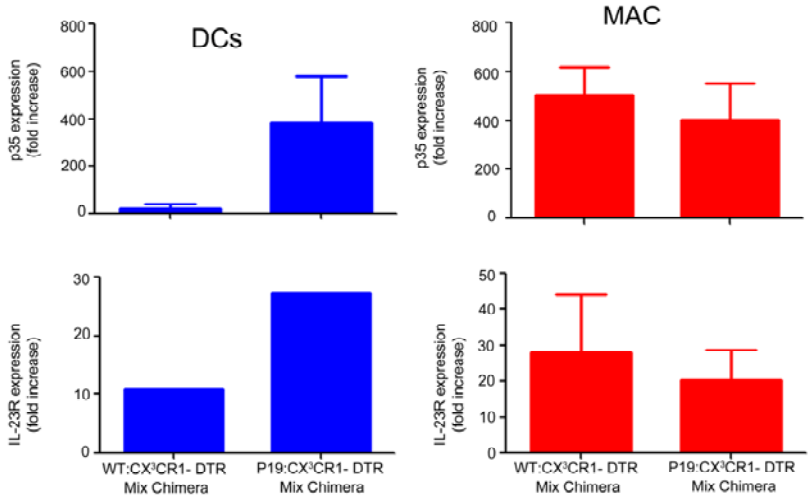
DCs
MAC
p35 expression (fold increase)
IL-23R expression (fold increase)
WT:CX3CR1- DTR Mix Chimera
P19:CX3CR1- DTR Mix Chimera

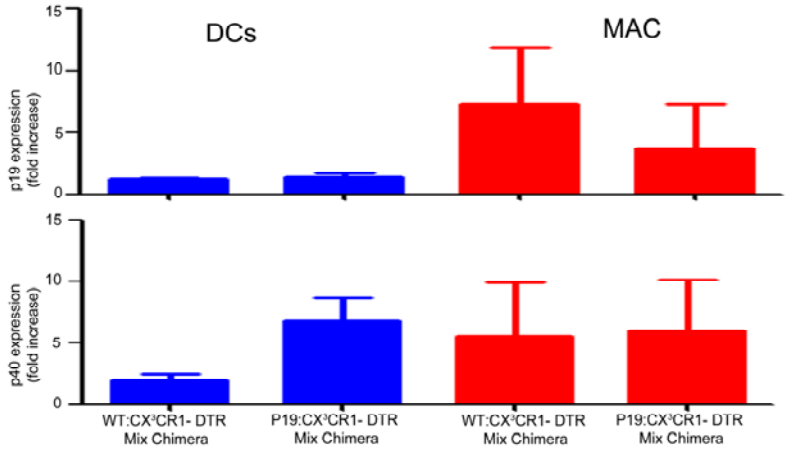
DCs
MAC
p19 expression (fold increase)
p40 expression (fold increase)
WT:CX3CR1- DTR Mix Chimera
P19:CX3CR1- DTR Mix Chimera

Figure 10: Production of IL-23 IL-12 and IL-23R in sorted cells from *C. rodentium* infected CX3CR1$^{+/gfp}$ mice. Mice were infected with ≈10^8–10^9 CFU of *C. rodentium* by gavage for three days. (a) Flow cytometric strategy for the sorting of CD103+ CD11c+ CD11b- CX3CR1- DCs and CD103- CD11c+ CX3CR1+ MΦs**,** pre and Post-sorting analysis. Data are representative of two experiments with lpDCs and lpMΦs pooled from 7-9 mice (b) RT-PCR analysis of lpDCs and lpMΦs was performed. IL-23p19 was found up regulated in lpMΦs. IL-12p35 and IL-23R were upregulated in lpDCs.(c) CD103+ CD11c+ CD11b- and CD103- CD11c+ CD11b+ MΦs were sorted from DTx treated WT:CX_3CR1-DTR and p19$^{-/-}$:CX_3CR1-DTR mixed chimeras,IL-12p35 and IL-23R were upregulated in DCs sorted from p19$^{-/-}$:CX_3CR1-DTR chimeras.IL-23p19 was down regulated in the MΦs sorted from p19$^{-/-}$:CX_3CR1-DTR mixed chimeras. Data were obtained from two independent experiments with lpDCs and lpMΦs pooled from 9-11 chimeras.

4.7 IL-12 secreted by CD103$^+$ DCs drives uncontrolled INF-γ production causing severe immunopathology.

IL-12 promotes the polarization of naïve T cells to TH1 cells and induces secretion of interferon-γ (IFNγ) from CD4$^+$ and CD8$^+$ T cells, as well as NK cells.

In order to evaluate whether IL-12 might trigger a TH1 response during *C. rodentium* infection, we analyzed tissue of the DTx-treated and infected groups of CX_3CR1:iDTR mixed BM chimeras for the presence of IL-12, IFNγ and IL-17A transcripts.

Mice that specifically lacked IL-23 in their MΦs displayed a significant increase of IL-12 transcripts, when compared to infected Wt or p40$^{-/-}$ chimeras **(Fig. 11a)**. In stark contrast, absence of both IL-12 and IL-23 from intestinal MΦs [p40$^{-/-}$ /CX_3CR1-iDTR > wt] animals did not result in an increase of IL-12 transcripts. Interestingly and in accordance with the observed upregulation of IL-12, the animals also displayed a rise in IFNγ transcripts **(Fig. 11a)**. IL-17A transcripts remained at the same level of expression in [p40$^{-/-}$ / CX_3CR1:iDTR > wt] and [p19$^{-/-}$ / CX_3CR1:iDTR > wt] chimeras **(Fig. 11a)**. Our results suggest that in an IL-23 deficient environment, IL-12 secreted by CD103$^+$ DCs drives uncontrolled IFN-γ production potentially causing immunopathology.

IFN-γ-dependent small intestinal pathology and dysfunction play a significant role in the lethality of super antigen exotoxins induced of Toxic shock syndrome (TSS) [74]. Therefore, we investigated whether in vivo neutralization of IFN-γ improves survival rates of mice inoculated with *C. rodentium* that lack MΦs or DC-derived IL-23 or only MΦs -derived IL-23 **(Fig. 11b**, **c).** We injected IFNγ neutralizing antibody to [p19$^{-/-}$ / CD11c-DTR > wt] and [p19$^{-/-}$ / CX_3CR1:iDTR > wt] chimeras; controls were injected

with isotype control and PBS. Neutralization of IFNγ prevented the immunopathology **(Fig.11b, c)**. IFNγ seems hence to drive the immunopathology in infected mice that have a specific deficiency of IL-23 in their MΦs. Since DC-derived IL-12 leads to upregulation of IFNγ, we hypothesized that direct neutralization of this compound will result in preventing the immunopathology upstream to IFNγ. To test this hypothesis p40 neutralizing antibody was administered to [$p19^{-/-}$ / CD11c-DTR > wt] and [$p19^{-/-}$ / CX_3CR1:iDTR > wt] chimeras **(Fig.11b, c)**. As expected neutralization of IL-12 protected mice from lethality further strengthening the notion that DC-derived IL-12 causes the IFNγ-mediated pathology.

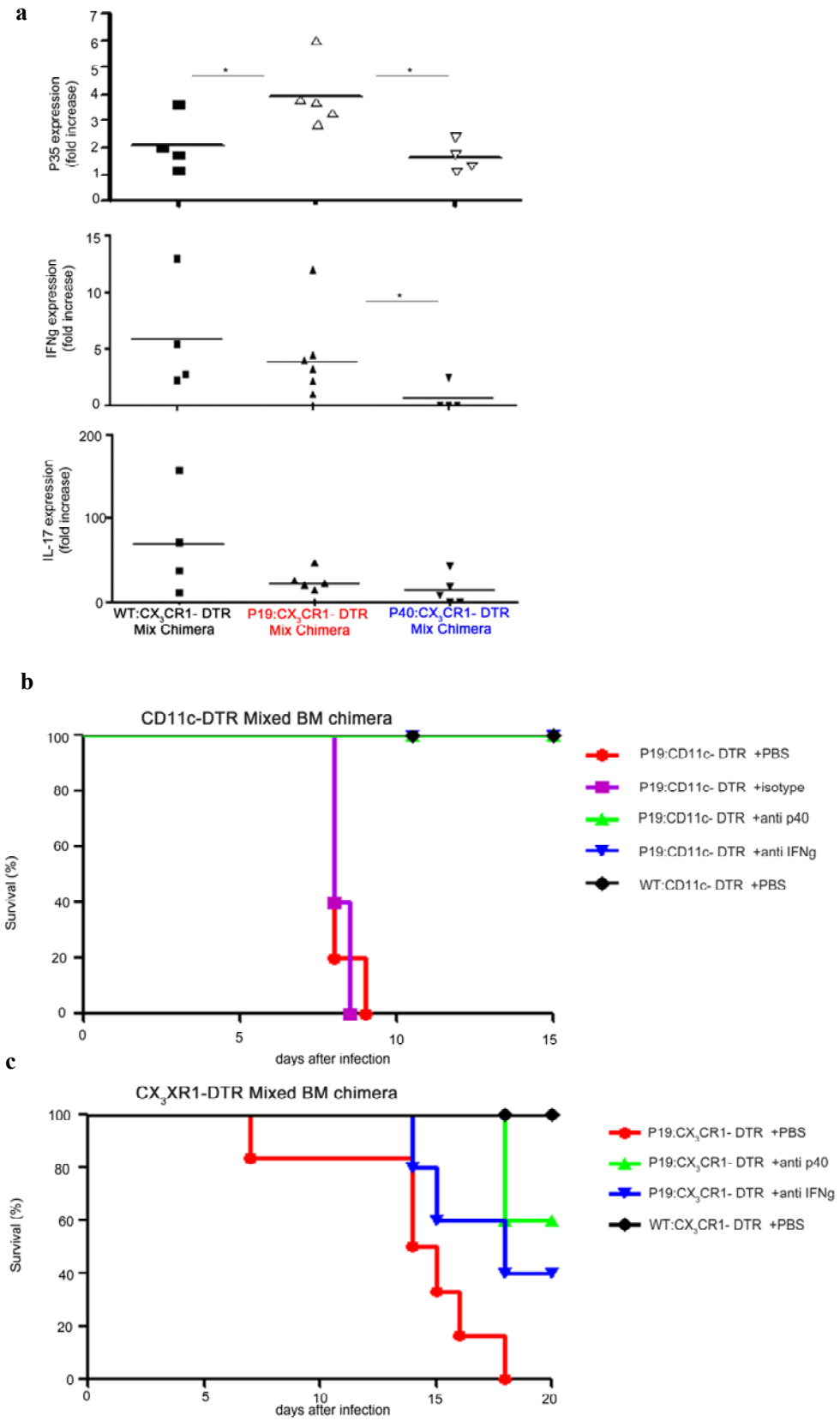
a
P35 expression (fold increase)
IFNg expression (fold increase)
IL-17 expression (fold increase)
WT:CX3CR1- DTR Mix Chimera
P19:CX3CR1- DTR Mix Chimera
P40:CX3CR1- DTR Mix Chimera
b
CD11c-DTR Mixed BM chimera
Survival (%)
days after infection
P19:CD11c- DTR +PBS
P19:CD11c- DTR +isotype
P19:CD11c- DTR +anti p40
P19:CD11c- DTR +anti IFNg
WT:CD11c- DTR +PBS
c
CX3XR1-DTR Mixed BM chimera
Survival (%)
days after infection
P19:CX3CR1- DTR +PBS
P19:CX3CR1- DTR +anti p40
P19:CX3CR1- DTR +anti IFNg
WT:CX3CR1- DTR +PBS

Figure 11: IL-12 secreted by CD103^{+} DCs drives uncontrolled INF-γ production causing severe immunopathology. Mice harboring a hematopoietic mixture of CX_3CR1:iDTR and p19$^{-/-}$and p40$^{-/-}$ cells were infected with ≈10^8−10^9 CFU *C. rodentium* by gavage . (a) Real-time PCR analysis IL-p35, IFNγ and IL-17A of colonic tissues collected on day 8 PI. p19$^{-/-}$ (n=6), p40$^{-/-}$ (n=5), WT (n=6). (b) Mice harboring a hematopoietic mixture of CD11c:DTR and p19$^{-/-}$ were infected with *C. rodentium* by gavage . (b) One p19$^{-/-}$ group received the IFNγ-neutralizing antibody, a second group was injected with p40 neutralizing antibody. A control. a third group of p19$^{-/-}$ mice received isotype control and wt mixture was injected with PBS. (c) Mice with a hematopoietic mixture of CX_3CR1:iDTR and p19$^{-/-}$ were infected as well, a group of p19$^{-/-}$ mice received IFNγ neutralizing antibody, a second group was injected with p40 neutralizing antibody and as a control was injected with PBS. Mice were monitored for survival. Note that in both cases IFNγ and p40 neutralizing antibody rescued the mice. Data are representative of two-three independent experiments each comprising 6-7 mice per group.

4.8 Th17 plasticity and acquisition of IFN-γ production

Recent studies indicate that Th17 cells retain plasticity and can acquire IFN-γ production that has been linked to their pathogenicity in vivo in EAE [75]. Th17 cells express the IL-23R, which is under control of the Th17 master regulator ROR-γt [76].

In order to evaluate whether DC-derived IL-12 **(Fig 11a, Fig 10a,b)** is required for polarization of naïve T cells to Th1 cells during *C. rodentium* infection, we analyzed colonic tissue of whole p19$^{-/-}$, p40$^{-/-}$ and wt BM chimeras in addition to the respective chimeras generated mixed with CD11c-DTR donor BM.

The results of our flow cytometric analysis of T cells isolated from the lamina propria and RT-PCR analysis for Th17 / IL-17A and Th1 / IFN-γ expression indicated a shift of the Th17 / Th1 balance towards Th1 cells in the IL-23-deficient BM chimeras and in chimeras that have a deficiency of IL-23 in DCs and MΦs. This suggests Th1 cells as the source of the IFN-γ that causes the severe immunopathology.

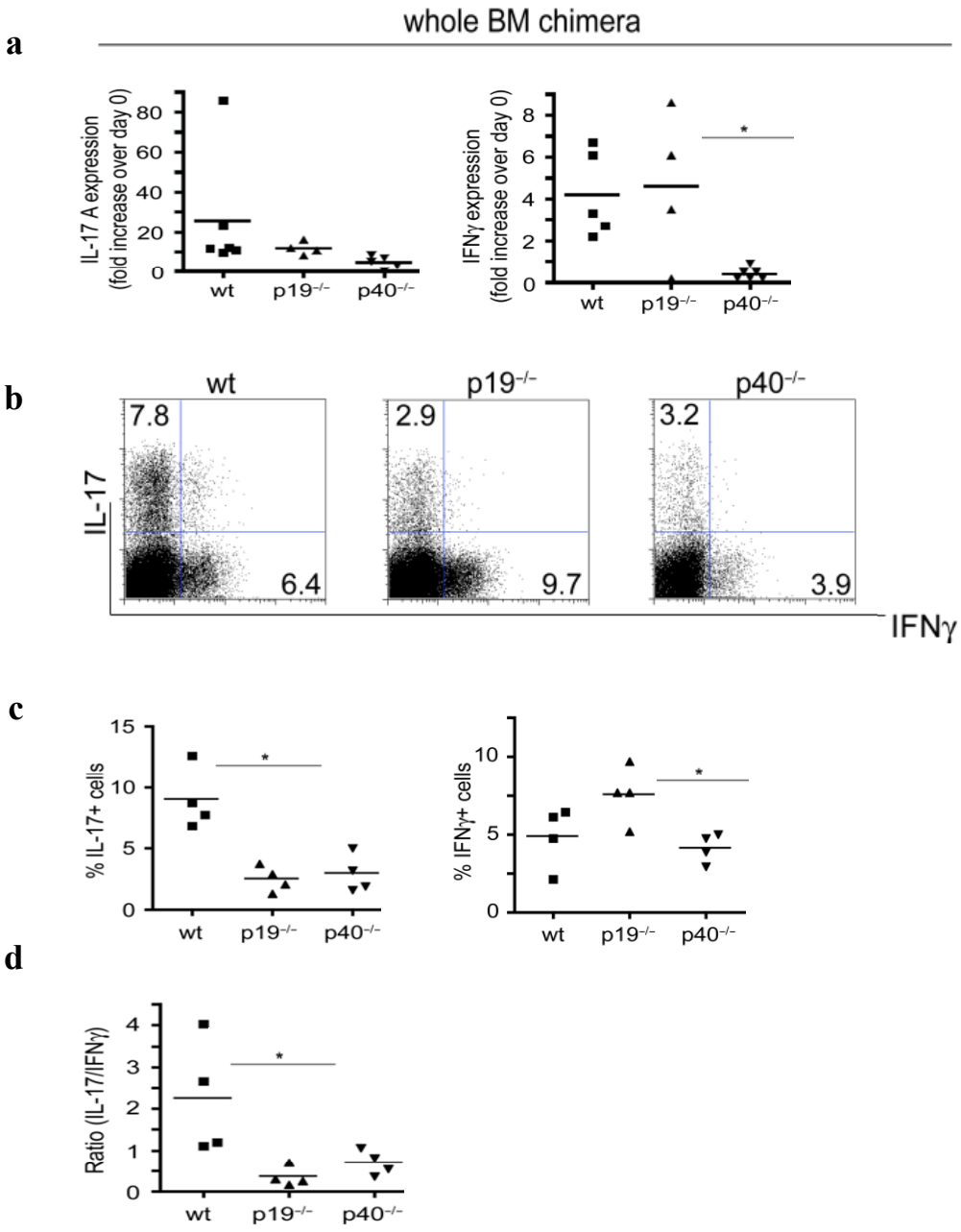
a
whole BM chimera
IL-17 A expression (fold increase over day 0)
IFNγ expression (fold increase over day 0)
wt
p19-/-
p40-/-
b
wt
p19-/-
p40-/-
7.8
6.4
2.9
9.7
3.2
3.9
IL-17
IFNγ
c
% IL-17+ cells
% IFNγ+ cells
d
Ratio (IL-17/IFNγ)

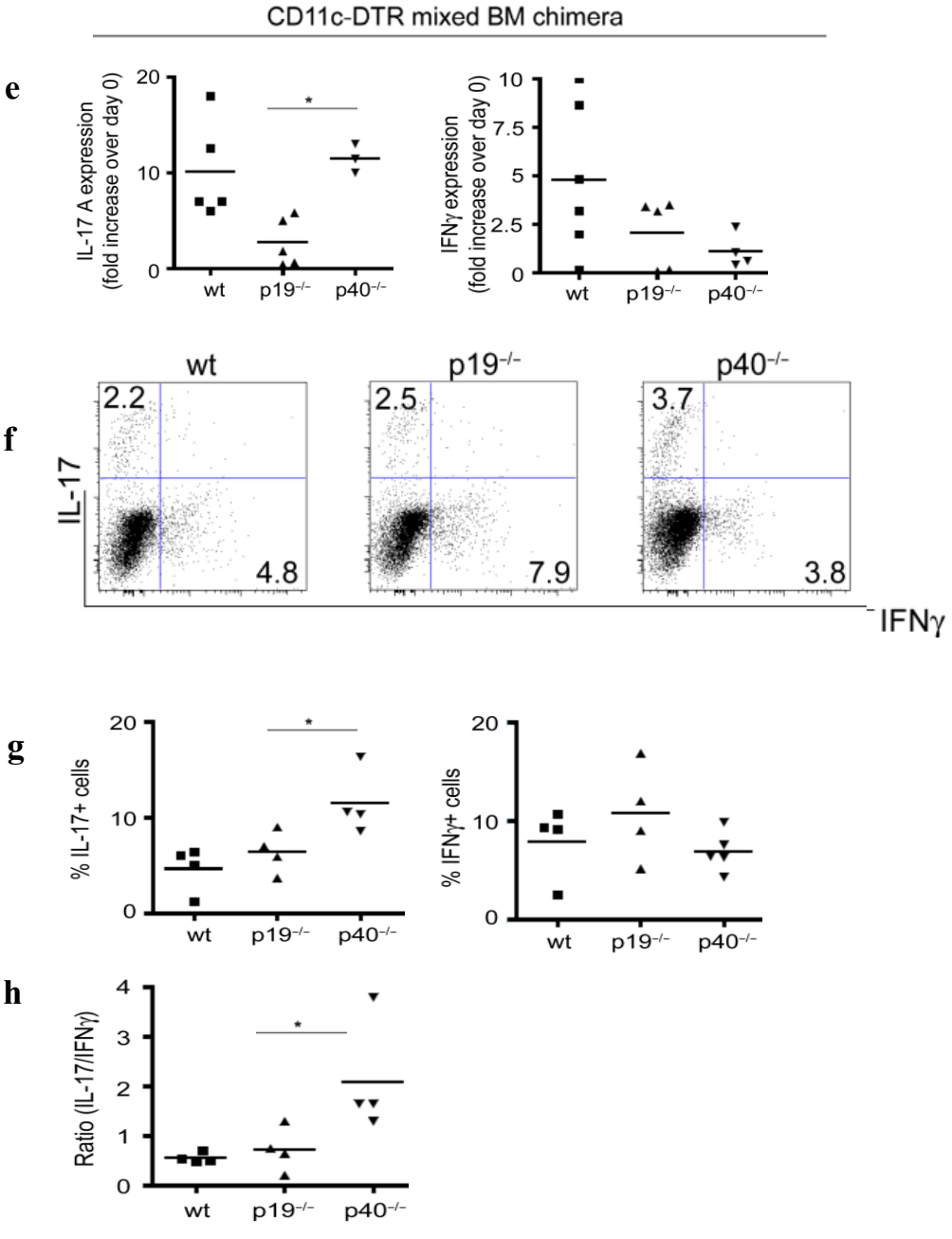
CD11c-DTR mixed BM chimera
e
IL-17 A expression (fold increase over day 0)
IFNγ expression (fold increase over day 0)
wt
p19-/-
p40-/-
f
IL-17
IFNγ
2.2
4.8
2.5
7.9
3.7
3.8
g
% IL-17+ cells
% IFNγ+ cells
h
Ratio (IL-17/IFNγ)

Figure 12: Th17 pasticity and acquisition of IFN-γ production.
$p19^{-/-}$, $p40^{-/-}$ and wt BM chimeras (a-d) or mice harboring hematopoietic mixture of CD11c:DTR (CD45.1) and $p19^{-/-}$, $p40^{-/-}$ and wt cells (e-h) were infected with $\approx 10^8 - 10^9$ CFU *C. rodentium* by oral gavage . (a and e) Real-time PCR analysis IFNγ and IL-17A of colonic tissues collected on day 8 PI. Flow cytometric analysis of TH17 and Th1 isolated from the lamina propria of whole hematopoietic cells BM chimers (b-d) or cells isolated from hematopoietic mixture of CD11c:DTR (f-h)

4.9 The contribution of $CD11b^+$ $Ly6C^+$ $F4/80^-$ CX_3CR1^{int} monocytes to the early host defense against C. *rodentium*.

$Ly6C^{hi}$ monocytes traffic to the colon and restore clearance of C. *rodentium* in $Ccr2^{-/-}$ mice [63].

To examine the contribution of $Ly6C^{hi}$ monocytes, we analyzed $CX_3CR1^{+/gfp}$ mice at different time points post infection (day 4, day 7, day 9 and day 12). The results showed that $CD11b^+$ $Ly6C^+$ $F4/80^-$ CX_3CR1^{inte} monocytes are indeed recruited to the colon on day 7, with the peak of the infiltration being on day 9 PI. On day 12 these cells seemed to have differentiated into $CD11b^+$ $Ly6C^-$ $F4/80^+$ CX_3CR1^{hi} cells **(Fig 13a)**.

In order to determine whether $Ly6C^+$ CX_3CR1^{int} monocytes contribute to the early host defense mediated by IL-23 and IL-22 we analyzed $CX_3CR1^{+/gfp}$ mice after depletion of $CD11b^+$ $Ly6C^+$ $F4/80^-$ CX_3CR1^{int} monocytes. The latter was achieved by injecting the anti-CCR2 antibody MC21 that depletes $Ly6C^+$ monocytes from the circulation. MC21 injection ablated $CD115^+$ $Ly6C^+$ monocytes from the spleen **(Fig 13b)**. In the colon treatment of MC21 led to a complete depletion of $Ly6C^+$ CX_3CR1^{int} monocytes **(Fig 13c)**. Most importantly, RT-PCR analysis of IL-23 of colonic tissues collected on day 4 PI and IL-22 RT-PCR analysis of colonic tissues collected on day 7 PI that was treated with MC21 antibody remained at the same level as the control mice **(Fig 13d)**. Collectively our data suggest that $Ly6C^+$ CX_3CR1^{int} monocytes do not contribute to the early host defense **(Fig 13a)**.

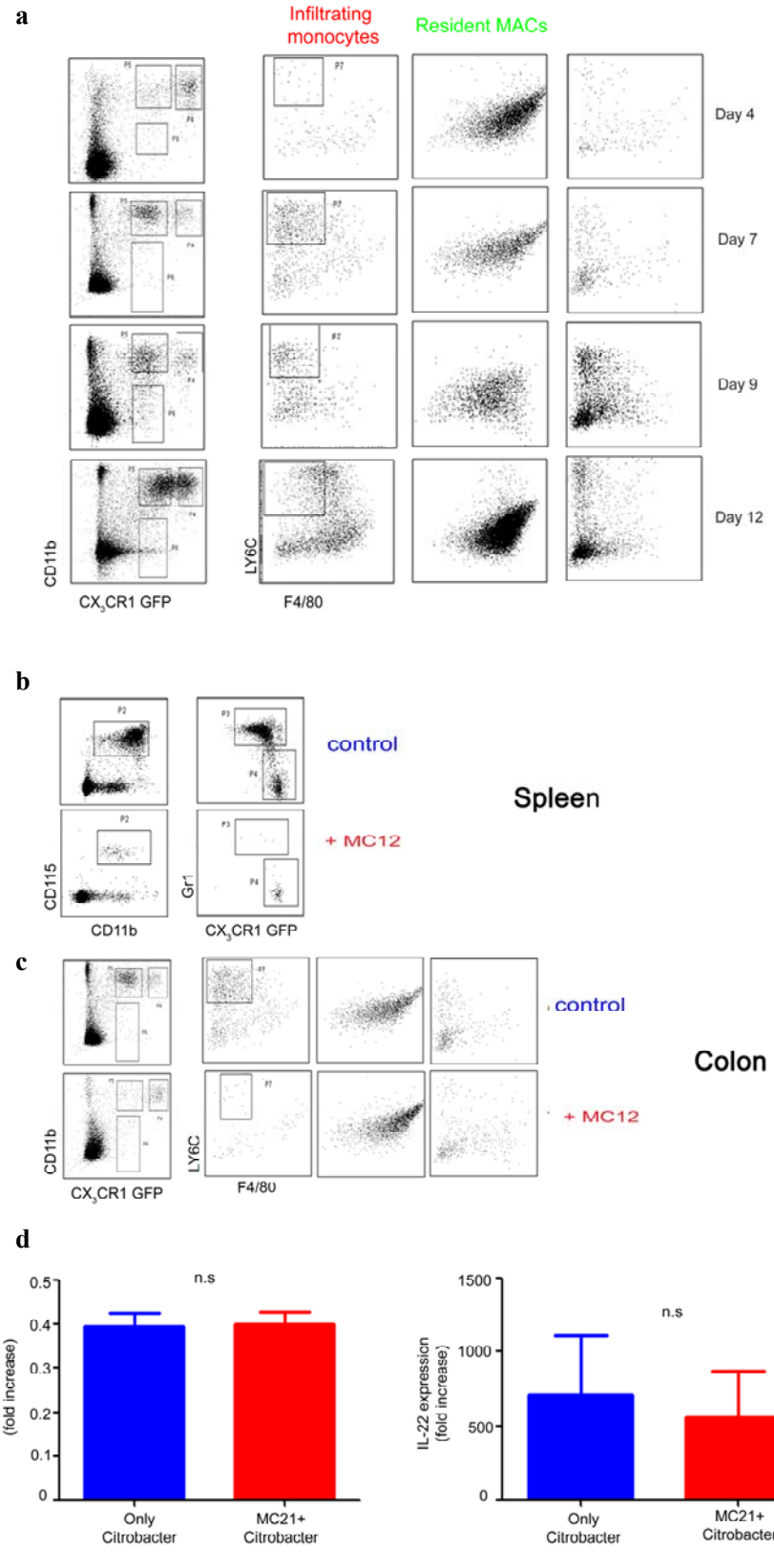
a
Infiltrating monocytes
Resident MACs
Day 4
Day 7
Day 9
Day 12
CD11b
CX3CR1 GFP
LY6C
F4/80
b
control
+ MC12
Spleen
CD115
Gr1
CD11b
CX3CR1 GFP
c
control
+ MC12
Colon
CD11b
CX3CR1 GFP
LY6C
F4/80
d
n.s
p19 expression (fold increase)
0.5
0.4
0.3
0.2
0.1
0
Only Citrobacter
MC21+ Citrobacter
n.s
IL-22 expression (folc increase)
1500
1000
500
0
Only Citrobacter
MC21+ Citrobacter

Figure 13: CD11b^{+} Ly6C^{+} F4/80^{-} CX$_3$CR1^{int} monocytes seem not contribute to the anti-*Citrobacter* response by IL-23 and IL-22 expression. FACS analysis of C. *rodentium* infected CX$_3$CR1$^{+/-}$ mice was performed at indicated time points post infection (a). C. *rodentium* infected CX$_3$CR1$^{+/-}$ mice were injected with MC21. Spleen (b) and Colon (C). Real-time PCR analysis of IL-23 and IL-22 of colonic tissues collected on day 4 and 7 PI.

Table 2: List of whole BM chimeras used in this study

Donor BM	Outcome the of chimeras	Outcome after C. *rodentium* infection
p19$^{-/-}$	Hematopoietic cells IL-23 deficiency	die
p40$^{-/-}$	Hematopoietic cells IL-12 and IL-23 deficiency	survive
wt	Hematopoietic cells contain IL-23 and IL-12	survive

Table 3: List of mixed BM chimeras used in this study

Donor BM 1	Donor BM 2	Outcome after DTx treatment of chimeras	Outcome after C. *rodentium* infection
CD11c-DTR	p19$^{-/-}$	DC/MF IL-23 deficiency	die
	p40$^{-/-}$	DC/ MF IL-12 and IL-23 deficiency	survive
	wt	DC/MF contain IL-23 and IL-12	survive
CX3CR1-DTR	p19$^{-/-}$	MF IL-23 deficiency	die
	p40$^{-/-}$	MF IL-12 and IL-23 deficiency	die
	wt	MF contain IL-23 and IL-12	survive

Table 4: Summary of cytokine expression in whole BM chimeras

Donor BM	IL-22	RegIIIβ	IFNγ	IL-17A
p19$^{-/-}$	+	+	+++	+
p40$^{-/-}$	+	+	+	+++
wt	++++	+++++	+++	+++

Table 5: Summary of cytokine expression in mixed BM chimeras

Donor BM 1	Donor BM 2	IL-22	RegIIIβ	IFNγ	IL-17A	IL-12p35
CD11c-DTR	p19$^{-/-}$	+	+	+++	+	ND
	p40$^{-/-}$	+	+	+	++	ND
	wt	++++	++++++	++++	+++	ND
CX3CR1-DTR	p19$^{-/-}$	++	+	+++	+	++++
	p40$^{-/-}$	+	+	+	++	+
	wt	++++	+++++	++++	+++	+

Table 6: Summary of histological analysis of whole BM chimeras

Donor BM	Colon length	Goblet cell	Enterocytes architecture	Mucosal hyperplasia
p19$^{-/-}$	reduced	depleted	destroyed	-
p40$^{-/-}$	reduced	depleted	normal	normal
wt	normal	normal	normal	increesed

Table 7: Summary of histological analysis of mixed BM chimeras

Donor BM 1	Donor BM 2	Colon length	Goblet cell	Enterocytes architecture	Mucosal hyperplasia
CD11c-DTR	p19$^{-/-}$	normal	depleted	destroyed	-
	p40$^{-/-}$	reduced	depleted	normal	normal
	wt	normal	normal	normal	increesed
CX3CR1-DTR	p19$^{-/-}$	ND	normal	destroyed	-
	p40$^{-/-}$	ND	depleted	normal	normal
	wt	ND	normal	normal	increesed

5. Discussion

The aim of this study was to investigate differential contributions of intestinal DCs and MΦs to the maintenance of gut homeostasis and the development of inflammatory bowel disorders. As a model system we used the oral challenge with the bacterial A/E pathogen *Citrobacter rodentium*, responses to which have been well defined in the past[61]. Specifically, this holds for a cytokine cascade involving IL-23 and IL-22[45]. The cell type that produces the IL-23 in the colon upon *Citrobacter* challenge and that triggers the defense cascade has however not been defined.

Our initial results involving BM chimeras established that IL-23 produced by hematopoietic cells was necessary to survive *C. rodentium* infection. This supports a aprevious report that showed that complete IL-23 knockout mice do not survive the infection[45]. Interestingly though, animals with hematopoietic deficiencies of both IL-23 and IL-12 survived the challenge. RT-PCR analysis of the colon of the infected mice revealed that IL-22 and RegIIIβ were significantly downregulated in chimeras, confirming that IL-23 was required for induction of these factors. It has recently been reported that induction of IL-22 and RegIIIβ is in the ileum following systemic TLR5 stimulation controlled by DC[32] . This suggests region and trigger-specific differences in the host responses. derived IL-23 Mice with the IL-12/23 deficiency also lacked the protective IL-22 response, but were found to survive the infection. Impaired IL-22 productioncould hence not explain the lethality. We also excluded the possibility that an overwhelming bacterial burden is causing lethality since the bacterial counts were similar in chimeras lacking IL-23 or IL-12/23. We however confirmed that the bacterial burden seems controlled by IL-22-induced antimicrobial activity because chimeras with IL-23 or IL-12/23 deficiency displayed higher levels of bacteria when compared to controls.

Using a conditional cell ablation strategy[11] we next established that CD11c-expressing myeloid cells are required for IL-23 production and the ensuing induction of

IL-22, which in turn results in epithelial expression of the antimicrobial protein RegIIIβ. Furthermore, the antimicrobial S100A9 defense and the IL-6 mediated response of TH17 cells[45, 76] seem not to be orchestrated by MΦs or DCs, strengthening the fact that DCs and MΦs are exclusively critical for IL-23 mediated host defense. On top of that, whole [CD11c-DTR > wt] BM chimeras survived the infection until day 12, as opposed to mixed [$p19^{-/-}$ / CD11c: DTR > wt] chimeras that died on day 8. The fact that mice deleted of DCs and MΦs were found protected indicated that the two cells types might regulate each other and that we deal with an immunopathology. Similar data describing the potential regulation of DCs and MΦ was reported for a DSS colitis model by using the CD11c-DTR mice and adoptively transferring monocytes. In this case mice that lacked both Dc and MΦ displayed less severed colitis than mice lacking only DC[11].

Next we took advantage of newly established "CX_3CR1-DTR" (CX_3CR1^{Cre}:iDTR) mice to specifically ablate MΦ but leave $CD103^+$ $CD11b^-$ *lamina propria* DCs untouched. Like [$p19^{-/-}$ / CD11c-DTR > wt] chimeras, in which both DCs and MΦ are ablated, [$p19^{-/-}$ / CX_3CR1-DTR > wt] chimeras succumbed to the *C. rodentium* infection suggesting that the critical IL-23 has to come from MΦ. When [$p40^{-/-}$ / CX_3CR1-DTR > wt] chimeras were infected, the mice also died. Since the IL-23 is comprised of p19 and p40 polypeptide chains, elimination of each one of them will result in the loss of IL-23 coming from the MΦ. This result corroborates MΦ as the source of IL-23. Moreover our data highlight the fact that MΦ are the sole producers of IL-23 under the infection of *C. rodentium* in the colon. This result together with the fact that IL-23 in the ileum is secreted from CD11b- DCs[32] establishes that different APCs are responsible to IL-23 production under the context of the intestine, and highlights the complexity of mucosal organs. Interestingly [$p40^{-/-}$: CD11c: DTR > wt] chimeras were protected from lethality. These mice lack both IL-23 and IL-12 coming from DCs and MΦ. Combined with the fact that MΦ are the sole source of IL-23, this suggests that (1) IL-12 could cause pathology and (2) that the IL-12 is derived from DCs. It is important to mention that in the succumbing [$p40^{-/-}$ / CX_3CR1-DTR > wt] chimeras, DCs are still present and a fraction of them is of wt genotype.

Our genetic models enabled us to critically investigate the source of IL-23 and IL-

12, but we decided to look also directly at cells isolated from $CX_3CR1^{gfp/+}$ that have wt phenotype and undergo minimal intervention. Analysis of mRNA of FACS-sorted MΦ and DCs isolated from unchallenged and *C. rodentium*-infected mice confirmed that IL-23 is definitely coming from the macrophages and that IL-12 can be derived from DCs. Moreover, we were able to demonstrate that DCs upregulated IL-23R expression upon *C. rodentium* infection and concomitantly downregulated IL-12 expression. Interestingly, it was reported that IL-23 can cross-regulate IL-12 p35/p40 expression, and that the lack of IL-23 leads in BM culture-derived DCs isolated from IL-23 p19-deficient mice to excessive IL-12 production [28]. This finding when combined with the results of our genetic approach, suggests that MΦ-derived IL-23 cross-regulates IL-12 expression by DCs. We further established that IL-23 is sensed by DCs and crossregulates their IL-12 expression by sorting DCs from mice that lack IL-23 in the MΦ compartment and analysing IL-12 and IL-23R in the DCs. So far IL23-R expression has been reported for lymphocytes, in particular TH17 cells both in the intestine and in the CNS[71-72,75,78] and the impact of IL-23 on these cells was mainly discussed in the framework of IL-22 production. Here we newly discovered that myeloid cells and more specifically DCs could respond to IL-23. MΦ also exhibited high levels of IL-12. However, we did not observe evidence for an autocrine loop controlling IL-12 production, as it was not affected by the IL23 deficiency of MΦ. This suggests that DC are the source of IL-12 causing immunopathology. In addition we measured high levels of MΦ -derived IL-12 in [wt / CX_3CR1- DTR > wt] mice. These mice survive the infection and do not have elevated transcripts of IL-12 in the DC. This result points at an importance of MΦ -derived IL-23 in the cross-regulation of DC- production of IL-12.

Mice that have a IL-23 deficiency in DCs and MΦ or in MΦ only died after C. *rodentium* infection. However, a combined IL-12/IL-23 deficiency in the DCs and MΦ resulted in the protection of the mice from the infection. We could exclude that the animals die as a result of an impaired host defense or due to an overwhelming bacterial load. On the other hand, we demonstrated that DCs sorted from the colon expressed IL-12. In order to identify the cause of the pathology in the dying mice, we performed a RT-PCR analysis for IL-12 (p40, p35) in the [$p40^{-/-}$ / CX_3CR1-DTR > wt] chimeras and in the [$p19^{-/-}$ / CX_3CR1- DTR > wt] chimeras. The results established that IL-12 was

upregulated in the mice that have macrophage-restricted IL-23 deficiency. This suggests that IL-12 is produced by DCs in the absence of IL-23 that would otherwise suppress its production. The suppressive capacity of IL-23 on IL-12 was reported previously in p19-/- BMDC who down regulated IL-12 expression however it was not the case in wt BMDC[28.] Our data confirm this notion in an *in vivo* system underlining its physiologicalrelevance. IL-12 promotes the polarization of naïve T cells to TH1 cells and induces the secretion of interferon-γ (IFNγ) by T and NK cells. Moreover, it has been linked to their pathogenicity in vivo in EAE [75]. To probe if IFNγ is the factor that leads to the immunopathology, we measured IFNγ expression in the colon of mice that had deficiency of IL-23 or IL-12/23, mice that are deficient of IL-23 or IL-12/23 in DCs or MΦ, as well as mice that are deficient of IL-23 in MΦ only. In all of the cases of single IL-23 deficiencies we observed an upregulation of IFNγ when comparing it to mice lacking both IL-12/IL-23. The opposite correlation was observed when we analyzed IL-17A expression. These experiments support our assumption that IL-12 induced IFNγ production is involved in the immunopathology. Most importantly we were able to rescue [$p19^{-/-}$ / CD11c-DTR > wt] mice by neutralizing IFNγ. Thus we identified IFNγ as the direct factor that leads to the immunopathology.

Interestingly when we examined IFNγ production in mice that had wt hematopoietic cells, wt DCs or macrophages or wt macrophages alone, we found IFNγ to be upregulated as well, however these mice had extremely high levels of IL-22 and RegIIIβ in contrast to the mice that lacked IL-23 in the different compartments. Therefore we conclude that IFNγ causes immunopathology only in an environment that lacks the IL-23-mediate host defense implemented by IL-22 and RegIIIβ.

IFNγ-dependent small intestinal pathology and dysfunction play a significant role in the lethality of superantigen exotoxins induced of Toxic shock syndrome (TSS) [74]. In addition IFNγ induces disassembly of tight junctions (TJ) through stimulation of endocytosis of junctional proteins in the intestinal epithelial cells. IFNγ thus generates leaky epithelial barriers [77]. These two studies may explain the phenomena that we observed, i.e. that *Citrobacter*-challenged "IL-23-deficient" mice die because they might succumb to a Toxic shock syndrome and impaired epithelial cell integrity. In an effort to identify the source of the IFNγ, we analyzed the TH1 and TH17 populations in the colon

in these experiments. We observed that the TH17 cell population was decreased in mice lacking IL-23 and in mice lacking IL-23 in DCs and MΦ, when compared to mice that lack both IL-12/IL-23 in the respective cells. The opposite result was obtained when we analyzed TH1 cells. This suggests that in the absence of MΦ -derived IL-23 DCs secrete IL-12 to polarize TH17 cells into TH1 cells that in turn secret deleterious IFNγ. The fact that IL-12 can polarize TH17 has been reported for the EAE model. Using TH17 reporter mice it was established that these cells can convert to TH1 cells [75]. Our data suggest that the same plasticity might occur in the intestine.

Goblet cells are mucus-secreting cells and the second most abundant epithelial cell in the colon; their lifespan is 5-6 days. Treatment with IL-22–binding protein was reported to suppress goblet cell reconstitution during the recovery phase of a DSS-induced acute colitis [48]. We observed that goblet cells were heavily reduced in chimeras that lack IL-23 or IL-12/IL-23. The same was observed for chimeras that display IL-23 or IL-12/IL-23 deficiency in DCs or MΦ, as well as in the chimeras that have IL-12/IL-23 deficiency only in the MΦ on 7 day after the infection. This establishes the importance of MΦ -derived IL-23 for the activation of IL-22 secretion that leads to goblet cell reconstitution after *C. rodentium* infection. At the same time it highlights the importance of MΦ in colonic tissue remodeling.

Intradermal administration of IL-23 into mouse skin initiates a TNF-dependent, but IL-17A independent cascade of events resulting in psoriasis-like epidermal hyperplasia[69]. Furthermore, histological evaluation of colons deficient in IL-23 signaling revealed decreased leukocytic infiltrate, less crypt loss, and reduced epithelial hyperplasia when subjected to pathogenesis in the DSS model of colitis[78]. These two studies offer the IL-23-IL-23R axis as important factor that mediates the colonic hyperplasia during colitis. In our experiments development of colonic hyperplasia was impaired in mice lacking IL-23 from hematopoietic cells. The same was observed for chimeras that have IL-23 deficiency in DCs or MΦ and chimeras that have IL-23 deficiency in the MΦ alone. Intestinal epithelial cells represent an important interface between the host, microbes and antigens. Here we established that MΦ-derived IL-23 reinforced the epithelial cell-mediated physical barrier by causing colonic hyperplasia and epithelial cell integrity.

Ly6C^{hi} monocytes traffic to the Colon and restore clearance of C. *rodentium* in Ccr2$^{-/-}$ mice. In addition Nod2 was reported to control the colonic recruitment of monocytes through the production of CCL2 in response to pathogen infection[79]. Thus, Nod2 mediates CCL2/CCR2-dependent recruitment of inflammatory monocytes, which is important in promoting bacterial eradication in the intestine.

Injection of an anti-CCR2 antibody depleted CD115+ Ly6C^{+} monocytes in the spleen as well as Ly6C^{+} CX_3CR1^{int} monocytes in the colon. Most importantly, RT PCR analysis of IL-23 and IL-22 post injection of the antibody showed no changes as compared to control mice. Collectively our data show that CX_3CR1^{int} monocytes do not contribute to early host defense mediated by IL-23 and IL-22. However they are certainly recruited to colon, as we see them differentiating into MΦ at day 12**.**

IBD is a group of chronic inflammatory conditions of the intestinal tract including ulcerative colitis and Crohn's disease [80]. While a combination of genetic susceptibility factors and altered immune responses has been suggested to cause the disease [81,] the etiology of IBD remains largely unknown, highlighting the need for research in this field. IL-23R and IL-12b[82] mutations in humans has been linked to colitis and Crohn's disease, however not with full penetrance highlighting the fact that an additional factors contribute. Here we suggest C. *rodentium* or his extended family the entero-pathogenic bacteria's including *E. coli* as the possible additional factors that drives genetic susceptibility to full disease.Additionally, MΦs from the patients display impaired cytokine secretion. Because of inadequate production of cytokines and chemokines, there might be insufficient attraction of granulocytes to mucosal breaches. This could result in defective clearance of bacteria and debris from the gut wall, ensuing chronic, granulomatous inflammation[83] .

While the IL-12 super family might be important in controlling and mediating the cross talk between myeloid and lymphoid cells in key organs, much remains to be learned. Including their cell type allocation, kinetics, and degree of expression, and the involvement of the innate TLR pathways that direct to their expression, on top of that the combinatorial usage of the limited number of transcription factors that control their

expression for example IRF1[84] needs to be studied in depth. The possibly potential of IL-12-related cytokines is remarkable, and it can be totally and carefully understood only through a close and full understanding of their immunobiology under the context of organ and the innate cell that secrets them.

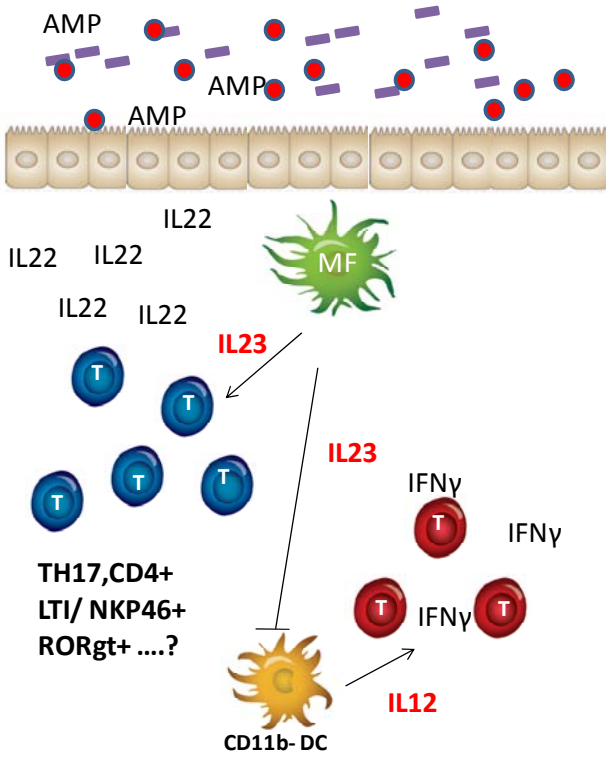

Conclusions

- MFs are critical producers of IL23 in *Citrobacter* response

Figure 13: MΦ restricted IL-23 controls the secretion of IL-22 which in triggers AMP mediated host defense against C. *rodentium*.

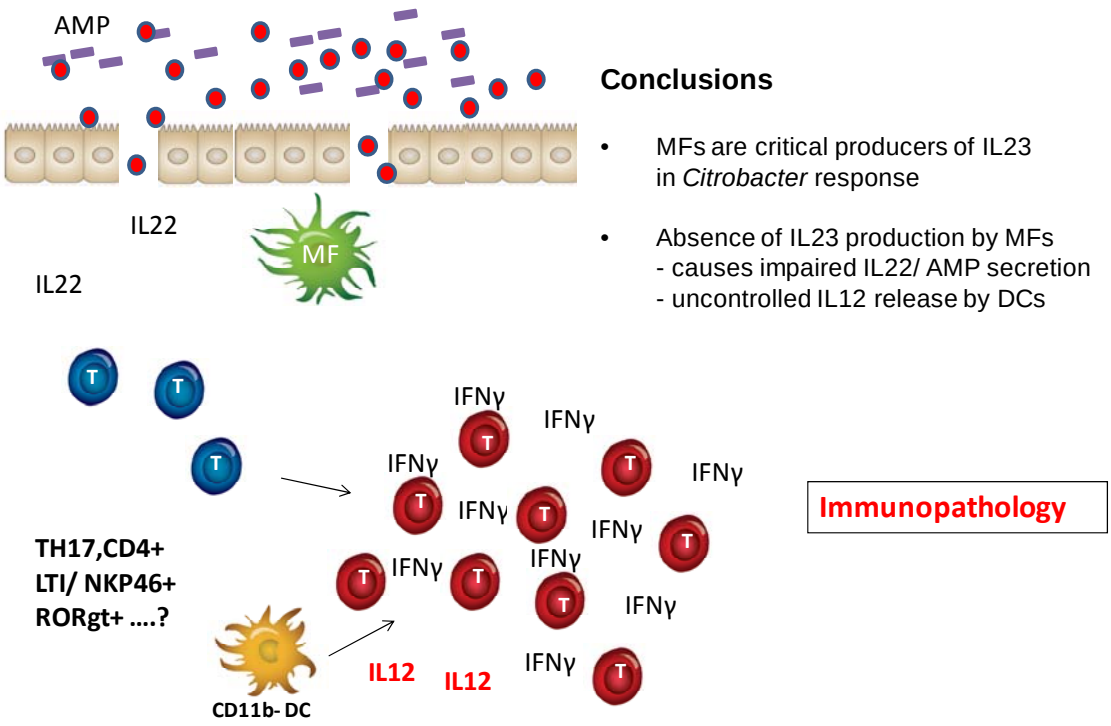

Figure 14: MΦ restricted IL-23 deficient environment leads to, IL-12 secretion by CD103^{+} DCs that drives uncontrolled IFN-γ production by T cells causing severe immunopathology.

6.Quantitative analysis of intravenously administered contrast media reveals changes in vascular barrier functions in a murine colitis model

6.1 Introduction

IBD is a group of chronic inflammatory conditions of the intestinal tract including ulcerative colitis and Crohn's disease [80]. While a combination of genetic susceptibility factors and altered immune responses has been suggested to cause the disease [81], the etiology of IBD remains largely unknown, highlighting the need for preclinical research. Hallmark pathological IBD features include leukocyte infiltration, intestinal mucosal damage and ulceration. In addition, IBD is associated with major alterations and dysfunction of the intestinal microvasculature, as indicated by clinical and preclinical studies that delineated a central role for microcirculation in initiation and perpetuation of inflammatory processes [89,.

Colitis induced by dextran sodium sulfate (DSS, a detergent leading to epithelial necrosis inducing lesions in the intestinal epithelium), is the most widely used chemically induced model of ulcerative colitis. Adding DSS to the drinking water for several days induces an acute intestinal inflammation with bloody diarrhea and ulcerations [89]. Endoscopic optical imaging, as well as MRI were found to be valuable for investigation of dynamic longitudinal changes during disease progression. Accordingly, in-vivo fiberoptic confocal imaging after surgical exposure [90] and side-view endomicroscopy of fluorescently labeled cells [91], have been used to study murine DSS colitis.

In the last decade, MRI has emerged as an important modality for abdominal imaging. T1-, T2-weighted, dynamic contrast enhanced (DCE) MRI, and diffusion-weighted MRI have been proven to be sensitive to inflammation in the small intestine and the colon. The MRI studies of colitis [92,95] and colorectal cancer in mice, reported so far, were performed using low molecular weight, clinically available Gd-DTPA [94,96]. Macromolecular contrast material, used as a blood pool agent in normal vasculature, can provide increased specificity for measurements of changes in blood volume and detection of elevation in vascular permeability, compared to low molecular weight Gd-DTPA [97]. Biotinylated

contrast material further enables histological validation of DCE-MRI data, using Gd-DTPA bound to bovine serum albumin (BSA) and biotin (biotin-BSA-GdDTPA) [98,102].

Our hypothesis was that changes in vascular permeability can be used as a sensitive biomarker for in-vivo monitoring of the progression of colitis. The aim of this study was to develop noninvasive quantitative fluorescence and MRI based methods to evaluate the changes in colonic vascular function for longitudinal preclinical research in a murine DSS colitis model. These tools were then applied for analysis of the ability to quantify disease severity in comparison to the pathological gold standard.

6.2 Results

6.2.1 Permeability of the colonic microvasculature in DSS-induced experimental colitis

In order to investigate vascular function in the colon of control mice and mice treated with DSS 3%, colonic blood vessels and the dynamics of macromolecular contrast agent were followed. The normal architecture of the colonic microcirculation in the mouse consists of polygonal subepithelial mucosal plexus drained by descending veins [106]. In control mice, fluorescent confocal endomicroscopy showed this well structured honeycomb pattern of microcirculation without leakage of macromolecular contrast agent. Mice exposed to DSS 3% in the drinking water for 7 days developed severe colitis. Fluorescent confocal endomicroscopy of the colon revealed distorted pattern of the microvasculature and dilated large vessels. FITC-dextran, a macromolecular fluorescent dye, leaked out of the blood vessel and accumulated in the tissue **(Fig 1 a, b; Supplementary 1, 2)**. Percent area of FITC-Dextran per FOV), including both vascular density and leakage, was significantly increased in animals with colitis compared to control animals (16.7±2.3% and 6.1±3.1% respectively; p=0.02; Figure 1c). The histogram of representative control and colitis images indicated an increased number of pixels with high intensity in colitis **(Fig 1d)**.

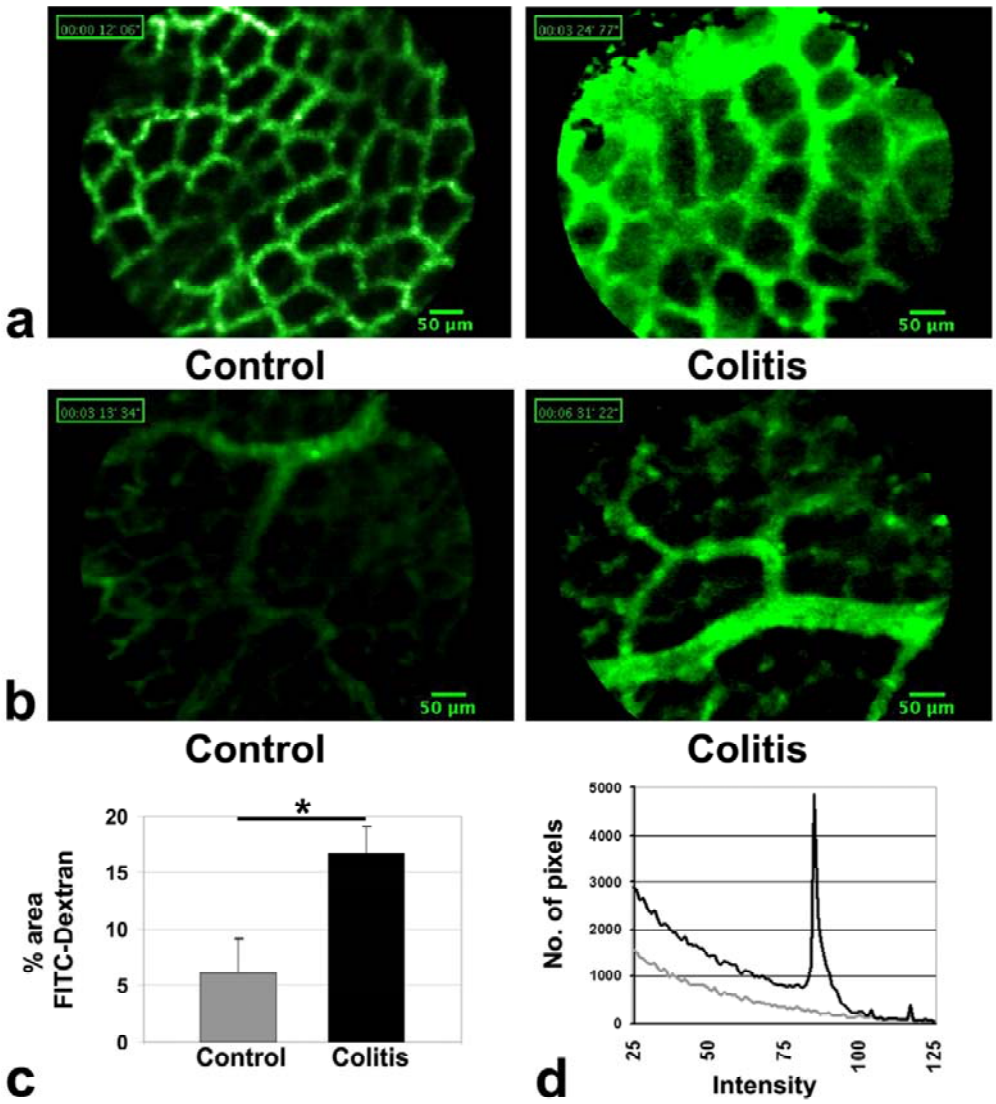

Figure 1. Fluorescent confocal endomicroscopy of representative mouse colon after intravenous injection of FITC-Dextran. (a) The polygonal subepithelial mucosal plexus with characteristic honeycomb pattern of microcirculation showed normal architecture of the colonic microcirculation in control colon. Highly distorted microcirculation in colon of 3% DSS-treated mouse (for 7 days) with leakage of FITC-Dextran from the vessels. (b) Descending veins, draining the subepithelial mucosal plexus, are dilated in animals with DSS colitis compared to control animals. (c) Quantification of the percent area of FITC-Dextran in control (n=5) compared to animals with colitis (n=6; *p=0.02). (d) Histogram of representative control and colitis of the entire grey scale image indicating an increased number of pixels with high intensity in colitis (Gray, control; Black, colitis). (See supplementary movies 1, 2).

Similar changes were detected by MRI. Animals were imaged by MRI before and 30min after iv administration biotin-BSA-GdDTPA **(Fig 2a)**. The blood volume fraction (fBV) and vascular permeability (PS) in the colon, as VOI, were derived by pharmacokinetic analysis **(Fig 2b)**.

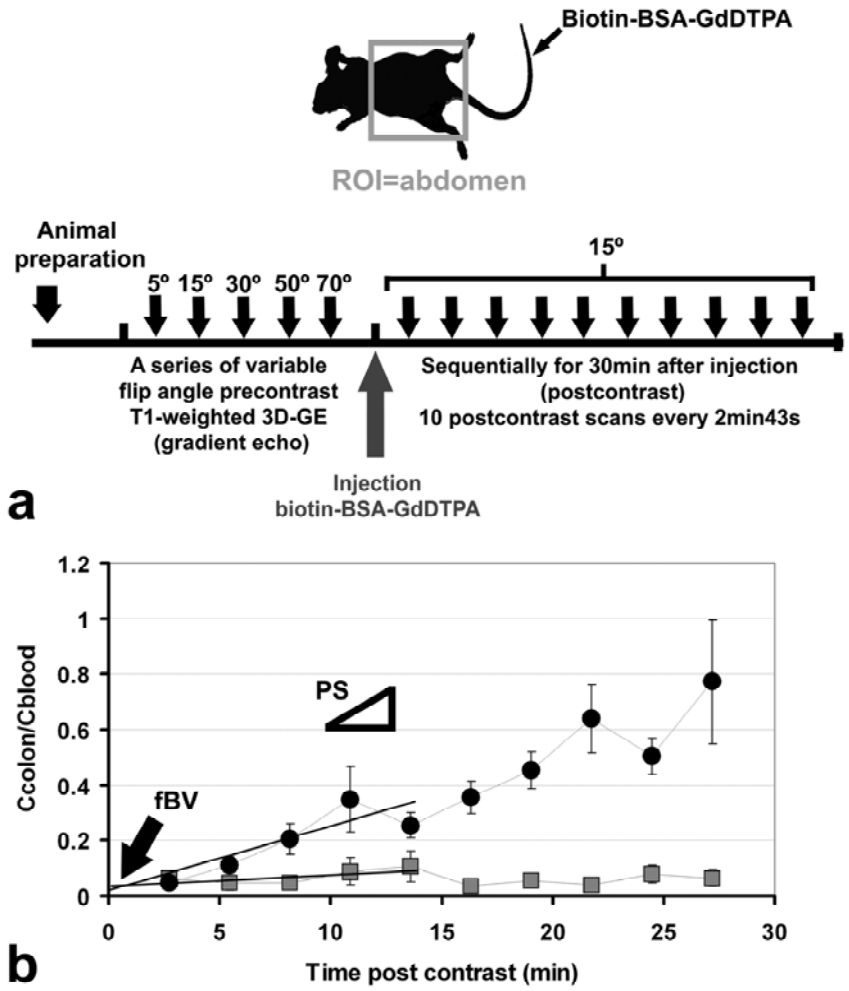

Figure 2. Macromolecular dynamic contrast-enhanced (DCE) MRI of the colon after 7 days of 3% DSS treatment. (a) Three dimensional gradient echo (3D-GE) images of the abdomen were acquired before and sequentially for 30min after intravenous injection of biotin-BSA-GdDTPA. The volume of interest (VOI) covered the abdomen. A series of variable flip angle precontrast T_1-weighted 3D-GE images were acquired to determine the endogenous precontrast R_1. (b) Contrast material accumulation was derived from consecutive MRI images of the abdomen of control (n=6; gray squares) and DSS treated mice (n=6; black circles). Images were acquired for 30min after macromolecular contrast injection (biotin-BSA-GdDTPA; intravenous, via a tail vein catheter; 10 time points). Fractional blood volume (fBV; intercept with time zero) and permeability surface area product (PS; the slope) were derived from the first 15min.

Immediately after administration, the contrast material was confined to blood vessels. No significant difference in fBV was found between control colon and colon after 7 days of DSS treatment (0.051±0.026 and 0.021±0.011 respectively; **Fig 3**). Vascular permeability was determined by the initial rate of accumulation of biotin-BSA-GdDTPA. During this period, the macromolecular contrast agent was not cleared from the blood circulation **(30min; Supplementary 3)**. The colon was analyzed in several axial slices and pixel-by-pixel analysis was done to derive values of vessel permeability. In control animals the contrast agent remained in the blood vessels, resulting in very low PS (0.002±0.001min^{-1}). However, in DSS-treated mice, PS values were markedly elevated, corresponding to enhanced rate of accumulation of the contrast media over time (0.022±0.005min^{-1}; p=0.003). Histogram analysis showed a significant increase in the number of voxels with high permeability in animals with colitis **(Fig 4)**. The leak was continuous, generating a flux of contrast material from mucosal vessels towards the lumen of the colon. Hot spots with increased flux of contrast material were present **(Fig 4; Supplementary 4)**.

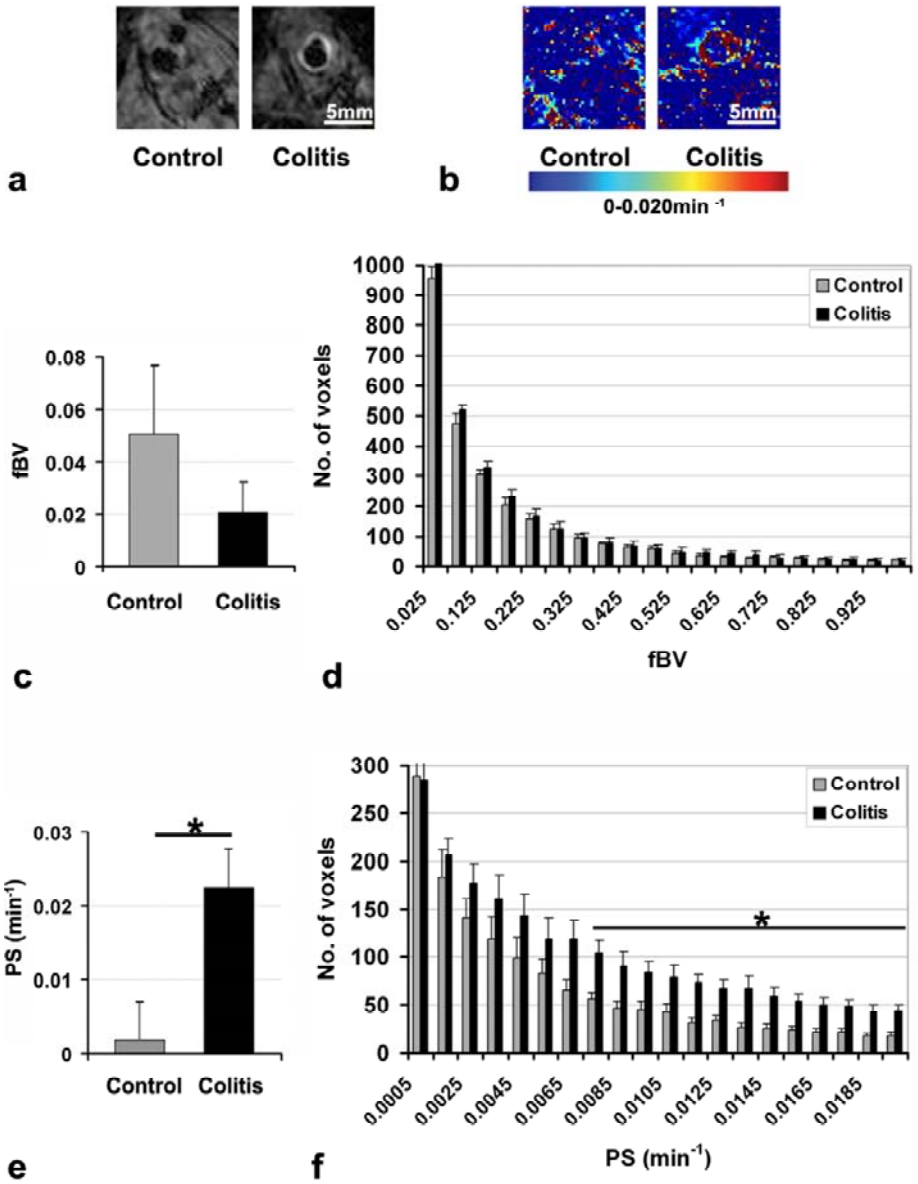

Figure 3. Fractional blood volume and permeability surface area product (a) axial MR images (3D gradient echo) 15min after contrast injection. (b) Permeability surface area product (PS; the slope of concentration curve normalized to blood concentration). (c) Mean fBV values and (d) histogram of fBV. (e) Mean PS values (n=6 per group; *p=0.003) indicating increased permeability in animals with colitis and (e) histogram of PS (n=6 per group; *p<0.01) showing a significant increase in the number of voxels with high permeability in animals with colitis. fBV and PS were calculated from a linear regression over 15min for each group. fBV and PS histograms represent values in the same pixels chosen for calculation of fBV and PS values.

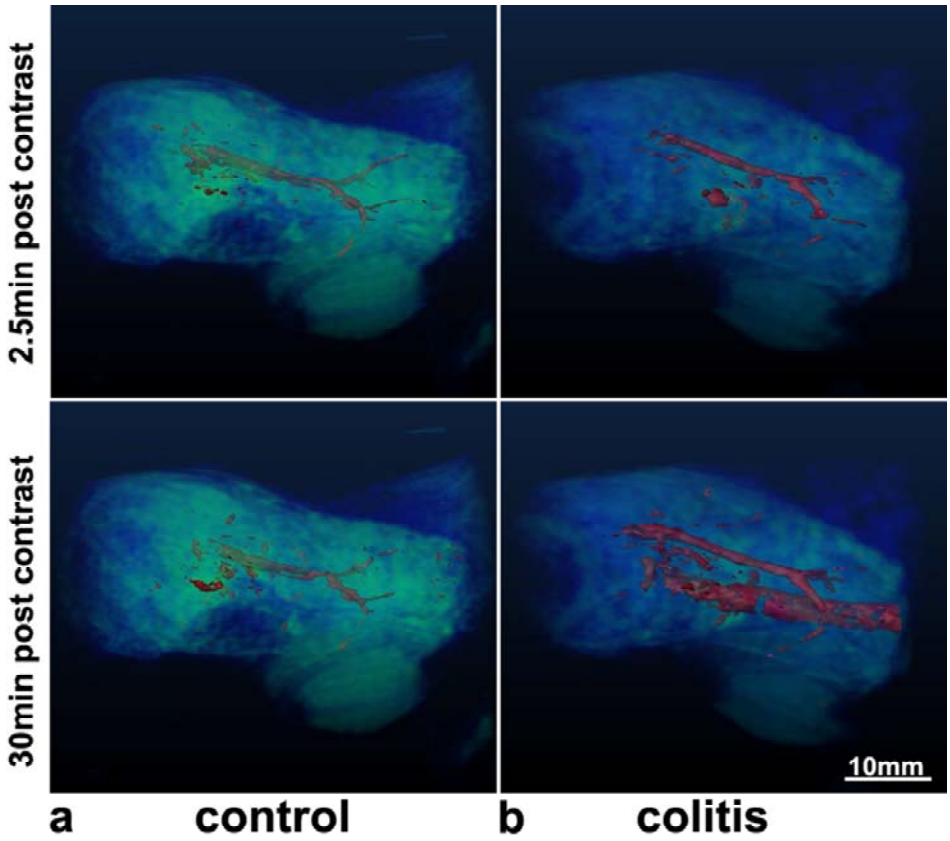

Figure 4. Three dimensional reconstruction of the abdomen of a control mouse (a) compared to a mouse with colitis (b). The first and last MRI scans (of the 10 sequential scans) after contrast injection are shown, enhancing only the vena cava in the control. For a representative mouse with colitis, in the first scan post contrast, no leakage of albumin into the colon is yet observed, but gradually, at each scan, the contrast agent leaked out, resulting in selective enhancement of the colon 30 min post contrast. (See supplementary movies 2 and 3).

Axial **(Fig 3b)** and coronal **(Fig 5a)** images showed concentric wall thickening and increased enhancement of the wall 30 min after administration of contrast media, in DSS-treated colon, after injection. The overlay of early and late maximal intensity projections (MIP), allows to assess the rate of extravasation of biotin-BSA-GdDTPA and the distribution of highly permeable foci along the colon **(Fig 5b)**. MIPs highlight regions with evident contrast enhancement. The colon wall was found significantly thickened in animals with DSS colitis compared to control animals (0.68±0.01mm and 0.29±0.05mm; p=0.00001; **Fig 5 c**).

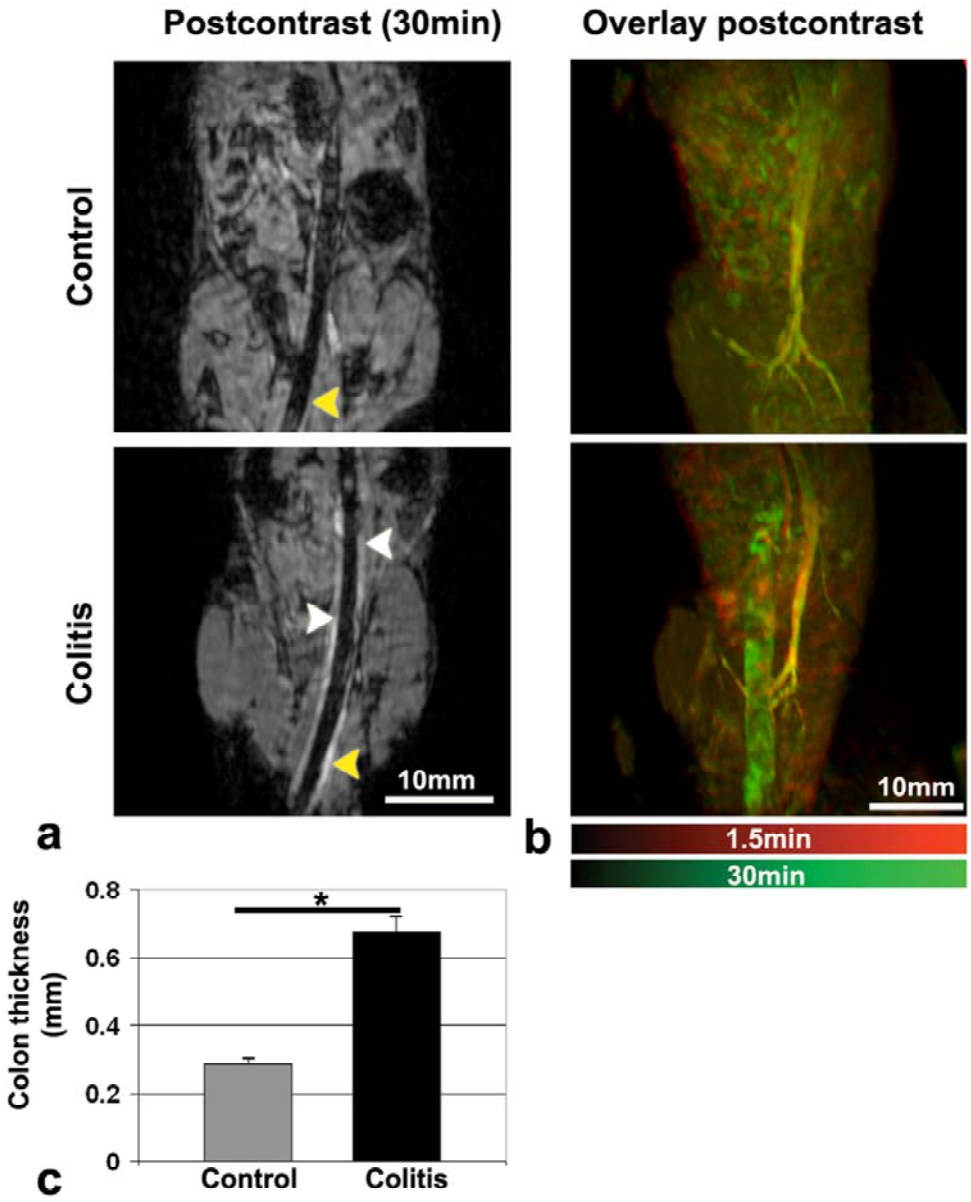

Figure 5. Macromolecular DCE-MRI of control mice and mice with colitis (7 days after 3% DSS treatment). (a) Coronal MR images (3D gradient echo) 30 min after contrast injection (arrows show selective enhancement of the colon; yellow arrow on (a) shows the region of the axial slice Figure 3a). (b) An overlay of maximal intensity projections (MIPs; right) of selected 3D images of control mouse, compared to a mouse with colitis (1.5 and 30 minutes postcontrast). Early time point in red and later time points in green (right), showing selective enhancement of the colon due to extravasation of biotin-BSA-GdDTPA (albumin). (c) Colon thickness measured on axial slices (n=6 per group; *p=0.00001).

6.2.2 Histology and biodistribution of macromolecular contrast agent in the colon

Pathological examination confirmed that all animals treated with 3% DSS containing water for 7 days, developed macroscopic and microscopic lesions. Macroscopically, the colon was shortened **(Fig 6a)**. Histological sections (stained with H&E) showed severe multifocal necro-ulcerative colitis affecting approximately 70% of the colon as examined by a pathologist **(Fig 6b)**.

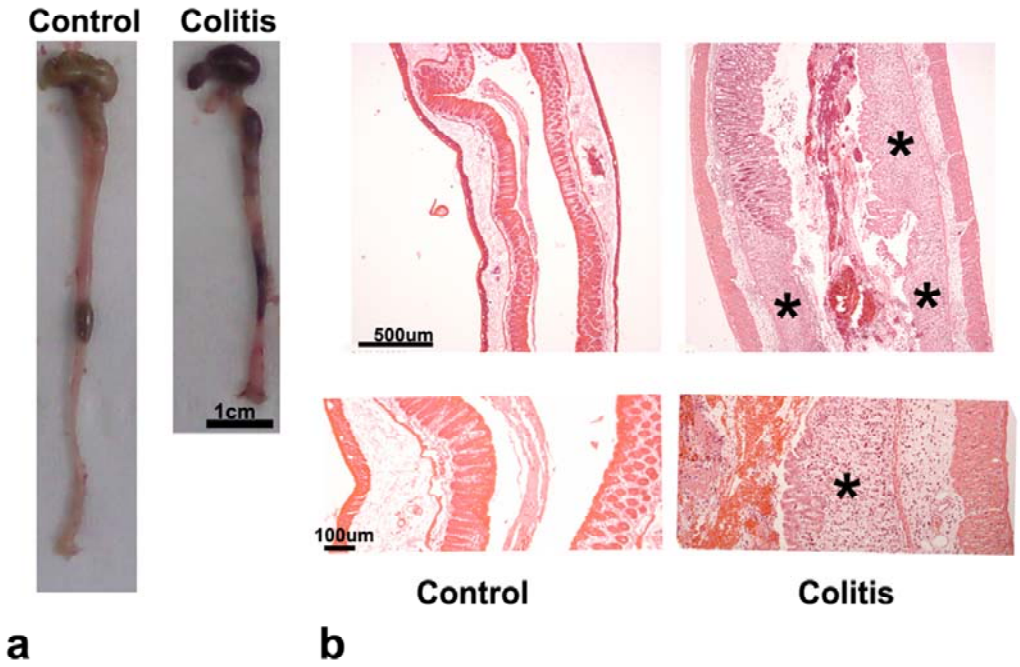

Figure 6. Macroscopic and microscopic lesions of DSS colitis. (a) The length of the colon is reduced in DSS treated mice. The intestinal contents are dark (hemorrhage) (b) H&E staining of control mice and mice with severe necro-ulcerative colitis (asterisks).

Histological staining of biotin-BSA-GdDTPA with avidin-FITC was used for validation of the microscopic biodistribution of the contrast material within the colon. Substantial extravasation of biotin-BSA-GdDTPA was observed, corresponding to the high permeability of the mucosal blood vessels, in the colon of mice exposed to DSS 3% for 7

days, as revealed by DCE-MRI. Colons of mice without administration of contrast agent, showed only background staining with avidin-FITC, due to endogenous biotin (data not shown). Therefore, we validated the extravasation of albumin in histology also by co-administration of BSA-FAM along with the bolus injection of MR contrast agent. The same distribution as detected in the avidin stained samples was observed. Therefore also, quantification of percent area of BSA-FAM, corresponding to permeability (PS) measurements of the MRI, revealed no leakage in the control animals, compared to significant extravasation in the animals with colitis (2.3±0.6% and 20.2±3.2% respectively; p=0.005). Blood vessels were highlighted by BSA-ROX staining, as an early vascular marker. Quantification of the percent area of blood vessels revealed no difference between control and colitis (1.6±0.1% and 1.4±0.3% respectively). These results are consistent with the MRI results showing no significant change in fBV **(Fig 7)**.

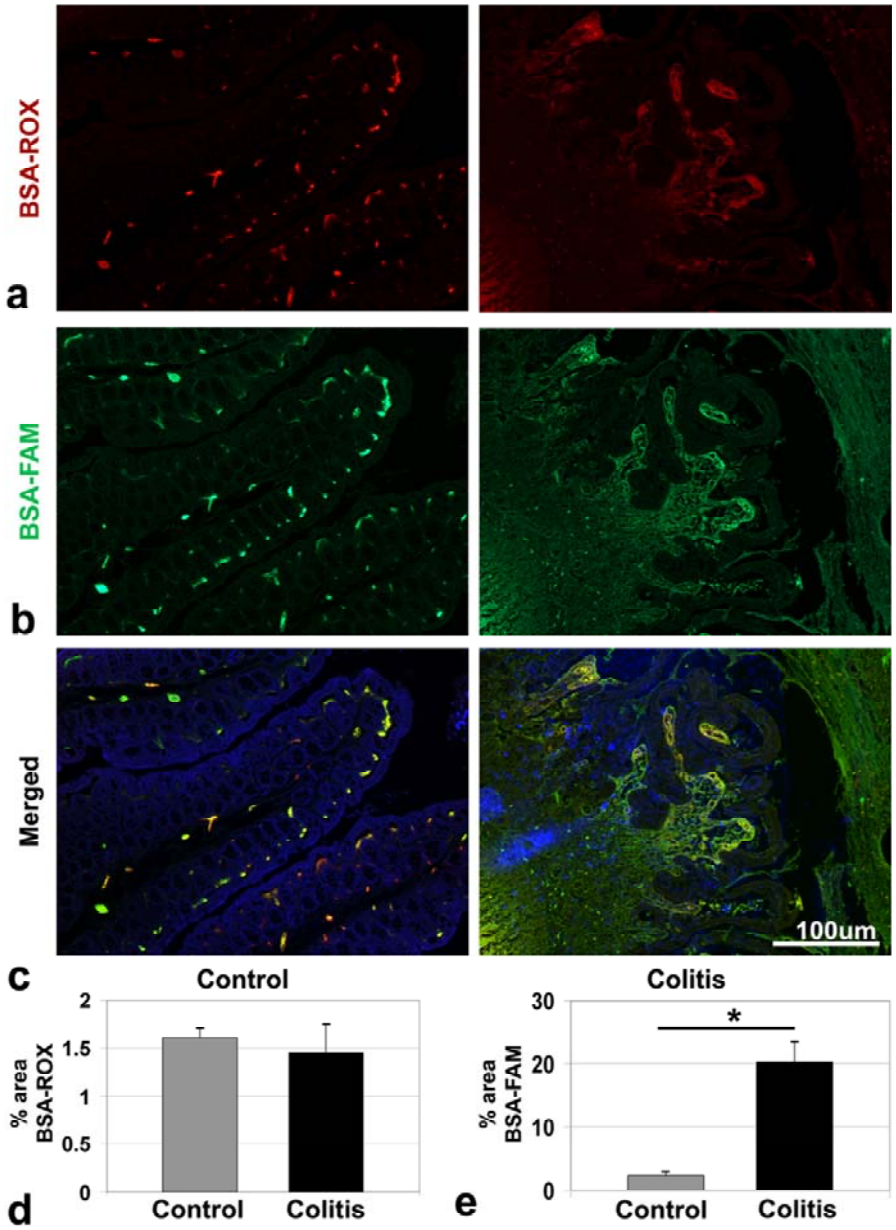

Figure 7. Microscopic histological analysis of the distribution of macromolecular contrast agent. (a) To stain blood vessels only, right after DCE-MRI and just before euthanizing, BSA-ROX, a red fluorescent dye attached to albumin was injected, corresponding to the fractional blood volume (fBV; Figure 2). Quantification of percent area of BSA-ROX revealed no difference between control (1.79±0.19%) and DSS colitis (2.05±0.66%). (b) BSA-FAM co-administered with the contrast agent of the MRI, showed no leakage in the control animals (percent area=2.05±0.66%) as opposed to significant extravasation seen in the animals with colitis (percent area=25.8±3.9%). (c) Composite image of (a) and (b) with DAPI staining nuclei in blue. (d) Percent area of BSA-ROX, corresponding to fBV, or initial enhancement in DCE-MRI. (e) Percent area of BSA-FAM, corresponding to PS, or rate of enhancement in DCE-MRI (n=3 per group; *p=0.005).

Supplementary movies: legends

Supplementary 1. Fiber-optic fluorescence microscopic imaging of representative control mouse colon after intravenous injection of FITC-Dextran. Honeycomb pattern of microcirculation in control colon without leakage of macromolecular dextran-FITC into the lumen.

Supplementary 2. Fiber-optic fluorescence microscopic imaging of representative mouse colon treated with DSS for 7 days after intravenous injection of FITC-Dextran. Highly distorted microcirculation in colon with leakage of FITC-Dextran from the vessels.

Supplementary 3. Dynamic three dimensional reconstruction of the abdomen of a control mouse after macromolecular contrast injection. Ten sequential scans after contrast injection, showing only the vena cava in a representative control animal. The second half of the movie shows a rotation of the last scan.

Supplementary 4. Dynamic three dimensional reconstruction of the abdomen of a mouse treated with 3% DSS for 7 days after macromolecular contrast injection. For a representative mouse with colitis, in the first scan post contrast, no leakage of albumin into the colon is yet observed, but gradually, at each scan, the contrast agent leaked out, resulting in selective enhancement of the colon 30 min post contrast. The second half of the movie shows a rotation of the last scan.

6.3 Discussion

Angiogenesis, manifested by remodeling of blood vessels and enhanced vascular permeability accompanies many diseases. Here, we reported noninvasive evaluation of vascular permeability in the colon as a biomarker of disease progression that enables longitudinal preclinical monitoring of a murine DSS colitis model. Plasma protein leakage to the colon lumen was imaged in-vivo using fluorescent confocal endomicroscopy and non-invasive quantitative macromolecular DCE-MRI, highlighting focal patches of colitis-induced vascular hyperpermeability.

Non-invasively quantifying vascular permeability in DSS-treated colon in living animals yields important dynamic information not available using a standard histo-pathological examination. Non-invasive fiber-optic fluorescent microscopy showed distorted blood vessels and hyperpermeability in the colon of mice after 3% DSS treatment. A honeycomb pattern of the vasculature in control colons and hyperpermeability in DSS-treated colons has been previously described in rats with surgical exposure of the abdomen [90]. Recently, imaging of fluorescently labeled cells and distorted vasculature in animals with DSS colitis has been performed using a custom-built non-invasive side-view endomicroscope [91]. Here, we report the use of a commercially available fluorescent confocal endomicroscopy system for imaging vascular hyperpermeability in DSS-treated colons.

Several studies involved the use of the use of two-dimensional T1- and T2-weighted and low-molecular weight DCE-MRI, for non-invasive detection of inflammation, edema and wall thickning in the colon [92-95]. Low-molecular weight DCE-MRI has also been recently used for semi-quantitative evaluation of colonic inflammation in ulcerative colitis, reporting an increased initial rate of Gd uptake in inflamed colon compared to normal colon [95]. High molecular weight biotin-BSA-GdDTPA, as used in the study reported here, extravasates at a slower rate than low molecular Gd-DTPA and this extravasation is selective and specific to diseased colon. The use of this contrast material thus increases the specificity for detection of small changes vascular permeability. Because of its high

molecular size, biotin-BSA-GdDTPA acts as a blood pool agent and can only extravasate from leaky vessels. Here, we employed 3D MRI visualizing the whole abdomen and allowing volume rendering, which revealed focal defects in the entire colon. As opposed to the low molecular Gd-DTPA, macromolecular MRI contrast agents such as biotin-BSA-GdDTPA, are not clinically approved. However, the approach reported here provides a powerful tool for monitoring the changes in colonic vascular permeability in the context of preclinical research and drug development.

Fractional blood volume (fBV) and permeability (PS) in the colon were measured in-vivo by 3D DCE-MRI using pharmacokinetic analysis of macromolecular biotin-BSA-GdDTPA. Although permeability was significantly increased, fBV, a measure of (micro)vascular density, was not increased for the analyzed region of the colon. This lack of change in fBV was confirmed by the percent area of BSA-ROX in fluorescent microscopy. A significant reduction in blood flow was noted before on days 4-6 of DSS colitis using intravital microscopy[107], in contrast with previous reports on Crohn's disease and ulcerative colitis containing numerous dilated vessels, implying an increased microvascular density based on immunohistochemistry [87,88]. Our method specifically detects functional blood vessels at day 7 of DSS colitis, a relatively advanced stage, in which reduction in vessel diameter and decreased vascular density were previously described [85].

Macromolecular DCE-MRI enabled us to identify severe colitis with loss of plasma proteins from the colonic vasculature due to elevation of capillary permeability and ulcerations in the colon wall. Elevation of capillary permeability, leading to extravasation of serum proteins and allowing detection by imaging the extravasation of macromolecular contrast materials, often accompanies angiogenesis, as a response to endothelial cell activation by vascular endothelial growth factor (VEGF) [104]. Indeed, angiogenesis and elevated expression of VEGF were previously reported to occur in inflammatory bowel disease [87,88]. In addition, modulation of the VEGF pathway affects angiogenesis and leukocyte adhesion in mice with DSS-induced colitis [108]. Leakage of plasma proteins from the vasculature to the colon lumen, enhances weight loss and is thus an important parameter in the disease progression of IBD. Leakage of plasma proteins and deposition of a provisional matrix can support inflammation and stimulate

remodeling of the colonic vasculature.

These results were validated by fluorescent microscopy using BSA-ROX for determination of the fractional blood volume. The permeability (PS) was validated both by staining the biotinylated contrast material with avidin-FITC, and by detection of BSA-FAM injected together with the contrast agent. Both markers showed significant extravasation, confirming the enhanced permeability seen in-vivo by macromolecular DCE-MRI. Thus vascular permeability provides a sensitive biomarker that can be used for quantitative in-vivo assessment of disease progression in preclinical models of colitis.

In summary, the results reported here demonstrate the derivation of quantitative measures for the severity of experimental colitis from in-vivo fluorescent confocal endomicroscopy and macromolecular DCE-MRI. Both techniques enable visualization of the entire tissue surface of the colon with complementary field of view and spatial resolution, while allowing in-vivo follow up. Macromolecular DCE-MRI can be used to visualize and quantify the changes in blood vessel permeability during progression and treatment of colitis. Quantitative biomarkers of disease progression are critical for evaluation of the genetic and environmental factors that affect colitis, as well as for the development of strategies for therapeutic intervention.

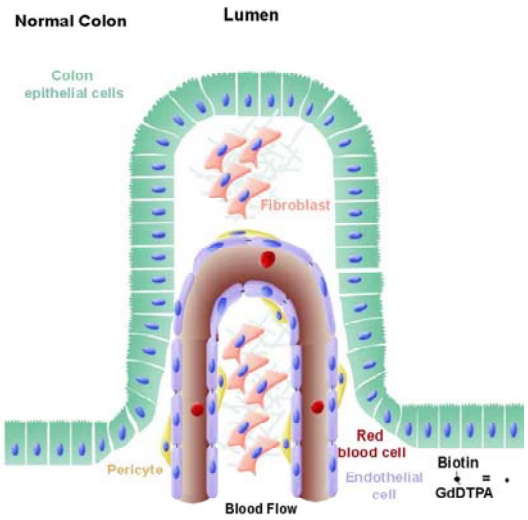

Control

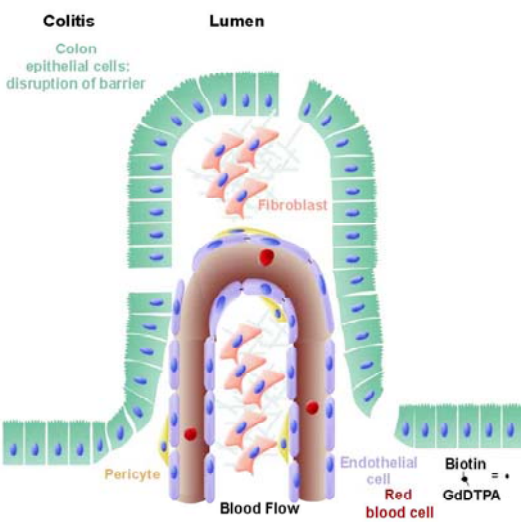

Colitis

Figure 8. Both MRI and fluorescent confocal endomicroscopy revealed a substantial increase in the permeability of the colonic microvasculature associated with colitis, resulting in extravascular accumulation of the macromolecular contrast agent in the lumen of the colon.

7. Concluding remarks

This study aspired to investigate differential contribution of intestinal DCs and macrophages in the maintenance of gut homeostasis and the development of inflammatory bowel disorders. We employed newly established mice to specifically ablate macrophages, but spare the population of $CD103^+$ $CD11b^-$ *lamina propria* DCs. As exemplified in our study, this system can be used to investigate different kinds of molecules of interest and probe for differential contributions of macrophages and DCs in the context of mucosal immunology. Here, we corroborated the earlier notion that the IL-23-IL-23R axis mediates colonic epithelial integrity during colitis and host defense process and newly established that the critical IL23 comes from macrophages. In addition we identified a novel role of IL23 in the crosstalk between macrophages and DC, in whose absence immunopathology develops.

In an independent line of experiments, we established that vascular permeability provides a sensitive biomarker that can be used for quantitative in-vivo assessment of disease progression in preclinical models of colitis.

8. Material and Methods

BM chimeric mice

C57BL/6 mice were purchased from Harlan and were lethally irradiated with 950rad. The next day, $5x10^6$ BM cells obtained from femora and tibiae of WT, $p19^{-/-}$, $p40^{-/-}$, CD11c-DTR , CX_3CR1^{Cre}:R26-YFP and CX_3CR1-iDTR mice were intravenously (*i.v*) injected into the irradiated recipient mice, which were kept to rest for 6-8 weeks before the experiment. $p19^{-/-}$ BM
was kindly provided by Dan Cua, *Merck Research Laboratories* [65].

Infection of Mice

Mice were orally inoculated with kanamycin (Kn)-resistant bioluminescent strain of *C. rodentium*, a kind gift of Gad Fraenkel (*Imperial College London, UK*) by oral gavage with 0.2 ml of PBS containing_$\approx 10^8 - 10^9$ CFU of *C. rodentium* [66].

cDNA Synthesis and Real-Time RT-PCR

Total RNA was extracted from the colon of WT, $p19^{-/-}$, $p40^{-/-}$, CD11c-DTR, CX_3CR1:iDTR chimeras by using the Gnetle-MACS (check) and RNA tissue kit (5prime, company). Then, cDNA synthesis was performed with 2-0.5 ug of total with High Capacity RNA-to-cDNA Kit (Applied Biosystems). Real-time PCR was performed with SYBR Green master mix (Applied Biosystems). Expression of each target gene was normalized to that of TAT binding protein (TBP).

Real-time RT-PCR primers. The sequences for primers used in this study are as follows:

Primers	Forward	Reverse
IL-17A	5’-GCT CCA GAA GGC CCTCAG A-3’	5’-CTT TCC CTC CGC ATT GAC A-3’
IL-6	5’-TCC AAT GCT CTC CTA ACA GAT AAG-3’	5’-CAA GAT GAA TTG GAT GGT CTT G-3’
IL-12p40	5’-ACA TCT ACC GAAGTC CAA TGC A-3’,	5’-GGA ATT GTA ATA GCG ATC CTG AGC-3’
IL-23p19	5’-GGT GGC TCA GGG AAA TGT-3’,	5’-GAC AGA GCA GGCAGG TAC AG-3’
IL-12 p35	5'- GCC ACC CTT GCC CTC CTA A -3'	5'- GGT TTG GTC CCG TGT GAT GTC -3'
IFN-γ	5'- ATG GCT GTT TCT GGC TGT TAC TG -3'	5'- ATC TGG CTC TGC AGG ATT TTC A -3'
IL-10	5'-CCCTTTGCTATGGTGTCCTT-3'	5'-TGGTTTCTCTTCCCAAGACC-3'
RegIIIβ	5’- ATG GCT CCT ACT GCT ATG CC-3’	5’- GTG TCC TCC AGG CCT CTT T-3’
IL-22	5’-TCC GAG GAG TCA GTG CTA AA-3’	5’-AGA ACG TCT TCC AGG GTG AA-3
TBP	5’-GAAGCTGCGGTACAATTCCAG-3’	5’-CCCCTTGTACCCTTCACCAAT-3’
IL-23R	5’-TGGTGTCACGGAGGAATCACAAGT3’	5’-AGATTCCTTGGTCGGCAGTGCTTA3’
S100A9	5’-GGT GGA AGC ACA GTT GGC A-3’,	5’-GTG TCC AGG TCC TCC ATG ATG-3’

Cell preparations

Blood monocytes; Blood was obtained from the tail vein of mice at 7 to 10 weeks of age. Erythrocytes and neutrophils were removed using a Ficoll density gradient (Amersham Biosciences Sunnyvale, CA). Ficoll was completely washed by PBS and cells were collected by the centrifugation at 1,400rpm for 5min at 4℃.

Lamina propria DCs and macrophages; Colonic epithelial cells were removed by the HBSS containing DTT and 5% of FCS. For the isolation of lamina propria cells (LPCs), colon pieces were digested by 5ml HBSS containing 10% FBS, 1mg/ml of collagenase VIII (sigma) and at 37℃ shaking incubator (300rpm) for 1h. Completely digested colon tissue was passed through a mesh and cells were collected by centrifugation at 1400rpm for 5min at 4℃.

T_H17 cells; To isolate T cells from the intestine, lamina propria cells were isolated and fractionated on a percoll density gradient (40% and 80%). To allow for the intracellular cytokine staining of T_H17 cells and T_H1, IL17A and IFNγ production was triggered and accumulated by PMA and ionomycin treatment for 2 hours and treated with

Brefeldin A (1:1000) for 2 hours at 37℃ 5% CO_2. Cells were permeabilized and fixed for the intracellular staining by the BD perm/fixation kit.

Splenic DCs; Spleens were digested with collagenase D (4mg/ml, Roche) at 37℃ for 1hour. Cells were passed through a mesh (100um) and washed by centrifugation at 1400rpm, 4℃ for 5min. Splenic cells were treated with ACK solution to remove erythrocytes, washed with PBS and stained.

Flowcytometric analysis

The following fluorochrome-labeled monoclonal antibodies and staining reagents were used according to manufacturers protocols: PE-conjugated anti-CD115 (eBioscience), APC-conjugated anti-Gr1 (Ly6C/G) (eBioscience) and PerCP-conjugated anti-CD11b were used for blood and spleen monocyte staining. Lamina propria cells were stained with CD11c-APC(1:100, eBioscience), CD11b-PerCP Cy5.5(1:200, Biolegend), CD103-PE(1:100, BD pharmingen) MHC II-PE-CY7 (1:300, eBioscience), CD45.2-(1:100, eBioscience) and DAPI (1:10,000). TH17 and TH1 cells were stained with IL17A-PE, CD3-PerCP , CD4-APC,CD45-FITC and IFNγ-PE-CY7. Monocytes isolated lamina propria were stained with CD11b-APC(1:200, Biolegend) , PerCP -conjugated anti Ly6C (eBioscience and F4/80-PE (EMR, 1:50, Serotec). Cells were analyzed on a FACS Calibur and LSR cytometer (BD) using Flow-Jo software (Treestar).

Neutralization of mouse IFNγ and in vivo

We intraperitoneally injected IFNγ specific mAb (Clone, XMG1.2) day 0, day 2, day 4, day 6 and day 8 after *C. rodentium* infection at a dose of 1 mg per mouse. Certain control groups also received isotype control IgG2a mAb.

Cell Sorting

Colonic epithelial cells from $CX_3CR1^{+/-}$ mice at the age of 6-10 weeks were removed and colon were digested and stained as indicated above. A FACSAria cytometer (Becton-Dickinson) was used for sorting.

In vivo measurement of *C. rodentium*

Mice were anaesthetized and imaged using IVIS (Xenogen, Almeda, CA). Greyscale reference images taken under low illumination were collected and overlaid with images capturing the emission of photons from the bioluminescent *C. rodentium* using LIVING IMAGE software (Xenogen). Live mice were euthanized and their colon was removed and imaged as above

DSS-induced experimental colitis

All animal experiments were approved by the Institutional Animal Care and Use Committee. After 7 days of exposure to 3% DSS in the drinking water, C57 black mice developed colitis [85]. Control C57 black mice were given regular drinking water. On day 7, animals were imaged by MRI and fluorescent endoscopy as listed below.

In-vivo fluorescent confocal endomicroscopy of the colon

DSS-induced colitis (n=6) and control animals (n=5) were imaged with fluorescent confocal endomicroscopy (Cellvizio, Mauna Kea Technologies, Newtown, PA). Anesthesized mice (75mg/kg ketamine, Fort Dodge Laboratories, IA, USA; and 3mg/kg xylazine 2%, VMD, Belgium; i.p.) were administered with the fluorescent contrast media fluorescein isothiocyanate (FITC)-Dextran (500kDa; 75mg/kg; Sigma-Aldrich, USA; i.v.), followed by insertion of the endoscopy probe (ProFlex Microprobe S-1500) into the anus. The colonic microcirculation was imaged with a field of view (FOV) of 400x280µm for 20 min after administration of the fluorescent contrast media. The fraction of area showing FITC-Dextran fluorescence, in each field of view (on 2-3 images per animal) was calculated using ImageJ software (http://rsbweb.nih.gov/ij/). The threshold for 8-bit grey scale images was set at 30 (in a range of 0 to 256) according to the visualization of the FITC in the images. Representative histograms of control and colitis were retrieved from the entire 8-bit grey scale image using ImageJ software.

In-vivo dynamic contrast enhanced MRI of the colon

Animal preparation

Mice displaying DSS-induced colitis and control mice (n=6 for each group) were imaged at 9.4T on a horizontal Biospec spectrometer (Bruker, Karlsruhe, Germany) using a quadrature resonator for excitation and detection (Bruker). Mice were anesthetized (isoflurane; induction 3.5% in oxygen in a box, maintenance 1.25% in oxygen inhaled through a nose cone) followed by addition acepromazine (intraperitoneal; 2.5µg/kg, Wyeth-Ayerst Laboratories, Canada) to suppress respiratory motion. A hollow rectal tube was inserted, in order to facilitate localization of the descending colon. The tail vein was catheterized with homebuilt catheters fitted with a heparin washed needle for administration of the contrast media. Animals were heated using a warming water blanket (Bruker)**.** Core temperature in a control animal under the same settings was measured using a MR compatible rectal system (Small Animal Imaging Inc., Stony Brook, NY, USA) and found to be around 34.5ºC**.**

DCE-MRI

Macromolecular biotin-BSA-GdDTPA (about 82kDa), was prepared as reported previously [96] and injected intravenously through a tail vein catheter as a bolus (10 mg/mouse in 0.2 ml).

Three dimensional gradient echo (3D-GE) images of the abdomen were acquired before and sequentially for 30min after administration of the contrast agent. A series of variable flip angle precontrast T_1-weighted 3D-GE images were acquired to determine the endogenous precontrast R_1. Imaging parameters: precontrast flip angles 5º, 15º, 30º, 50º, 70º; postcontrast flip angle 15º; TR 10ms; TE 4ms; two averages; spectral width 50,000Hz; matrix 128x128x64; zero-filled to 256x256x128; FOV 40x40x40mm; acquisition time 163s per time frame. We used 3D gradient echo acquisition with hard pulse excitation (no slice selection), so as to minimize in flow effects on R_1 relaxation [99].

DCE-MRI data analysis

MRI data were analyzed using voxel-by-voxel MATLAB program (MathWorks Inc., USA) to derive concentrations of biotin-BSA-GdDTPA for selected slices containing the

colon in the 3D datasets [100,101]. Briefly, precontrast longitudinal relaxation rate (R_1 pre) values were derived from the variable flip angle data by nonlinear best fit to Eq.[1]:

[1]

$$I = \frac{M_0 \sin\alpha(1 - e^{-TR \bullet R_1 pre})}{1 - \cos\alpha \bullet e^{-TR \bullet R_1 pre}}$$

Where I is the signal intensity as a function of pulse flip angle α, TR is the repetition time (10 ms), and the preexponent term M_0 includes the spin density and the T_2 relaxation, which are assumed to be constant. Post contrast R_1 values ($R_{1\ post}$) were calculated from the precontrast and postcontrast signal intensities (I_{pre} and I_{post}, respectively, acquired with a flip angle of 15º). Finally, concentrations were calculated based on the measured relaxivity (r_1) of biotin-BSA-GdDTPA (99 $mM^{-1}s^{-1}$ per BSA, at 9.4T) [100,101].

The concentration of the contrast material was calculated on axial slices of the colon, over a length of 10.6 mm from the anus cranially for 10 time points after administration of the contrast material. For each time point, the biotin-BSA-GdDTPA concentration in the volume of interest (VOI) of colon (C_{colon}) was divided by the corresponding concentration of biotin-BSA-GdDTPA in blood (C_{blood}; calculated in VOI depicting the vena cava).

From the temporal changes in the concentration maps, two parameter maps were derived from the first 5 time points (first 15 minutes postcontrast). The blood volume fraction (fBV) was derived from the ratio between the concentration of biotin-BSA-GdDTPA in the colon and the concentration in the blood extrapolated to the time of administration of the contrast media. Linear regression was used to derive the rate of change in C_{colon} /C_{blood}, *to yield* the permeability surface area product (PS; min^{-1}). PS measured with biotin-BSA-GdDTPA reflects the extravasation of macromolecules such as albumin from blood vessels and their accumulation in the tissues. PS maps (generated for slices of interest) were projected to show the mean value in each pixel in the axial plain. The percentage diseased colon, was calculated using the percentage of slices with PS>0.005min^{-1}. Rendering of the 3D MRI data was done using Amira software (Visage Imaging Inc, USA). Because of the inserted rectal tube, the anatomy of the descending colon could be easily identified. The dimensions of the colon were delineated manually

and colonic thickness was calculated on axial slices (3 slices containing the colon per animal) using ImageJ software.

Histology and fluorescent microscopy

The distribution of the biotinylated MRI contrast media, biotin-BSA-GdDTPA was determined in histological sections by staining with fluorescent avidin-FITC. Since endogenous tissue biotin could interfere with validation of the MRI contrast agent by histology, BSA labeled with fluorescein (BSA-FAM; 1.4μmol/kg; Molecular Probes, USA) was added to the MRI contrast agent and injected together as a bolus for two animals per group. At the end of the MRI experiment, 30 min after contrast injection, BSA labeled with red fluorescent rhodamine (BSA-ROX; 1.4μmol/kg; Molecular Probes, USA), as an early vascular marker, was iv injected via a tail vein catheter 2min prior to animal sacrifice, as reported previously [100]. The colons were fixed (Carnoy's solution for fluorescence) and embedded in paraffin, sectioned serially at 4μm thickness and stained for the biotinylated contrast agent with avidin-FITC (Molecular Probes, CA, USA) [100]or BSA-FAM directly examined when it was added in the bolus. BSA-ROX and BSA-FAM injected just before collection of the tissue, remained intact throughout the processing mentioned above. The percent area with fluorescent BSA-FAM and BSA-ROX staining (2-3 slices per animal) in each field of view was calculated using ImageJ software. Adjacent sections were stained with hematoxylin and eosin (H&E) for pathological scoring.

Statistical analysis

A two-tailed unpaired t-test ± standard error (s.e.m.) was applied for the analysis of significance of the MRI permeability data. Values are presented as mean ± standard error. The authors had full access to the data and take responsibility for its integrity. All authors have read and agreed to the manuscript as written.

9. References

1. Xavier, R.J. & Podolsky, D.K. Unravelling the pathogenesis of inflammatory bowel disease. *Nature* 448, 427-434 (2007).

2. Varol, C., Zigmond, E. & Jung, S. Securing the immune tightrope: mononuclear phagocytes in the intestinal lamina propria. *Nat Rev Immunol* 10, 415-426.

3. Iwasaki, A. Mucosal dendritic cells. *Annu Rev Immunol* 25, 381-418 (2007).

4. Rescigno, M.*, et al.* Dendritic cells express tight junction proteins and penetrate gut epithelial monolayers to sample bacteria. *Nat Immunol* 2, 361-367 (2001).

5. Coombes, J.L. & Powrie, F. Dendritic cells in intestinal immune regulation. *Nat Rev Immunol* 8, 435-446 (2008).

6. Worbs, T.*, et al.* Oral tolerance originates in the intestinal immune system and relies on antigen carriage by dendritic cells. *J Exp Med* 203, 519-527 (2006).

7. Uematsu, S.*, et al.* Regulation of humoral and cellular gut immunity by lamina propria dendritic cells expressing Toll-like receptor 5. *Nat Immunol* 9, 769-776 (2008).

8. Fogg, D.K.*, et al.* A clonogenic bone marrow progenitor specific for macrophages and dendritic cells. *Science* 311, 83-87 (2006).

9. Naik, S.H.*, et al.* Intrasplenic steady-state dendritic cell precursors that are distinct from monocytes. *Nat Immunol* 7, 663-671 (2006).

10. Liu, K.*, et al.* In vivo analysis of dendritic cell development and homeostasis. *Science* 324, 392-397 (2009).

11. Varol, C.*, et al.* Intestinal lamina propria dendritic cell subsets have different origin and functions. *Immunity* 31, 502-512 (2009).

12. Rakoff-Nahoum, S., Paglino, J., Eslami-Varzaneh, F., Edberg, S. & Medzhitov, R. Recognition of commensal microflora by toll-like receptors is required for intestinal homeostasis. *Cell* 118, 229-241 (2004).

13. Rimoldi, M.*, et al.* Intestinal immune homeostasis is regulated by the crosstalk between epithelial cells and dendritic cells. *Nat Immunol* 6, 507-514 (2005).

14. Niess, J.H.*, et al.* CX3CR1-mediated dendritic cell access to the intestinal lumen and bacterial clearance. *Science* 307, 254-258 (2005).

15. Vallon-Eberhard, A., Landsman, L., Yogev, N., Verrier, B. & Jung, S. Transepithelial pathogen uptake into the small intestinal lamina propria. *J Immunol* 176, 2465-2469 (2006).

16. Chieppa, M., Rescigno, M., Huang, A.Y. & Germain, R.N. Dynamic imaging of dendritic cell extension into the small bowel lumen in response to epithelial cell TLR engagement. *J Exp Med* 203, 2841-2852 (2006).

17. Schulz, O.*, et al.* Intestinal CD103+, but not CX3CR1+, antigen sampling cells migrate in lymph and serve classical dendritic cell functions. *J Exp Med* 206, 3101-3114 (2009).

18. Arques, J.L.*, et al.* Salmonella induces flagellin- and MyD88-dependent migration of bacteria-capturing dendritic cells into the gut lumen. *Gastroenterology* 137, 579-587, 587 e571-572 (2009).

19. Atarashi, K.*, et al.* ATP drives lamina propria T(H)17 cell differentiation. *Nature* 455, 808-812

(2008).

20. Murai, M., *et al.* Interleukin 10 acts on regulatory T cells to maintain expression of the transcription factor Foxp3 and suppressive function in mice with colitis. *Nat Immunol* 10, 1178-1184 (2009).

21. Zhou, L., Chong, M.M. & Littman, D.R. Plasticity of CD4+ T cell lineage differentiation. *Immunity* 30, 646-655 (2009).

22. Ivanov, II, *et al.* Specific microbiota direct the differentiation of IL-17-producing T-helper cells in the mucosa of the small intestine. *Cell Host Microbe* 4, 337-349 (2008).

23. Gaboriau-Routhiau, V., *et al.* The key role of segmented filamentous bacteria in the coordinated maturation of gut helper T cell responses. *Immunity* 31, 677-689 (2009).

24. Izcue, A., Coombes, J.L. & Powrie, F. Regulatory lymphocytes and intestinal inflammation. *Annu Rev Immunol* 27, 313-338 (2009).

25. Bogunovic, M., *et al.* Origin of the lamina propria dendritic cell network. *Immunity* 31, 513-525 (2009).

26. Commins, S., Steinke, J.W. & Borish, L. The extended IL-10 superfamily: IL-10, IL-19, IL-20, IL-22, IL-24, IL-26, IL-28, and IL-29. *J Allergy Clin Immunol* 121, 1108-1111 (2008).

27. Kobayashi, M., *et al.* Identification and purification of natural killer cell stimulatory factor (NKSF), a cytokine with multiple biologic effects on human lymphocytes. *J Exp Med* 170, 827-845 (1989).

28. Becker, C., *et al.* Cutting edge: IL-23 cross-regulates IL-12 production in T cell-dependent experimental colitis. *J Immunol* 177, 2760-2764 (2006).

29. Collison, L.W., *et al.* The inhibitory cytokine IL-35 contributes to regulatory T-cell function. *Nature* 450, 566-569 (2007).

30. Collison, L.W., *et al.* IL-35-mediated induction of a potent regulatory T cell population. *Nat Immunol* 11, 1093-1101.

31. O'Neill, L.A. & Bowie, A.G. The family of five: TIR-domain-containing adaptors in Toll-like receptor signalling. *Nat Rev Immunol* 7, 353-364 (2007).

32. Kinnebrew, M.A., *et al.* Interleukin 23 production by intestinal CD103(+)CD11b(+) dendritic cells in response to bacterial flagellin enhances mucosal innate immune defense. *Immunity* 36, 276-287.

33. Xue, X., *et al.* Microbiota downregulates dendritic cell expression of miR-10a, which targets IL-12/IL-23p40. *J Immunol* 187, 5879-5886.

34. Weaver, C.T., Hatton, R.D., Mangan, P.R. & Harrington, L.E. IL-17 family cytokines and the expanding diversity of effector T cell lineages. *Annu Rev Immunol* 25, 821-852 (2007).

35. Goriely, S., Neurath, M.F. & Goldman, M. How microorganisms tip the balance between interleukin-12 family members. *Nat Rev Immunol* 8, 81-86 (2008).

36. Becker, C., *et al.* Constitutive p40 promoter activation and IL-23 production in the terminal ileum mediated by dendritic cells. *J Clin Invest* 112, 693-706 (2003).

37. Kotenko, S.V., *et al.* Identification, cloning, and characterization of a novel soluble receptor that binds IL-22 and neutralizes its activity. *J Immunol* 166, 7096-7103 (2001).

38. Wolk, K., *et al.* IL-22 increases the innate immunity of tissues. *Immunity* 21, 241-254 (2004).

39. Zenewicz, L.A., *et al.* Innate and adaptive interleukin-22 protects mice from inflammatory bowel disease. *Immunity* 29, 947-957 (2008).

40. Radaeva, S., Sun, R., Pan, H.N., Hong, F. & Gao, B. Interleukin 22 (IL-22) plays a protective role in T cell-mediated murine hepatitis: IL-22 is a survival factor for hepatocytes via STAT3 activation. *Hepatology* 39, 1332-1342 (2004).

41. Ma, H.L., *et al.* IL-22 is required for Th17 cell-mediated pathology in a mouse model of psoriasis-like skin inflammation. *J Clin Invest* 118, 597-607 (2008).

42. Zheng, Y., *et al.* Interleukin-22, a T(H)17 cytokine, mediates IL-23-induced dermal inflammation and acanthosis. *Nature* 445, 648-651 (2007).

43. Liang, S.C., *et al.* Interleukin (IL)-22 and IL-17 are coexpressed by Th17 cells and cooperatively enhance expression of antimicrobial peptides. *J Exp Med* 203, 2271-2279 (2006).

44. Boniface, K., *et al.* IL-22 inhibits epidermal differentiation and induces proinflammatory gene expression and migration of human keratinocytes. *J Immunol* 174, 3695-3702 (2005).

45. Zheng, Y., *et al.* Interleukin-22 mediates early host defense against attaching and effacing bacterial pathogens. *Nat Med* 14, 282-289 (2008).

46. Aujla, S.J., *et al.* IL-22 mediates mucosal host defense against Gram-negative bacterial pneumonia. *Nat Med* 14, 275-281 (2008).

47. Sonnenberg, G.F., Monticelli, L.A., Elloso, M.M., Fouser, L.A. & Artis, D. CD4(+) lymphoid tissue-inducer cells promote innate immunity in the gut. *Immunity* 34, 122-134 (2011).

48. Sugimoto, K., *et al.* IL-22 ameliorates intestinal inflammation in a mouse model of ulcerative colitis. *J Clin Invest* 118, 534-544 (2008).

49. Ota, N., *et al.* IL-22 bridges the lymphotoxin pathway with the maintenance of colonic lymphoid structures during infection with Citrobacter rodentium. *Nat Immunol* 12, 941-948 (2011).

50. Geddes, K., *et al.* Identification of an innate T helper type 17 response to intestinal bacterial pathogens. *Nat Med* 17, 837-844 (2011).

51. Takatori, H., *et al.* Lymphoid tissue inducer-like cells are an innate source of IL-17 and IL-22. *J Exp Med* 206, 35-41 (2009).

52. Satoh-Takayama, N., *et al.* Microbial flora drives interleukin 22 production in intestinal NKp46+ cells that provide innate mucosal immune defense. *Immunity* 29, 958-970 (2008).

53. Cella, M., *et al.* A human natural killer cell subset provides an innate source of IL-22 for mucosal immunity. *Nature* 457, 722-725 (2009).

54. Martin, B., Hirota, K., Cua, D.J., Stockinger, B. & Veldhoen, M. Interleukin-17-producing gammadelta T cells selectively expand in response to pathogen products and environmental signals. *Immunity* 31, 321-330 (2009).

55. Pickert, G., *et al.* STAT3 links IL-22 signaling in intestinal epithelial cells to mucosal wound healing. *J Exp Med* 206, 1465-1472 (2009).

56. Li, M.O. & Flavell, R.A. Contextual regulation of inflammation: a duet by transforming growth factor-beta and interleukin-10. *Immunity* 28, 468-476 (2008).

57. Liu, Z., *et al.* Interleukin (IL)-23 suppresses IL-10 in inflammatory bowel disease. *J Biol Chem* 287, 3591-3597 (2012).

58. Wales, A.D., Woodward, M.J. & Pearson, G.R. Attaching-effacing bacteria in animals. *J Comp*

Pathol 132, 1-26 (2005).

59. Deng, W., Li, Y., Vallance, B.A. & Finlay, B.B. Locus of enterocyte effacement from Citrobacter rodentium: sequence analysis and evidence for horizontal transfer among attaching and effacing pathogens. *Infect Immun* 69, 6323-6335 (2001).

60. Schauer, D.B. & Falkow, S. The eae gene of Citrobacter freundii biotype 4280 is necessary for colonization in transmissible murine colonic hyperplasia. *Infect Immun* 61, 4654-4661 (1993).

61. Lupp, C., *et al.* Host-mediated inflammation disrupts the intestinal microbiota and promotes the overgrowth of Enterobacteriaceae. *Cell Host Microbe* 2, 119-129 (2007).

62. Kamada, N., *et al.* Regulated virulence controls the ability of a pathogen to compete with the gut microbiota. *Science* 336, 1325-1329 (2012).

63. Kim, Y.G., *et al.* The Nod2 sensor promotes intestinal pathogen eradication via the chemokine CCL2-dependent recruitment of inflammatory monocytes. *Immunity* 34, 769-780 (2011).

64. Fritz, J.H., *et al.* Acquisition of a multifunctional IgA+ plasma cell phenotype in the gut. *Nature* 481, 199-203 (2012).

65. McGeachy, M.J. & Cua, D.J. Th17 cell differentiation: the long and winding road. *Immunity* 28, 445-453 (2008).

66. Wiles, S., Robertson, B.D., Frankel, G. & Kerton, A. Bioluminescent monitoring of in vivo colonization and clearance dynamics by light-emitting bacteria. *Methods Mol Biol* 574, 137-153 (2009).

67. Ivanov, II, *et al.* Induction of intestinal Th17 cells by segmented filamentous bacteria. *Cell* 139, 485-498 (2009).

68. Takahashi, A., *et al.* Production of beta-defensin-2 by human colonic epithelial cells induced by Salmonella enteritidis flagella filament structural protein. *FEBS Lett* 508, 484-488 (2001).

69. Chan, J.R., *et al.* IL-23 stimulates epidermal hyperplasia via TNF and IL-20R2-dependent mechanisms with implications for psoriasis pathogenesis. *J Exp Med* 203, 2577-2587 (2006).

70. Jung, S., *et al.* In vivo depletion of CD11c(+) dendritic cells abrogates priming of CD8(+) T cells by exogenous cell-associated antigens. *Immunity* 17, 211-220 (2002).

71. Ivanov, II, *et al.* The orphan nuclear receptor RORgammat directs the differentiation program of proinflammatory IL-17+ T helper cells. *Cell* 126, 1121-1133 (2006).

72. Ishigame, H., *et al.* Differential roles of interleukin-17A and -17F in host defense against mucoepithelial bacterial infection and allergic responses. *Immunity* 30, 108-119 (2009).

73. Sapoznikov, A., *et al.* Perivascular clusters of dendritic cells provide critical survival signals to B cells in bone marrow niches. *Nat Immunol* 9, 388-395 (2008).

74. Tilahun, A.Y., Holz, M., Wu, T.T., David, C.S. & Rajagopalan, G. Interferon gamma-dependent intestinal pathology contributes to the lethality in bacterial superantigen-induced toxic shock syndrome. *PLoS One* 6, e16764 (2011).

75. Hirota, K., *et al.* Fate mapping of IL-17-producing T cells in inflammatory responses. *Nat Immunol* 12, 255-263 (2011).

76. Lee, J., *et al.* IL-17E, a novel proinflammatory ligand for the IL-17 receptor homolog IL-17Rh1. *J Biol Chem* 276, 1660-1664 (2001).

77. Bruewer, M., *et al.* Interferon-gamma induces internalization of epithelial tight junction proteins via

a macropinocytosis-like process. *FASEB J* 19, 923-933 (2005).

78. Cox, J.H., *et al.* Opposing consequences of IL-23 signaling mediated by innate and adaptive cells in chemically induced colitis in mice. *Mucosal Immunol* 5, 99-109 (2012).

79.Yun-Gi Kim, Nobuhiko Kamada, Michael H. Shaw, Neil Warner, Grace Y. Chen, Luigi Franchi, andGabriel Núñez. The intracellular sensor Nod2 Promotes Intestinal Pathogen Eradication via the chemokine CCL2-Dependent Recruitment of Inflammatory Monocytes. Immunity 2009; 34, (5), 769-780.

80.Podolsky DK. Inflammatory bowel disease. N Engl J Med 2002;347(6):417-429.2.Bouma G, Strober W. The immunological and genetic basis of inflammatory bowel disease. Nat Rev Immunol 2003;3(7):521-533.

81.Hulten L, Lindhagen J, Lundgren O, Fasth S, Ahren C. Regional intestinal blood flow in ulcerative colitis and Crohn's disease. Gastroenterology 1977;72(3):388-396.

82.Abraham C, Cho JH. Inflammatory bowel disease. N Engl J Med 2009; 19;361(21):2066-2078.

83.Casanova JL, Abel L. Revisiting Crohn's disease as a primary immunodeficiency of macrophages. J Exp Med 2009; 31;206(9):1839-1843.

84.Liu J, Cao S, Herman LM, Ma X. Differential regulation of interleukin (IL)-12 p35 and p40 gene expression and interferon (IFN)-gamma-primed IL-12 production by IFN regulatory factor 1. 2003 ; 20;198(8):1265-1276.

85.Hulten L, Lindhagen J, Lundgren O, Fasth S, Ahren C. Regional intestinal blood flow in ulcerative colitis and Crohn's disease. Gastroenterology 1977;72(3):388-396.

86.Chidlow JH, Jr., Langston W, Greer JJ, Ostanin D, Abdelbaqi M, Houghton J, Senthilkumar A, Shukla D, Mazar AP, Grisham MB, Kevil CG. Differential angiogenic regulation of experimental colitis. Am J Pathol 2006;169(6):2014-2030.

87.Deban L, Correale C, Vetrano S, Malesci A, Danese S. Multiple pathogenic roles of microvasculature in inflammatory bowel disease: a Jack of all trades. Am J Pathol 2008;172(6):1457-1466.

88.Danese S, Sans M, de la Motte C, Graziani C, West G, Phillips MH, Pola R, Rutella S, Willis J, Gasbarrini A, Fiocchi C. Angiogenesis as a novel component of inflammatory bowel disease pathogenesis. Gastroenterology 2006;130(7):2060-2073.

89.Wirtz S, Neufert C, Weigmann B, Neurath MF. Chemically induced mouse models of intestinal inflammation. Nat Protoc 2007;2(3):541-546.

90.McLaren W, Anikijenko P, Barkla D, Delaney TP, King R. In vivo detection of experimental ulcerative colitis in rats using fiberoptic confocal imaging (FOCI). Dig Dis Sci 2001;46(10):2263-2276.

91.Kim P, Chung E, Yamashita H, Hung KE, Mizoguchi A, Kucherlapati R, Fukumura D, Jain RK, Yun SH. In vivo wide-area cellular imaging by side-view endomicroscopy. Nat Methods 2010;7(4):303-305.

92.Larsson AE, Melgar S, Rehnstrom E, Michaelsson E, Svensson L, Hockings P, Olsson LE. Magnetic resonance imaging of experimental mouse colitis and association with inflammatory activity. Inflamm Bowel Dis 2006;12(6):478-485.

93.Melgar S, Gillberg PG, Hockings PD, Olsson LE. High-throughput magnetic resonance imaging in murine colonic inflammation. Biochem Biophys Res Commun 2007;355(4):1102-1107.

94.Young MR, Ileva LV, Bernardo M, Riffle LA, Jones YL, Kim YS, Colburn NH, Choyke PL. Monitoring of tumor promotion and progression in a mouse model of inflammation-induced colon cancer with magnetic resonance colonography. Neoplasia 2009;11(3):237-246.

95.Mustafi D, Fan X, Dougherty U, Bissonnette M, Karczmar GS, Oto A, Hart J, Markiewicz E, Zamora M. High-resolution magnetic resonance colonography and dynamic contrast-enhanced magnetic resonance imaging in a murine model of colitis. Magn Reson Med 2010;63(4):922-929.

96.Heilmann M, Walczak C, Vautier J, Dimicoli JL, Thomas CD, Lupu M, Mispelter J, Volk A. Simultaneous dynamic T1 and T2* measurement for AIF assessment combined with DCE MRI in a mouse tumor model. MAGMA 2007;20(4):193-203.

97.Vandoorne K, Addadi Y, Neeman M. Visualizing vascular permeability and lymphatic drainage using labeled serum albumin. Angiogenesis 2010;13(2):75-85.

98.Ziv K, Nevo N, Dafni H, Israely T, Granot D, Brenner O, Neeman M. Longitudinal MRI tracking of the angiogenic response to hind limb ischemic injury in the mouse. Magn Reson Med 2004;51(2):304-311.

99.Plaks V, Kalchenko V, Dekel N, Neeman M. MRI analysis of angiogenesis during mouse embryo implantation. Magn Reson Med 2006;55(5):1013-1022.

100.Dafni H, Israely T, Bhujwalla ZM, Benjamin LE, Neeman M. Overexpression of vascular endothelial growth factor 165 drives peritumor interstitial convection and induces lymphatic drain: magnetic resonance imaging, confocal microscopy, and histological tracking of triple-labeled albumin. Cancer Res 2002;62(22):6731-6739.

101.Vandoorne K, Magland J, Plaks V, Sharir A, Zelzer E, Wehrli F, Hemmings BA, Harmelin A, Neeman M. Bone vascularization and trabecular bone formation are mediated by PKB alpha/Akt1 in a gene-dosage-dependent manner: in vivo and ex vivo MRI. Magn Reson Med 2010;64(1):54-64.

102.Brasch R, Pham C, Shames D, Roberts T, van Dijke K, van Bruggen N, Mann J, Ostrowitzki S, Melnyk O. Assessing tumor angiogenesis using macromolecular MR imaging contrast media. J Magn Reson Imaging 1997;7(1):68-74.

103.Kim YR, Rebro KJ, Schmainda KM. Water exchange and inflow affect the accuracy of T1-GRE blood volume measurements: implications for the evaluation of tumor angiogenesis. Magn Reson Med 2002;47(6):1110-1120.

104.Dafni H, Landsman L, Schechter B, Kohen F, Neeman M. MRI and fluorescence microscopy of the acute vascular response to VEGF165: vasodilation, hyper-permeability and lymphatic uptake, followed by rapid inactivation of the growth factor. NMR Biomed 2002;15(2):120-131.

105.Dafni H, Gilead A, Nevo N, Eilam R, Harmelin A, Neeman M. Modulation of the pharmacokinetics of macromolecular contrast material by avidin chase: MRI, optical, and inductively coupled plasma mass spectrometry tracking of triply labeled albumin. Magn Reson Med 2003;50(5):904-914.

106.Ravnic DJ, Konerding MA, Tsuda A, Huss HT, Wolloscheck T, Pratt JP, Mentzer SJ. Structural adaptations in the murine colon microcirculation associated with hapten-induced inflammation. Gut 2007;56(4):518-523.

107.Mori M, Stokes KY, Vowinkel T, Watanabe N, Elrod JW, Harris NR, Lefer DJ, Hibi T, Granger DN.

Colonic blood flow responses in experimental colitis: time course and underlying mechanisms. Am J Physiol Gastrointest Liver Physiol 2005;289(6):G1024-1029.

108.Scaldaferri F, Vetrano S, Sans M, Arena V, Straface G, Stigliano E, Repici A, Sturm A, Malesci A, Panes J, Yla-Herttuala S, Fiocchi C, Danese S. VEGF-A links angiogenesis and inflammation in inflammatory bowel disease pathogenesis. Gastroenterology 2009;136(2):585-595 e585.

10. List of publications

10.1 Articles published in refereed journal (included in my thesis).

1. Tegest Aychek[1]*, Katrien Vandoorne[2]*, Ori Brenner[3], Steffen Jung[1**] and Michal Neeman[2**"], *Quantitative analysis of intravenously administered contrast media reveals changes in vascular barrier functions in a murine colitis mode"* **Magn Reson Med. (2011).**

2. **Tegest Aychek**, *Alexander Mildner,* Simon Yona, *Ki-wook Kim,* and Steffen Jung, *Critical IL-23-based crossregulaion of intestinal DCs by macrophages protects mice from Citrobacter challenge* .***Manuscript in preparation.***

10.2 Articles published in refereed journal (not included in my thesis).

1. Varol C, Vallon-Eberhard A, Elinav E, **Aychek T**, Shapira Y, Luche H, Fehling HJ, Hardt WD, Shakhar G, Jung S. *Intestinal lamina propria dendritic cell subsets have different origin and functions.*I**mmunity. 2009.**

2. Mishalian I, Ordan M, Peled A, Maly A, Eichenbaum MB, Ravins M, **Aychek T**, Jung S, Hanski E. *Recruited macrophages control dissemination of group A Streptococcus from infected soft tissues.* **J Immunol. 2011**

3. Mildner A, Chapnik E, Manor O, Yona S, Kim KW, **Aychek T**, Varol D, Beck G, Itzhaki ZB, Feldmesser E, Amit I, Hornstein E, Jung S. *Mononuclear phagocyte microRNome analysis identifies miR-142 as critical regulator of murine dendritic cell homeostasis.***Blood. 2012**

11. Statement about independent collaboration

The manuscript entitled "*Quantitative analysis of intravenously administered contrast media reveals changes in vascular barrier functions in a murine colitis mode"* Summarized a study initiated by me, I identified the phenotype and established the DSS colitis model an addition I established the usage of the Cell-Vizio to visuals colonic blood vessel. I also wrote the article with the help of Katrien Vandoorne who performed the MRI imaging and the analysis of the data resulting from the MRI.